The effect of radiation on cellular ageing

A Thesis submitted for the Degree Award of Master of Philosophy

by

Rebecca Jane Sabin

School of Health and Social Care

Brunel University

December 2012

Abstract

Humans are exposed to low and moderate doses of ionising radiation (IR) from a range of diagnostic and occupational sources which may lead to cellular effects including genomic damage, cellular senescence and cell death. Cellular senescence is interesting because it is a normal, metabolically active form of tumour-suppressive growth arrest initiated in response to intrinsic and extrinsic stressors helping to prevent the proliferation of ageing/damaged cells. However, in addition to this tumour-suppressive mechanism, senescent cells and tissues have also been linked with the development of a pro-oncogenic environment resulting from the secretion of an inflammatory phenotype. Indeed, senescence is thought to be important in a number of age-related pathologies and may influence the biological effects of radiation exposure. To assess the relationship between IR and stress-induced senescence we exposed mid and late passage primary normal human bronchial epithelial (NHBE) cells to low-LET Cobalt^{60} γ-rays (0-2 Gy) and fixed cells 0 min – 792 hours after exposure. DNA damage in both proliferating and senescent NHBE cells was quantified in nuclei co-stained for 53BP1 DNA damage foci (average foci/nucleus and foci size), and Ki-67 proliferation antigen, utilising manual and automated foci (AutoRIF) scoring methods. As expected, 53BP1 foci were significantly induced in mid (5.3 and 6.48 53BP1 foci/nucleus) and late (6.86 and 8.21 foci/nucleus) passage NHBE cells 30 minutes after exposure to 0.3 and 0.5 Gy respectively compared to sham (mid; 1.1 and late; 2.44 foci/nucleus); the elevated numbers of foci in the late passage cells reflect the increased background. By contrast, cells that were cultured beyond this time did not reveal any elevations in foci number and instead a decline was observed at extended times. This may result from cells with persistent DNA damage being removed from the population by apoptosis. AutoRIF analysis also determined that the proportion of medium and large foci in late passage NHBE cells was increased compared to mid passage nuclei, however no IR-induced increase in foci size was seen at late times after exposure. Additionally, approximately 30% of mid-passage NHBE cells were senescent (Ki-67 negative) compared to 64% in late-passage cells, the fractions of which were also not influenced by our single dose exposures.

In conclusion, our preliminary experiments do not show any IR-modifying effects after the single acute doses examined, however the end-points studied and the base-line data generated offer an excellent platform from which to assess the long-term cellular effects of exposure to acute and fractionated exposures of IR in primary NHBE cells.

Declaration

I hereby declare that all of the work presented in this thesis embodies the results of my own work undertaken at Brunel University. Where appropriate I have made acknowledgement of the work of others or referenced work carried out in collaboration with other persons. I understand that as a student of the University I am required to abide by the Regulations of the University.

Rebecca Jane Sabin

BSc Hons

Table of Contents

1 Introduction

1.1 Ionising Radiation

Ionising radiation (IR) is energy that is released from atoms in the form of electromagnetic waves, such as x-rays, gamma rays (γ-rays) or as particles, such as alpha (α), beta (β) and neutron particles and which are of sufficient energy (~>10 electron volts (eV)) to result in the ionisation of an atom or molecule. Such ionisation events are capable of inducing biologically relevant damage including the formation of DNA double strand breaks (DSB) which may result in modifying cellular effects. Other electromagnetic waves including UV-A, UV-B, visible light and microwaves are not energetic enough to detach electrons from atoms and are therefore non-ionising. Different types of IR show different patterns of energy deposition in the form of radiation track structures (Nikjoo *et al*. 1997) and these track structures will determine the spatial deposition of ionisation events and potentially the complexity of damage induced. For example 1 Gray (Gy) of low linear energy transfer (LET; defined as the amount of energy deposited per unit distance) γ-rays corresponds to approximately 1000 electron tracks within a nucleus which on average results in the induction of ~40 double strand breaks (DSB) per cell, of which ~30% can be categorized as complex DSB. Complex DSB are defined as lesions that include two or more individual lesions within one or two turns of helical DNA (Nikjoo *et al*. 1997, Brenner, Ward 1992) and are difficult to repair (Asaithamby, Chen 2011). Compare this to 1 Gy of high LET α-particles that corresponds to ~2 alpha tracks and 40 DSB, of which 70% are complex (Nikjoo *et al*. 1998, Anderson *et al*. 2000) and it is clear to see the differences between induction and repair of damage between differing radiation qualities (Figure 1.1). Thus, in addition to radiation dose, radiation of varying LET will induce a varying spectrum of damage at the molecular, cellular, tissue and organismal levels.

The Sievert (Sv) is a unit that takes the differing relative biological effectiveness (RBE) of different types of IR into account and provides an equivalent radiation dose absorbed by the tissue. The equivalent dose is calculated by multiplying a weighting factor (W_R) by the absorbed dose in Gy, and this weighting factor takes

into account radiation type and energy (ICRP. 2007). For example, α-particles have a W_R of 20 which equates to a 1 Gy absorbed dose providing an equivalent dose in tissues of 20Sv, compared to γ-rays which have a W_R of 1 whereby the equivalent dose (Sv) is equal to the absorbed dose (Gy) (figure 1.1).

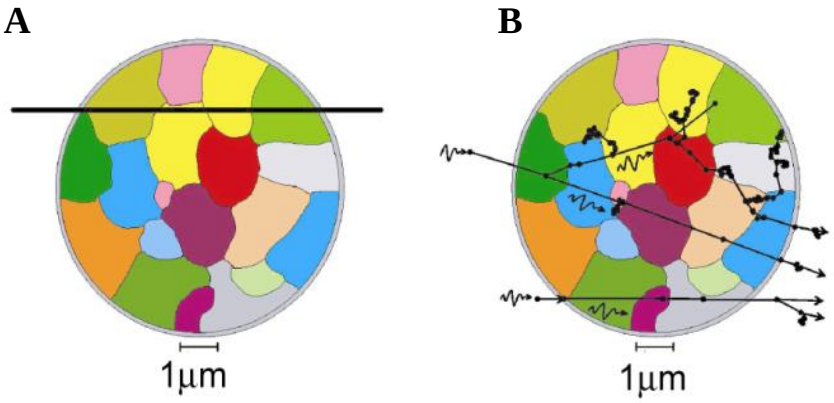

Figure 1.1 Schematic of a transverse section of a peripheral blood lymphocyte (PBL) cell nucleus crossed with high and low LET radiation. Individual chromosome domains are shown in colour, being crossed by an α-particle (A) and electron tracks from two x-ray interactions (B). Courtesy of Anderson RM, Stevens DL and Goodhead DT, 2002 (Anderson, Stevens & Goodhead 2002).

1.1.1 Sources and health effects of ionising radiation

As a population we are continually being exposed to IR from a range sources including the natural radioactive gas, Radon and cosmic and γ-rays. Other sources include radionuclides that are present within the soil, water and air that may be ingested with our food and water. According to the Health Protection Agency (HPA) the average annual exposure to IR in the UK is 2.7 mSv which is mainly made up of background radon exposure from our homes (~1.3 mSv per annum/7.8 mSv in Cornwall per annum), as well as from use of diagnostic procedures such as x-rays (dental = 0.005 mSv, chest = 0.02 mSv) and computed tomography (CT) scans (head = 1.4 mSv, chest = 6.6 mSv, whole body = 10 mSv). It is easy to see how an increase in the use of x-rays and CT scans for diagnostic purposes could quickly increase the annual exposure (Hall, Brenner 2008, Hall, Brenner 2008, Brenner *et al*. 2000). The average annual occupational exposure received by nuclear power station workers is 0.18 mSv with an annual exposure limit of 20 mSv, which is well above the population average (Health Protection Agency 2012). Other sources include acute accidental exposures to

ionising radiation such as those as a result of the explosions at the Fukishima nuclear plant (March 2011), as well as Chernobyl (1986) and Hiroshima (1945).

It has been known for many decades that human exposure to high levels of radiation can cause acute radiation poisoning, cancer and even death. The earliest known radiation-induced cancers were documented in Uranium miners in 1493-1541 in Saxony and a causal link between high dose and low dose residential exposures and lung cancer was made at the beginning of the 20th century (Schuttman 1993, Tirmarche *et al*. 1993, Darby *et al*. 2005, Darby *et al*. 2006, Krewski *et al*. 2006). In striking contrast to a link between domestic radon exposure and lung cancer that has been well documented, evidence of a hormesis effect after low dose IR exposure forms the basis of Radon spa treatments that are still used today to treat a variety of ailments (Franke *et al*. 2000, Gastein's Mountain – Helistollen, 2012).

The lethal dose of radiation that is expected to cause death in 50 percent of exposed individuals (LD50) is ~ 4 Gy (UNSCEAR. 2000) while partial-body or lower dose exposure (<1-2 Gy) will result in acute radiation effects or the promotion of cancers (Asaithamby, Chen 2009). The HPA determine 100 mSv to be the level at which changes in blood cells can be readily observed, although as discussed later, maximum adaptive protection responses have been shown after single tissue doses of 100-200mSv and are absent at higher doses (Feinendegen, Pollycove & Neumann 2009). The effects of exposures to moderate and high levels of ionising radiation are therefore relatively well understood, however the risks or benefits of low (<100 mGy/100mSv of whole body low LET) dose exposures are less understood. As a result of this there is continuing controversy surrounding the shape of the dose-response curve for cancer risk, which according to the current Linear-no-threshold (LNT) extrapolation models are based on the paradigm that cellular effects are due to the direct damaging effects of radiation on DNA (figure 1.2; I). Increasingly, the importance of non-targeted effects (NTE) (1.1.3) for example, genomic instability, bystander effects, the phenomena of persisting inflammation and adaptive/hormesis responses, may be of importance after low dose exposures (UNSCEAR. 2006). Indeed non-cancer diseases including cardiovascular disease have been well documented in Atomic

bomb survivors (Yamada *et al*. 2004b) and as a result the relevance of NTE, especially after low dose exposures are becoming increasingly studied for radiation protection. Interestingly, these effects may increase the complexity of radiation responses and potentially give rise to outcomes that were not previously predictable using standard (LNT) models of cancer risk (HLEG Report. 2009).

1.1.2 The linear no-threshold (LNT) hypothesis

Current radioprotection is based on the LNT model of cancer risk which describes that there is no dose-threshold for excess risk and that dose is directly proportional to risk at low doses (Pearce *et al*. 2012). This model suggests that cellular targets must be 'hit' in order to cause damage, however this has been shown to be contradictory at low doses with some experimental and epidemiological findings suggesting the model may be overestimating or underestimating the risks (ICRP. 2007, UNSCEAR. 2000, Tubiana 2005, NRC (National Research Council). 2006). Of potential importance at low doses are the roles that radiation-related bystander effects, genomic instability and adaptive responses, play in cancer-associated risks. Figure 1.2 highlights the contradicting potential risk responses to low dose exposures below 100 mGy.

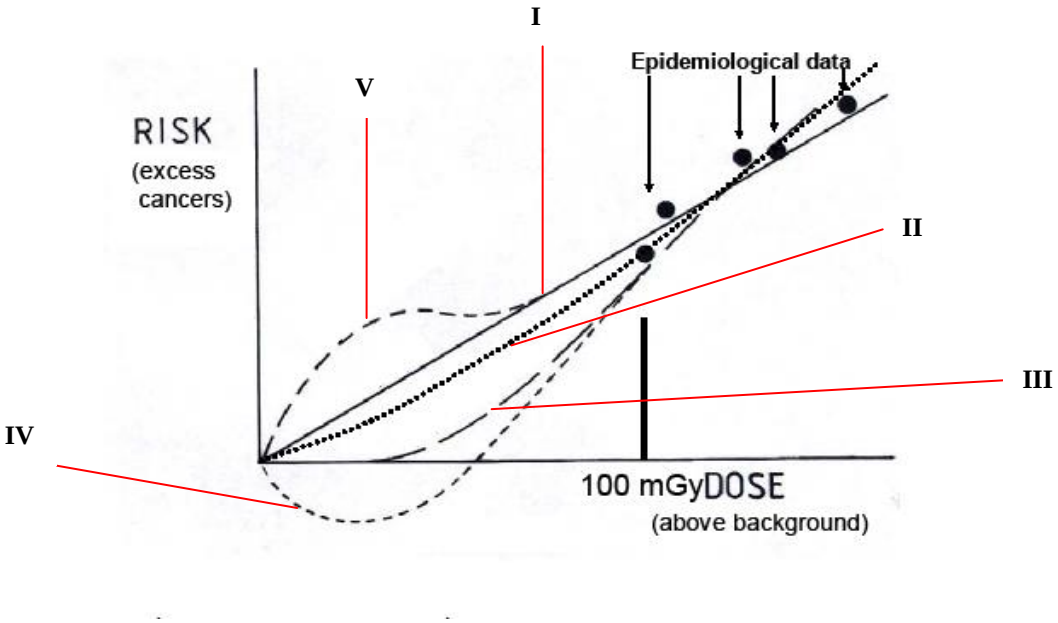

Figure 1.2 Low dose risk extrapolation: Current models for low dose responses (HLEG Report. 2009)**.** I) Linear-no-threshold (LNT); II) Upwardly curving with no threshold; III) Linear or upwardly curving but with a zero-effect interval below a given threshold dose; VI) Bi-modal relationships (beneficial hormesis/adaptive responses); V) Supra-linearity (hypersensitivity at low doses).

1.1.3 Non-targeted effects (NTE)

Non-targeted effects (NTE) or radiation-induced bystander effects (RIBE) describe a whole range of cellular effects that are observed in un-irradiated cells upon communication with irradiated cells. Collectively these factors are known to dominate at low radiation doses, are seen to saturate with increasing dose and mediate a range of cellular effects such as DNA damage (Azzam, de Toledo & Little 2001, Little J *et al*. 2003), cell death (Lyng F, Seymour C & Mothersill C. 2002), cell proliferation, adaptive protective effects and malignant transformation (Nagasawa 1992, Mothersill, Seymour 1997, Lorimore *et al*. 1998, Sawant *et al*. 2001, Dickey *et al*. 2009, Belyakov *et al*. 2005). Many of the experimental systems describing these bystander phenomena have utilised the targeted properties of low fluence high-linear energy transfer (LET) α-particles enabling known fractions (Little *et al*. 1997), or known compartments (Wu, Pandolfi 2001, Wu *et al*. 1999) of cells to be intersected by α-particle tracks. For instance Nagasawa and Little (1992) observed elevated sister chromatid exchanges (SCE) in ~30% of cells after direct exposure of less than 1% of the cell population (Nagasawa, Little 1992), while Wu *et al* (1999) showed an increase in spontaneous mutation frequency after cytoplasmic traversal of defined numbers of α-particles, demonstrating that the target for NTE is greater than the cell nucleus (Wu *et al*. 1999). NTE have also been observed after exposure to low-LET radiations (Law, Wong & Yu 2010). Mothersill and Seymour (1997) found that medium transferred from epithelial cells previously irradiated with low LET γ-rays reduced the clonogenic survival of un-irradiated cells of the same type (Mothersill, Seymour 1997). The authors subsequently utilised this medium transfer model to show that cell-cell contact was not a requirement for NTE but that factors released into the extracellular medium after radiation exposure, mediated the effect (Mothersill, Seymour 1997, Mothersill, Seymour 1998, Seymour, Mothersill 2000, Sokolov 2005, Hamada *et al*. 2007). Contrastingly, adaptive effects have been shown in peripheral blood lymphocytes (PBL), whereby the frequency of chromosome aberrations (CA) was reduced in cells exposed to a priming dose of 3H-Thymidine 48 hours before exposure to 1.5 Gy x-rays, and accordingly after an adaptive dose of 0.1 Gy followed by a 2 Gy challenging dose (Olivieri, Bodycote & Wolff 1984). To date, this bystander

phenomena has also been observed in cells cultured in non-irradiated tumour or senescent cell conditioned medium (Dickey *et al*. 2009, Coppe *et al*. 2008), microbeam-irradiated human tissue (Belyakov *et al*. 2005, Sedelnikova *et al*. 2007) and *in vivo* animal models (Coates, Lorimore & Wright 2004, Coates *et al*. 2008, Ilnytskyy, Koturbash & Kovalchuk 2009). Candidate sources for the mediation of NTE include activated macrophage, nitric oxide (NO), interleukin 6 (IL-6), interleukin 8 (IL-8), interferon-gamma (IFN-γ) and transforming growth factor-beta (TGF-β) (Coates, Lorimore & Wright 2004, Coates *et al*. 2008, Dieriks *et al*. 2010), implicating that there are multiple complex mechanisms involved in the transmission of NTE including oxidative stress and inflammation, whereby inflammation-associated cytokines and chemokines are secreted from irradiated (or otherwise stressed) cells.

1.2 Cellular effects of ionising radiation

1.2.1 The DNA double strand break

Exposure to IR results in a wide spectrum of damage including base damage and single strand breaks, however the most dangerous and critical form of DNA damage is the DSB (Burma *et al*. 2001, Anderson, Henderson & Adachi 2001). Endogenous and exogenous damage alone typically produces approximately 50,000 lesions per cell per day, and therefore cells have developed complex response mechanisms involving over 100 genes that are involved in the response and repair of this cellular damage.

Formation of a DSB is initially sensed by the Mre11-Rad50-Nbs1 (MRN) complex which results in Nijmegen breakage syndrome 1 subunit (NBS1) recruiting the initiating phosphoinositide (PI)-3/4-kinase Ataxia telangiectasia mutated (ATM) bringing it to the site of the DSB. ATM undergoes rapid autophosphorylation which triggers phosphorylation of histone H2AX at serine 139 (γ-H2AX) and the binding of the mediator protein MDC1. This interacts with the MRN complex and tethers it to the site of the DSB within 1-3 minutes (Lee, Paull 2005, Rogakou *et al*. 1998). Further ubiquitinylation and methylation of H2A histones in the vicinity of the DSB results in chromatin modifications that allow access of DNA repair proteins such as tumour suppressor p53 binding protein 1 (53BP1) and breast cancer type 1 susceptibility protein (BRCA1) to the

site, where they form large nuclear domains known as foci (Maser *et al*. 1997, Rogakou *et al*. 1999, Mailand *et al*. 2007, Mailand *et al*. 2007). 53BP1 protein is thought to be a conserved checkpoint protein that also acts as an early sensor of DNA DSBs (Anderson, Henderson & Adachi 2001, Schultz *et al*. 2000b, Rappold *et al*. 2001, Mochan *et al*. 2003). The protein consists of 1972 amino acids, a tudor domain and 2 tandem BRCT domains (Iwabuchi *et al*. 1998) and its gene is located on chromosome 15. 53BP1 identifies with the central binding protein of tumour suppressor p53 and as a result becomes hyperphosphorylated in response to radiation and co-localizes with phosphorylated H2AX at sites of DSB (Ward *et al*. 2003). As well as being dependent on γ-H2AX, localization of 53BP1 has also been shown to be dependent on MDC1 and changes in higher-order chromatin structure (Bekker-Jensen *et al*. 2005, Xie *et al*. 2007, Huyen *et al*. 2004). 53BP1 foci were seen to form independently of ATM at DSB sites after irradiation (Schultz *et al*. 2000a) localizing in discreet nuclear foci at the sites of DSBs within 5-15 minutes in response to IR, peaking at 30 minutes and then declining in number thereafter as a result of cellular repair mechanisms (Schultz *et al*. 2000b).

The sensing of DSB also leads to the phosphorylation of checkpoint proteins CHK1 and CHK2 results in phosphorylation of the tumour suppressor p53, and via up-regulation of the cyclin dependant kinase (cdk) inhibitor p21, p53 inhibits the action of cdk2-kinase activity causing the cell cycle to be arrested in G_1 (Abraham 2002). This allows time for initiation of non-homologous end-joining (NHEJ) or homologous recombination (HR) repair to occur; however if a cell fails to correctly repair DNA damage, apoptosis may be initiated in order to prevent the continuation of mutations and chromosome rearrangements (Paull *et al*. 2000, Shimada, Nakanishi 2006). Alternatively cells may enter a permanent state of arrest known as cellular senescence.

1.3 Cellular Senescence

Cellular senescence is a metabolically active form of irreversible growth arrest that halts the proliferation of ageing and/or damaged cells and as a consequence, prevents the transmission of damage to daughter cells. It is essentially a protective mechanism to prevent neoplastic transformation in cells that may have accumulated unrepaired DNA damage and replication errors as a result of

increasing replication cycles or as a result of the exhaustion of a cell's determined replication capacity. This occurs when normal diploid cells lose their ability for cell division, which irreversibly arrests cellular proliferation. This complicated cellular event is initiated in response to a variety of stimuli (Campisi 2001, Wright, Shay 2001, Ben-Porath, Weinberg 2005) including intrinsic factors, oncogenic damage and intrinsic/extrinsic genotoxic stressors (Davalos *et al*. 2010). It is mediated by tumour suppressor pathways involving p53, and p16INK^{4a}/pRb (Kulju, Lehman 1995, Narita *et al*. 2003) that lead to the inhibition of cyclin-dependant kinases (Mehta *et al*. 2007, Blagosklonny 2003). Accordingly, cellular senescence can be thought of as a tumour suppressor mechanism. Indeed the majority of cancers have mutations in p53 and/or the pRb/p16 pathways, while germ-line mutations in these pathways result in a cell-specific ability to overcome senescence-inducing signals, greatly increasing susceptibility to cellular transformation (Ohtani *et al*. 2004, Gil, Peters 2006, Collins, Sedivy 2003). The importance of senescence as a tumour suppressor mechanism is further demonstrated by evidence that shows senescent cells to have a strong influence over the growth of proliferating cells and cellular oncogenes of tumour cells (Smith, Pereira-Smith 1996). For instance, when proliferating cells were fused with senescent cells, DNA replication was inhibited even in the presence of mitogens, and when senescent cells were fused with tumour cells, DNA replication was similarly inhibited (Yanishevsky, Stein 1980). These findings led to the assumption that senescent cells contained control elements capable of exerting a dominant effect over proliferating pre-senescent cells. Importantly, this tumour suppressive mechanism of cellular senescence has been supported in both mice and human studies (Serrano, Collado 2010). Senescence has also been shown to play an important role in wound healing and tissue repair and/or communication to surrounding tissues/cells of damage crisis to assist healing (Coppe *et al*. 2008, Coppé *et al*. 2010). For example, senescent cells have been shown in *in vivo* mouse models to play a role in the resolution of fibrosis through the action of matrix metalloproteinases (MMPs) after acute liver injury. Under normal conditions, proliferating hepatic stellate cells, triggered in response to acute liver injury, produce fibrotic scars in advance of entering into a senescent state and secretion of MMPs results in dissolution of the scars. However in cells deficient in either p53/pRb pathways, liver injury results in severe, irresolvable

fibrosis (Krizhanovsky *et al*. 2008). Similarly, the matricellular protein CCN1, which is expressed at sites of cutaneous wound repair, has been shown to initiate DNA damage response pathways and reactive-oxygen species-dependent activation of p16INK4A/pRb pathway, resulting in fibroblast senescence and the expression of anti-fibrotic genes in wild-type mice. Mutant mice that express a senescence-defective CCN1 protein show increased fibrosis at sites of wound repair (Jun, Lau 2010). Another primarily beneficial function of senescence is the prevention of epithelial-mesenchymal transition (EMT) and thus prevention of metastatic dissemination of cancerous cells (Evan, d'Adda di Fagagna 2009, Birchmeier, Birchmeier 1995)

Senescent cells may also have an impact on neighbouring non-senescent cells, and tissue function and integrity in ageing, (Stein *et al*. 1999). Senescent fibroblasts cause an inflammatory response through release of cytokines and metalloproteinases that break down the collagen matrix secreted by normal fibroblasts, a mechanism which may contribute further to the ageing of tissues (Bassi, Sacco 2009).

The major phenotype of senescence that characteristically distinguishes senescence from quiescence is irreversible growth arrest associated with resistance to apoptosis and increased sensitivity to cellular injury (Wang 1995, Campisi 2000, Ryu, Oh & Park 2007, Rochette, Brash 2008, Chaturvedi *et al*. 2004, Hampel *et al*. 2004, Labinskyy *et al*. 2006). Other characteristic alterations of senescence include but are not exclusive to, altered gene expression with increased expression of proteins including p53, p16, p19 and p21 (Shelton *et al*. 1999, Kristnamurthy 2006), an increase in senescence-associated beta galactosidase (SA-β-gal) activity at pH 6.0 (Dimri 1995) the presence of persistent telomere and non-telomere DNA damage foci (Herbig *et al*. 2004, Bakkenist *et al*. 2004, Sedelnikova 2004), senescence-associated heterochromatic foci (SAHF) (Narita *et al*. 2003, Kosar *et al*. 2011) and a senescence-associated secretory phenotype (SASP) (Campisi 2005, Kuilman, Peeper 2009). Cellular stains that can be used in addition to SA-β gal include the proliferation cell-cycle specific marker Ki-67 (Bridger, Kill & Lichter 1998, Gerdes *et al*. 1984, Gerdes 1990). Kill *et al* (1996) showed that human dermal fibroblasts (HDFs) were 56% Ki-67 positive at early passage 4 (Kill 1996) compared to only 30% at passage 38

(Bridger *et al*. 2000), with the decrease in fraction of Ki-67 positive cells indicating an increasing fraction of senescent cells within culture.

Morphological changes are also evident in the nuclear structures and nuclear morphology of senescent cells, with senescent fibroblasts showing an enlarged and flattened morphology that is accompanied by loss of elongated, spindle-like properties, when compared to normal proliferating fibroblasts. Mean nuclear area was shown to be 255μm^2 at early passage, compared to 293μm^2 at later passage (Mehta *et al*. 2007). Interestingly, the sub-nuclear organisation of chromosomes has also been shown to be different in senescent and proliferating mammalian somatic cells, whereby gene poor chromosomes such as 13 and 18 are thought to relocate from the nuclear periphery to the nuclear interior, with their radial positioning correlating to their size, instead of gene density (Bridger *et al*. 2000, Meaburn *et al*. 2007). To date though, no unique biological marker has been found, and, consequently, the identification of senescent cells relies on assaying for a combination of the above characteristics.

1.3.1 Stress-induced premature senescence (SIPS)

In contrast to replicative senescence that occurs when a normal cells division capacity is exhausted, stress-induced senescence, also known as premature senescence, culture shock and STASIS (stress or aberrant signalling-induced senescence) (Chen 2004, Serrano 1997, Ramirez *et al*. 2001), also occurs rapidly in response to a variety of intrinsic or extrinsic stressors, including DNA damage from IR and non-IR radiation, cytotoxic DNA damaging agents, oxidative stress, as well as a consequence of oncogenic activation (oncogene-induced senescence) (Ben-Porath, Weinberg 2005, Davalos *et al*. 2010, Blagosklonny 2003, Serrano, Blasco 2001). Serrano *et al* (1997) were among the first to identify a form of SIPS that was not attributable to telomere attrition that they described as oncogene-induced senescence (OIS). The group showed that oncogenic ras expression permanently arrested primary human and rodent cells in G_1, which was accompanied by an accumulation of p53 and p16 and evidence of phenotypic characteristics similar to cells in replicative senescence (Serrano 1997). Further, expression of the catalytic subunit of the telomerase enzyme hTERT has been shown not to abrogate SIPS, demonstrating that cellular senescence can be triggered prematurely independently of telomere attrition. Expression profiles of

p53, p21 and p16INK4A have also been shown to resemble those of replicatively senescent cells (Robles, Adami 1998, Wei, Wei & Sedivy 1999). Thus, stressors that lead to DNA damage but which are independent of loss or dysfunction of telomeres, initiate a response that results in a cellular phenotype indistinct to that observed for replicative senescence (Pazolli, Stewart 2008, Zglinicki *et al*. 2005).

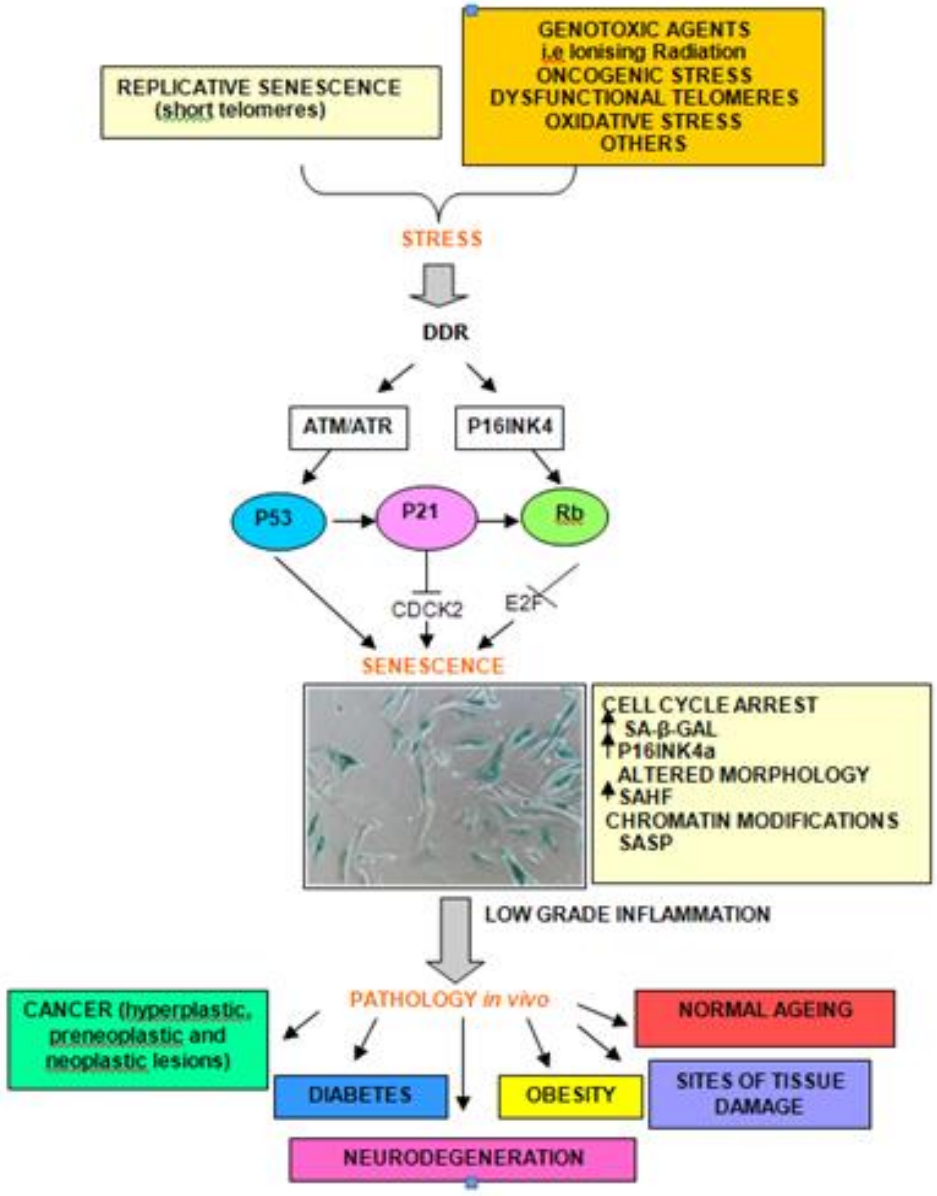

Figure 1.3 Scheme highlighting initiating and molecular mediators of cellular senescence. The senescent phenotype includes expression of SA-β-galactosidase (SA-β-gal), increased expression of p16INK4a leading to cell cycle arrest and an increase in the secretion of pro inflammatory factors termed as senescence-associated secretory phenotype (SASP). Senescent cells have been observed in normal ageing cells and in cells/tissues of various age-related pathologies (Sabin, Anderson 2011). See appendix for journal article.

1.3.2 The molecular pathways of senescence

The initiating event for both replicative senescence and SIPS involves the recognition of DNA damage and activation of the DNA damage response (DDR) pathway (Ben-Porath, Weinberg 2005, Rodier *et al*. 2005, Ben-Porath, Weinberg 2004, Nakamura *et al*. 2008, d'Adda di Fagagna *et al*. 2003, Kastan *et al*. 1992).
Activation of the DNA damage response kinase ATM, a key mediator in the cellular response to ionising radiation, and γ-H2AX foci, have both been shown to increase in both murine and human senescent cells *in vitro* (Nakamura *et al*. 2008, d'Adda di Fagagna *et al*. 2003, Kastan *et al*. 1992).
This activation results in downstream phosphorylation of p53 which leads to up-regulation of the cyclin-dependant kinase inhibitor p21, resulting in inhibition of CDK2 kinase activity and cell cycle arrest in G_1 (Abraham 2002). Stress-induced cellular senescence is thought to depend upon the P16INK4 family of tumour suppressor proteins, activated upstream to pRb and described for its ability to arrest the cell cycle and induce cellular senescence (Gil, Peters 2006, Finkel, Serrano & Blasco 2007). Accordingly, increased P16INK4a expression is another useful marker of senescence *in vitro*, and was detected in ageing baboon fibroblasts along with markers of telomere damage and SAHF (Jeyapalan *et al*. 2007). p21 also activates pRb through the inhibition of E/CDK2 (Campisi 2001). The hypophosphorylated state of pRb results in inhibition of the transcription factor gene E2F and this brings about G_1 cell cycle arrest. For this reason, the p53 and p16/pRB dependent senescent pathways are not completely separable and as well as the common link through p21, pRB has been shown to regulate the activity of MDM2 which acts to control the stability of p53 (Yap *et al*. 1999).

The p53 target of p21 is found to be increasingly expressed during replicative senescence, whilst playing a role in premature senescence in response to DNA damage, oxidative stress or oncogenic over-expression (Zhang 2006). The DNA damage response, senescence and apoptotic pathways therefore share common lineages through p53 and p21. What directs a cell to senesce or apoptose remains unclear, but cell type, the type of damaging agent and the dose administered is thought to be important; as well as the post-translational modifications that p53 undergoes (Webley *et al*. 2000). What is clear is that the convergence of multiple pathways through p53 and pRb are required to maintain the senescent state and

removal of either of these has shown to prevent senescence in mouse embryonic fibroblasts (Dirac, Bernards 2003). In humans, it is thought that both p53 and pRb pathways must be inactivated in order to prevent the onset of cellular senescence (Smogorzewska, de Lange 2002) and accordingly research suggests that 50% of tumours show evidence of mutated/non-functional p53 highlighting its importance in tumour suppression (Kaul *et al*. 2003, Shay, Pereira-Smith & Wright 1991). p53 is also associated with apoptosis of cells that have obtained irreparable damage and it has been found that cells deficient in p53 are unable to arrest cell growth at G_1 in response to γ-radiation, including a reduced ability to apoptose. Interestingly though, senescence has been found to be triggered independently of Rb in humans (Ben-Porath, Weinberg 2005) with activation of p53 and pRb occurring through activation from p19ARF and p16INK4A products from the INK4A locus respectively, and suppression of mitogenic stimuli.

1.3.3 Cellular senescence and age-related pathology

Senescence has also been linked to reduced tissue functionality and is increasingly thought to play a role in age-related pathologies such as cancer, Alzheimer's, diabetes and obesity (Erusalimsky, Kurz 2005, Price *et al*. 2002). Cancer is commonly defined as an age-related pathology with an increasing incidence of carcinomas reported in the older population, namely of the breast, colon, lung and prostate (Wu, Pandolfi 2001, DePinho 2000, Beghe, Balducci 2005, Artandi *et al*. 2000). Senescent cells have been observed in many ageing mice tissues (Wang 1995, Wang *et al*. 2009) baboon skin fibroblasts (Jeyapalan *et al*. 2007) and human tissues (Dimri 1995) indicating that senescence may have a causal role in ageing *in vivo* as well as *in vitro*. Senescent endothelial cells have been shown to increase in atherosclerosis, thrombosis and at sites of inflamed vascular endothelium (Evan, d'Adda di Fagagna 2009, Erusalimsky 2009, Erusalimsky 2009) further to which, the accumulation of senescent haemopoietic stem cells has been suggested as a possible mediator for the decline in tissue regeneration and repair with age. Indeed markers of DNA damage are known to accumulate in ageing stem cells (Chen 2004, Rossi *et al*. 2007, Nijnik *et al*. 2007, Janzen *et al*. 2006). Similarly γ-H2AX foci indicative of DSBs, were seen to accumulate in normal human fibroblasts, WI38 fibroblasts and PrEC prostate epithelial cells with increasing passage that correlated with an increasing fraction of SA-β gal

positive cells (Sedelnikova 2004). Thus it can be suggested that there is a relationship between cellular ageing and the accumulation of residual DNA damage *in vitro* and *in vivo*, however there is no evidence yet to conclusively determine whether senescence is a resultant part of ageing and age-related pathologies or whether it is a state that contributes to the development of ageing tissues and tissue pathology. Interestingly, mouse models of accelerated ageing that are deficient for p16INK4a show delayed onset of age-related phenotypes, highlighting the role of increasing p16INK4a in maintaining the senescent state and its role in age-related decline of tissue regeneration and repair (Baker, Jin & van Deursen 2008). Recently Baker and colleagues showed for the first time that cellular senescence is causally implicated in the generation of age-related phenotypes by the development of a transgenic mouse system that allowed for the inducible removal of p16INK4A positive cells upon administration of a drug that induces FK506-binding-protein-caspase8 activation. Removal of these life-long senescent cells resulted in a delayed onset of age-related pathology of the adipose, skeletal and eye tissue, and although it did not result in an increased lifespan, an increased 'health span' was observed in the mice (Baker *et al*. 2011). More studies are needed to determine what the effect would be on life-long removal of these cells as they are known to have beneficial effects as described above, however this is an important development that will hopefully decipher the evidential link between increasing populations of senescent cells/tissues and the contribution they have in the development of age-related pathologies such as cancer, through tissue damage and persistent inflammation (Sikora *et al*. 2011, Vijg, Campisi 2008).

1.3.4 Senescence-associated secretory phenotype

Senescent cells have been shown to secrete factors such as interleukins, chemokines, growth factors and proteases which encompass what is known as a senescence-associated secretory phenotype (SASP) (Coppé *et al*. 2010, Campisi 2005, Freund *et al*. 2010). SASP is thought to mediate growth arrest via the autocrine activities of pro-inflammatory cytokines (IL-6 and IL-8), as well as pro-apoptotic protein insulin growth-factor binding protein 7 (IGFBP7), epithelial growth factors (heregulin and VEGF), matrix metalloproteinases including MMP-3 and plasminogen activator inhibitor 1 (PAI-1) (Acosta *et al*. 2008, Wajapeyee *et*

al. 2008, Kortlever, Higgins & Bernards 2006). Although SASP remains to be fully characterised, it is known to influence the proliferation of neighbouring cells and disrupt tissue architecture (Parrinello *et al*. 2005), principally through pro-inflammatory influences. For instance, an increase in VEGF has been seen in human and mouse fibroblasts, stimulating tumour vascularisation and invasion of basement membranes as a result of senescent fibroblasts stimulation (Coppé *et al*. 2006). Indeed the name 'senescence-messaging secretome' (SMS) was proposed to highlight that the associated factors of the secretory phenotype were not only essential for the maintenance of the senescent state, but that they also possessed communicative functions mediated by autocrine and paracrine signals (Kuilman *et al*. 2008, Kuilman *et al*. 2010). A study to highlight this communication showed that re-activation of endogenous p53 in p53-deficient tumours in a mosaic mouse model of hepatocellular carcinoma led to tumour regression. This was proposed to occur through the induction of cellular senescence and up-regulation of inflammatory cytokines, triggering an innate immune response *in vivo* that ultimately led to tumour clearance (Xue *et al*. 2007). Thus, inflammatory cytokines are highlighted in the establishment and maintenance of senescence, suggesting an essential function of the SASP/SMS products in the suppression of malignancy (Acosta *et al*. 2008, Kuilman *et al*. 2008). Several *in vivo* and *in vitro* studies have indicated that senescent cells can actually promote the progression of malignancy; a relationship that is described as antagonistically pleiotrophic (Campisi 2000, Coppé *et al*. 2006, Yeager *et al*. 1998, Reddel 2000, Campisi, d'Adda di Fagagna 2007, Campisi 2007). For instance, senescent human fibroblasts have been shown to stimulate pre-malignant and malignant fibroblasts to hyperproliferate and form tumours in mouse models when senescent cells comprised ~10% of the fibroblast population (Krtolica *et al*. 2001). Close proximity of senescent fibroblasts to pre-neoplastic cells are thought to be the trigger for this change. Additionally, after exposure to the DNA-damaging agent bleomycin, human SIPS fibroblasts co-transplanted into xenografts of immunodeficient mice were also seen to stimulate nearby cancer cells to proliferate, either directly or through local tissue damage and inflammation mediated by MMPs (Liu, Hornsby 2007). Inflammation is thought of as a key mediator in cancer development and inflammatory cytokines and MMPs are being increasingly implicated as a contributing factor in this multistep process.

Alteration of the tissue microenvironment and promotion of epithelial cell growth as a consequence of the senescent phenotype, through inflammation, persistent tissue damage, cellular proliferation, angiogenesis and cell motility (Davalos *et al*. 2010, Coppé *et al*. 2010, Bassi, Sacco 2009) may thereby provide a mechanism that may contribute to cancer promoting effects in ageing tissues (Krtolica, Campisi 2002). Models that assess the effects of senescent cells on nearby pre-neoplastic or neoplastic cancer cells therefore support the theory that senescence is antagonistically pleiotrophic; being thought to protect young animals from cancer by mechanisms of tumour suppression, whilst contributing to deleterious effects in aged organisms through persistent inflammation and tissue injury (Bassi, Sacco 2009, Krtolica *et al*. 2001).

1.3.5 Relationship between senescence and ionising radiation

Ionising radiation has been shown to induce a SIPS phenotype instead of apoptosis in fibroblasts both *in vitro* and *in vivo* after exposure to high and low levels of damage, with cells showing a preference towards entering premature cellular senescence as a result of small levels of cellular damage (Suzuki *et al*. 2001, Tsai *et al*. 2005, Tsai *et al*. 2009). In normal cells with intact signalling pathways, senescence, in place of apoptosis has shown to be the more favourable route after low levels of DNA damage, perhaps as the cell makes the decision to attempt to repair instead of removing the cell (Ben-Porath, Weinberg 2005). The status of the tumour suppressor phosphate and tensin homolog (PTEN) was shown to affect the cellular response of glioma cells with PTEN-deficient cells seen to enter senescence, and PTEN-proficient cells seen to enter apoptosis in response to ionising radiation exposure. It was therefore determined in this instance that premature senescence was a compensatory mechanism in the place of apoptosis in the absence of the PTEN tumour suppressor (Lee *et al*. 2010). By contrast, adult human dental pulp stem cells (DPSCs) were found to enter premature senescence in the G_2 phase of the cell cycle after exposure to high doses (2-20 Gy) of ionising radiation, as detectable by SA-β-gal activity, phosphorylated p53 and increased p16 expression. The increased p16 expression was observed for the experimental period of 13 days, coinciding with SA-β-gal activity at day 3 after irradiation, demonstrating the induction of a premature senescent state in response to ionising

radiation exposure and highlighting the complexities of damage response phenomena (Muthna *et al*. 2010). It has been noted that some cell types have delayed onset of senescence upon inactivation of p16 only, whereas others require a deficiency in p53, or both in order to abrogate senescence, This pathway abrogation in turn allows a cancer to develop more invasive features and undergo metastatic dissemination (Ansieau *et al*. 2008).

In addition to this, immunological ageing or immunosenescence is known to result in decreased cellular proliferation, increased resistance to apoptosis and alterations in the T-cell balance (Spaulding, Guo & Effros 1999, De Martinis *et al*. 2007, Giovannetti *et al*. 2008). Interesting observations in human and animal studies show that a correlation exists between the immunological imbalances caused as a result of exposure to ionising radiation and, those effects which are seen in normal aged immune cells, implying ionising radiation may accelerate immunological ageing (Park, Jo 2011). For instance, the normal age-related decrease of total $CD4^+$ T-cells was found to be ~4% per 10 years, compared to a radiation-induced decrease of ~2% Gy^{-1}, equivalent to a 5 year age increase per 1 Gy (Kusunoki *et al*. 2010, Kusunoki *et al*. 1998). This group also demonstrated a dose-dependent increase in $CD25^+/CD127^-$ regulatory T-cells and attributed T-cell immunosenescence to a higher level of inflammatory markers in Atomic bomb survivors. For instance, changes in the immunological profiles of cytokines, known to be involved in the coordination of the inflammatory response (tumour necrosis factor –alpha (TNF-α), IFN-γ, IL-6 and IL-10), are seen in both Atomic bomb survivors and liquidators which may contribute to the persistent subclinical inflammatory status that is seen in these individuals (Hayashi *et al*. 2003, Hayashi *et al*. 2005, Kusunoki *et al*. 2003, Nakachi *et al*. 2004). Therefore radiation-induced enhancement of inflammatory reactions may contribute to the development of radiation-induced disorders and premature ageing (Kusunoki *et al*. 2010, Yamada *et al*. 2004a). Indeed, it is also well known that Atomic bomb survivor's show increased cardiovascular and respiratory diseases associated with persistent inflammation (Van der Meeren *et al*. 2008, Neriishi 2001, Lehnert, Goodwin 1997, Rubin *et al*. 1995, Yentrapalli *et al*. 2013). The potential role of senescent cells in the mediation of NTE (e.g. via SASP) as discussed in section 1.3.4, the relevance of exposure to radiation in the initiation of SIPS, and the long

term tissue damage and pathological alterations that may arise as a consequence remain to be elucidated (Nagasawa 1992).

1.3.6 The lungs as a target for Ionising Radiation exposure

The biology of radiation-induced lung cancers is becoming of increasing importance and a causal link between domestic exposure to Radon gas and small cell lung carcinoma (SCLC) has been well documented (Darby *et al*., 2005). The main target tissue for inhaled radon gas is the lungs and bronchioles and therefore this highlights the relevance of studying radiation effects in an important target organ.

The normal human bronchial epithelium is composed of specialised epithelia cell types including ciliated columnar epithelium, mucous-secreting goblet cells (non-ciliated secretory columnar cells) and the smaller more predominant basal cells, as well as the presence of immune and inflammatory cells that assist and aid epithelial cell function (Knight, Holgate, 2003). These basal cells are thought to be undifferentiated epithelial cells that make up the progenitor population of the cells and have the ability to differentiate into both ciliated and goblet cells in culture (Fig 3.1) (Vaughan *et al*. 2006). Differentiation of these normal human bronchial epithelial cells (NHBE) by culturing at the air liquid interface (ALI) which effectively mimics a more *in vivo* environment (Danahay *et al*. 2002, Sedelnikova *et al*. 2007) results in the formation of ciliated-columnar epithelial cells and mucous-secreting goblet cells, which can be detected by β-tubulin IV and mucin respectively (Vaughan *et al*. 2006). This technique is therefore widely used to allow better representation of an in vivo environment and represents and provides a focus for future work in this study.

1.4 Aims and objectives

The aim of this project is to understand and assess the early and late effects of ionising radiation (IR) in primary human bronchial epithelial cell models after exposure to low-moderate doses. Specifically we aim to determine IR effects on DNA damage and cellular senescence. Beyond this, we aim to determine inflammatory responses, and whether initiation of a premature stress-induced cellular senescence phenotype may amplify radiation-induced effects at extended times after low dose exposures.

2 Materials and Methods

2.1 Preparation of cell culture environment

All cell culture work and preparation for experimental work was performed using aseptic techniques within the University cell culture suite using a Class II HeraSafe Laminar flow hood to maintain the sterility of cultures and of the equipment used. All bio-hazardous waste including cell culture medium and equipment was decontaminated in Virkon disinfectant overnight prior disposal and autoclaving for sterility. Disposal of all reagents was undertaken according to risk assessment and COSHH forms.

2.2 Cell Culture

Four different cell types were used; AGO1522 and 1HD (human dermal fibroblasts) and MCF-7 cells (human breast adenocarcinoma cell line) were used in method development, while primary human bronchial epithelial (NHBE) cells were the model cell type used for the majority of the experimental procedures. All 4 cell types grew as adherent cultures on plastic dishes/flasks (NUNC).

2.2.1 Cell Types

2.2.1.1 Primary Normal Human Bronchial Epithelial Cells (NHBE)

Primary normal human bronchial epithelial (NHBE) cells were obtained from Lonza, Clonetics® frozen in cryovials at passage (P) 1. These NHBE cells are directly obtained from explants derived from areas of bronchial tissue distant from any pathology; these cells were assigned as P2 once they were reintroduced back into culture (2.2.2). Frozen cells were thawed rapidly by warming the cryovials to 37°C and diluted into an appropriate volume of specialized bronchial epithelial growth medium (BEGM) detailed in section 2.2.3.1. The cells were passaged continually from this point in order to cryopreserve cells at each subsequent passage for future stocks until the population ceased to maintain normal exponential growth (~P11) or morphological changes suggested differentiation. In order to maintain viability and steady growth, NHBE cells were seeded at approximately 3500 cells/cm^2 (2.62 x 10^5 cells in a T75 flask) and were passaged once they reached no more than ~85% confluence. This initial seeding density was increased as the cells reached later passages to ensure viability was maintained.

Details of the NHBE cell donors are shown in table 2.1, with Donor 2 being a 52 year old Hispanic female, and Donor 3 a 43 year old Caucasian male. All experimental work was carried out using donor 3 NHBE, unless otherwise stated in which case, donor 2 cells were used.

According to the manufacturer's guidelines, all primary cells from Lonza have been tested and are negative for HIV-1, mycoplasmas, Hepatitis B and C, bacteria, yeast and fungal infections

Table 2.1 Lonza NHBE cell donor information

Donor Lot No	Age	Sex	Race	Cell passage	Cell count (cell/ml)	Doubling time (hours)	Total population doublings
4F1624 (Donor 2)	52	Female	Hispanic	1	572500	19	18
6F4180 (Donor 3)	43	Male	Caucasian	1	665000	25	15

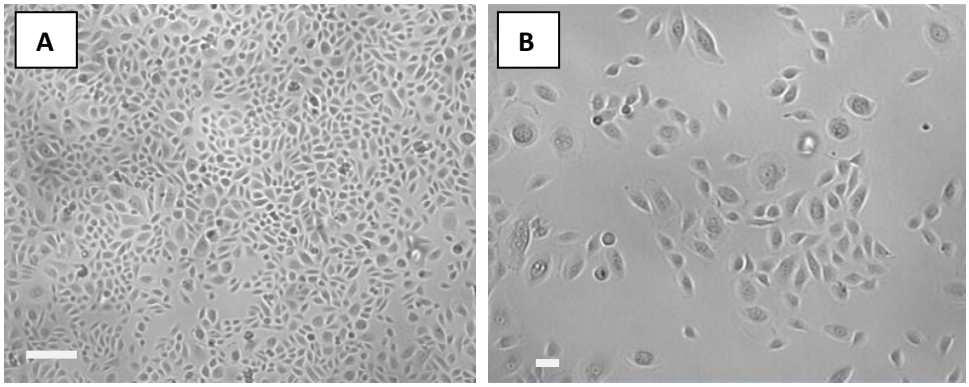

Figure 2.1 Phase contrast images of P4-P5 NHBE cell morphology in culture.

Images acquired using JuLi Cell Analyser microscope (Montreal Biotech) with a 4x objective and 10x digital zoom. A stage graticule was used to identify the pixel aspect ratio of 0.746 pixels/µm. Scales bars represent 100µm (A) and 25µm (B).

Three different cell types are present in the NHBE population; mucus secreting goblet cells, columnar epithelial cells and basal cells. The normal morphology of these cells in culture show approximately 30% to be goblet cells and the predominating epithelial types to be basal and then columnar cells respectively.

2.2.1.2 Human Dermal Fibroblasts 1HD/AGO1522

The human dermal fibroblasts used in this study were initially derived from juvenile foreskin by Dr Bridger (1998), and termed 1HD (Bridger *et al*. 1998); or

normal human skin fibroblasts (AGO1522) were obtained from Coriell Cell Repositories.

1HD/AGO1522 cells were thawed as described in section 2.2.2 to 37°C, before placement into 20mls of pre-warmed Dulbecco's modified eagle medium (DMEM; 2.2.3.2) in a T75 culture flask. Cells were maintained in 20mls of medium until cells were 85-90% confluent and passaged as described (section 2.2.5). 1HD/AGO1522 dermal fibroblasts were seeded at a density of 1-5 x 10^5 cells per T75 flask depending on the rate of growth required.

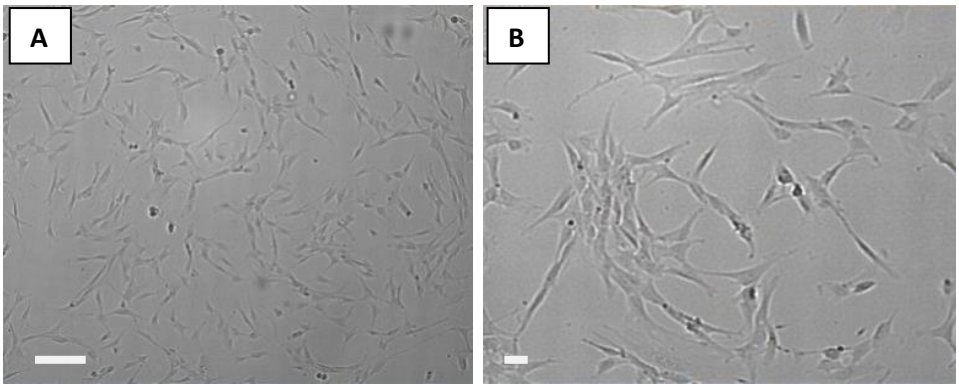

Figure 2.2 Phase contrast images of P20 AGO1522 dermal fibroblasts.
Images taken with JuLi Cell Analyser.

2.2.1.3 Human breast adenocarcinoma cell line MCF-7

A cryovial of the human breast adenocarcinoma cell line, MCF-7 (P215) was kindly donated for use courtesy of Dr Mariann Rand-Weaver. The MCF-7 cell line was originally isolated from the breast tissue of 69 year old Caucasian woman in the 1970's and was assigned as MCF-7 after the Michigan Cancer Foundation-7 where the cell line was first established (Soule *et al*. 1973). The donated cryovial was thawed quickly to 37°C as in 2.2.2 and seeded into a T75 flask with 15mls pre-warmed DMEM/F12(1:1)1X medium (section 2.2.3.3). For maintenance of MCF-7 cells, a seeding density of ~1 x 10^5 cells took approximately 1 week grow to confluence and medium was replenished every 3-4 days.

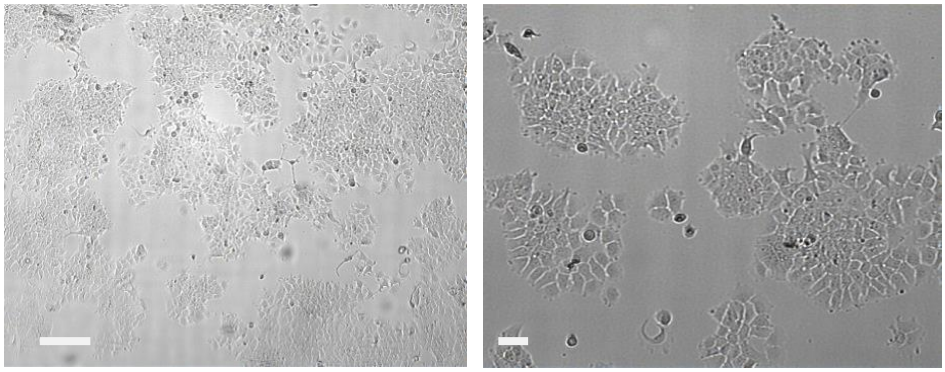

Figure 2.3 Phase contrast images of MCF-7 cell line.

2.2.2 Recovery of cryopreserved cells

Cryovials were quickly removed from liquid nitrogen storage and thawed to 37°C before being introduced into the appropriate volume and type of pre-warmed medium needed for each cell type, and gently mixed. Cells were then left to adhere overnight/24 hours (T75 flasks were used unless otherwise stated) before the medium was changed to remove any residual dimethyl sulphoxide (DMSO) which had been used to previously cryopreserve the cells (2.2.7).

2.2.3 Maintenance of cells in culture

2.2.3.1 Human Bronchial Epithelial Cells (NHBE)

NHBE cells were maintained in specialised serum-free BEGM medium and defined supplements (Lonza Clonetics®, BEGM® Singlequots® bulletkits). 500ml bottles of BEGM were prepared (shelf life of approximately 3-4 weeks at 4°C) by the addition of singlequots supplements containing: 0.2% bovine pituitary extract (BPE), 0.1% insulin, 0.1% hydrocortisone, 0.1% gentamycin sulphate and amphotericin-B (GA), 0.1% retinoic acid (RA), 0.1% transferrin, 0.1% triiodo-L-thyronine, 0.1% epinephrine and 0.1% human recombinant epidermal growth factor in buffered bovine serum albumin saline solution (rhEGF). BEGM medium was changed one day after seeding and then every other day to maintain viability.

NHBE cells were passaged according to section 2.2.5 when they reached no more than 85% confluency as they become irreversibly contact-inhibited when grown to confluence. The specialised subculturing reagents including HEPES buffered saline solution, Trypsin/EDTA and Trypsin neutralising solution (Lonza ReagentPack™) were used throughout.

In addition, passage 8 NHBE cells were also cultured with a pre-prepared supplemented, serum-free basal medium (LHC-9 1X) from GIBCO for a period of

13 days alongside normal cell culture in Lonza BEBM medium. It was noted that NHBE cells cultured in the GIBCO medium were morphologically different after 1 passage, and although the majority of the cells continued to represent small basal cells, there was an increasing number of long, spindly (fibroblast-like) cells seen which were never present during BEGM culture. The presence of these morphologically abnormal cells within the NHBE culture was also coupled with an increased time to reach the desired confluence to passage, and lower cell counts per ml than seen in the NHBE cells grown in Lonza medium, and increased floating dead cells within the culture. As a result of this, it was decided to halt the culture of the cells in the GIBCO medium and dispose of the flasks. All cell culture of NHBE cells was continued using BEBM.

2.2.3.2 Human dermal fibroblasts

Normal human dermal fibroblasts were maintained in Dulbecco's Modified Eagle Medium (DMEM), with phenyl red indicator and without l-glutamine; or low glucose DMEM, with GlutaMAX™, all supplied by GIBCO®, Invitrogen. In order to maintain stable concentrations of L-glutamine in culture, GlutaMAX™ supplements (200mM L-alanyl-L-glutamine dipeptide in 0.85% NaCI) and medium were used as an alternative to L-Glutamine which breaks down quickly in culture to form ammonia. Complete DMEM medium was made up with 10-15% fetal bovine serum (FBS), 1% penicillin/streptomycin, and 1% l-glutamine (or 1% GlutaMAX in non-supplemented media).

2.2.3.3 Human breast adenocarcinoma cell line MCF-7

MCF-7 cells were maintained in Dulbecco's modified eagle medium/Hams F12 (1:1) 1X supplemented with 10-15%FBS, P/S and L-glutamine/Glutamax. DMEM without phenol red was used as this can act as a weak oestrogen and may affect the proliferation of the oestrogen-receptor positive control cell line (Berthois, Katzenellenbogen & Katzenellenbogen 1986).

2.2.4 Seeding Density

In order to ensure normal growth of cells as a monolayer, as stated in section 2.2.1.1, NHBE cells were seeded at a density of approximately 3500 cells/cm^2, and 1HD/AGO1522 and MCF-7 cells on average between 1333-3500 cells/cm^2.

A range of vessel sizes were used for experiments. The seeding density of NHBE cells was also increased when a higher passage was reached or to accommodate for cell death during extended culture after exposure to ionising radiation.

To calculate the volume (ml), of cell suspension needed for each flask to obtain the correct cell concentration per ml, the following equation was used:

$$\frac{\text{Total cells needed per flask}}{\text{Desired seeding density}} = \text{Volume (ml) needed per flask}$$

2.2.5 Harvesting Cells

The old culture medium was removed and discarded into a beaker of Virkon disinfectant and the cell sheet washed twice with 10mls of Versene (0.197g EDTA per 1L of phosphate buffered saline [PBS]), being careful at all times not to touch the cell sheet with the pipette tips or to cause too much mechanical disruption to the cells. For NHBE cells, the cell sheet was washed twice with 5-10mls of HEPES-BSS (Lonza Clonetics®), and discarded. It was important that these wash steps were not missed as the medium contains complex proteins and calcium that can neutralise and reduce the efficiency of the trypsin enzyme. To enzymatically hydrolyse the connective proteins and dissociate adherent cells, 2-3ml of a porcine trypsin 1X working solution or 2-3ml of the recombinant fungal trypsin-like serine protease TrypLE™ Express (GIBCO, Invitrogen) was added to fibroblast and MCF-7 cells. NHBE cells were dissociated specifically with 2-3 ml of Trypsin/EDTA (NHBE) (Lonza Reagent Pack™) per flask. Flasks were incubated at 37°C (5% CO_2) for 2-5 minutes and checked under phase contrast until 90% of the cells had rounded up. The trypsin/TrypLE Express activity was neutralized with 4-6mls of DMEM with 10% FBS (2.2.3) for fibroblast/MCF-7 cultures (TrypLE Express does not require deactivation with trypsin inhibitors), or 4-6mls of Trypsin neutralizing solution (TNS, soybean derivative) (Lonza Reagent Pack™) for NHBE cultures. The cell suspension was then pelleted by centrifugation for 5 minutes at 1100rm (NHBE) and 10 minutes at 1200 for other cultures, before removal of the supernatant. The cell pellets were then re-suspended in a total of 1ml of fresh complete DMEM or BEBM medium for cell counting (section 2.2.6).

2.2.6 Cell Counts

A 20µl aliquot of cell suspension was added to 20µl of Trypan blue (GIBCO, Invitrogen) gently mixed and added to a haemocytometer chamber for counting. Viable cells were counted in 4 of the large squares and the average multiplied by the dilution factor of trypan blue (1:2) and by a conversion factor of 10^4 ($0.1mm^3$ volume) or 5000 ($0.2mm^3$ volume) to give the total number of cells per ml.

Where possible, the percentage of viable cells was calculated by dividing the number of viable cells per ml by the total number of cells per ml (dead and alive), and multiplying by 100.

According to the derived cell count, the volume of cell suspension required per new culture flask was calculated by:

$$\frac{\text{No. of cells needed}}{\text{Total number of cells/ml}} = \text{volume (ml) per flask to obtain required seeding density.}$$

2.2.7 Cryopreservation of cells

Cells were prepared for cryopreservation after harvesting as described in section 2.2.5 in sterile freezing cryovials at approximately $5 \times 10^5 – 1.5 \times 10^6$ cells per vial. Cell pellets were re-suspended in fresh medium and the required volumes of cell suspension made up to 1ml with 10% DMSO. The freezing mix of DMSO and fresh medium was left to sufficiently cool before addition of the cell suspension in order to reduce the cell damaging exothermic effects of DMSO that occur above room temperature. Cryovials were immediately stored at -80°C for 24 hours before being transferred to liquid nitrogen (-179°C) for permanent storage.

2.2.8 Observations

Regular observations were made of the cells in culture, especially for the more fragile NHBE cells, including cell morphology and % confluency to ensure cells were harvested at the correct time. It was also essential to ensure that the cultures remained free of infectious agents such as bacteria/fungus by microscopic examination of the medium and cells. The epithelial characteristics of NHBE and the predominance of large ‘fried egg’ goblet cells within the culture were both

noted as the occurrence of the latter increase within the ageing cultures or as a potential sign of differentiation.

2.3 Cell-based Experimental Protocols

2.3.1 Optimisation of senescence-associated beta galactosidase (SA-β gal) assay

Positive controls

Determination of an appropriate positive control was performed using MCF-7 breast adenocarcinoma cell line/AGO1522 and 1HD dermal fibroblasts. According to manufacturer recommendations, MCF-7 cells were treated with a sub-lethal dose of the topoisomerase II inhibitor Etoposide (Ascent Scientific) to induce premature senescence. Further optimisations were carried out using sub-lethal doses of ethanol and hydrogen peroxide and the most effective method chosen.

Etoposide treatment

Old medium was discarded from sub-confluent culture wells of either MCF-7 or AGO1522/1HD dermal fibroblasts prior to treatment for 24 hours in 12.5μM Etoposide (2.5μl of 50mM Etoposide stock in DMSO, per 10 mls of medium). Etoposide medium was then removed carefully from wells and the cells washed twice with PBS, before adding fresh medium and cell recovery allowed for 4-5 days. Medium was replenished every 2 days and non-treated cells were trypsinised into a larger flask if necessary. Cells were then fixed and stained according to the SA-β-gal chromogenic assay (section 2.3.1.1). Use of MCF-7 cells as a positive control for SA-β gal staining after etoposide treatment was not optimised due to the growth characteristics of the cells which resulted in subjective uniform staining.

Ethanol treatment

Sub-confluent cells were treated with 2-3 mls of 5% ethanol/DMEM mix for 2 hours. Treatment medium was removed and cells washed twice with PBS before addition of fresh medium. This treatment was repeated everyday for a 5 day period, prior to staining.

Hydrogen peroxide treatment

Sub-confluent cells were treated with 2-3 mls (per 35mm dish) of 150μM H_2O_2/DMEM medium mix for 2 hours. After two PBS washes, medium was replenished and cells allowed to recover for 3-4 days.

2.3.1.2 Cytochemical detection of SA-β gal

Senescence β-galactosidase staining kit was sourced from Cell signalling Technology (BioLabs, UK) to stain for β-galactosidase activity at pH 6.0 in senescent cells. The kit includes 10X fixative solution (20% formaldehyde, 2% gluteraldehyde in 10X PBS); X-gal powder (5-bromo-4-chloro-3-indoyly-β-D-galactopyranoside, 20X, 20mg), which can be stored at -20°C in a light resistant container for 1 month as an X-gal in N-N-dimethlyformamide stock; 10X Staining solution (400mM Citric acid/sodium phosphate, at pH 6.0, 1.5 M NaCl, 20mM $MgCl_2$); 100X staining solution supplement A (500mM potassium ferrocyanide) and 100X staining solution supplement B (500mM potassium ferricyanide). Whilst protected from direct light, the growth medium was removed from wells (all volumes given are for 35mm dishes) the cell sheets washed once gently with PBS and then fixed with 1ml of 1X fixative solution (10X diluted in distilled water) for 10-15 minutes at room temperature. 930μl of 1X staining solution (10X previously diluted with distilled water), 10μl of supplement A, 10μl of supplement B and 50μl 20mg/ml X-gal in DMF were made up to pH 6.0. The 1X Fixative solution was removed from the wells and washed three times with PBS. 1ml of the prepared staining solution at pH 6.0 was added to each well and incubated overnight (staining maximal after 12-16 hours) at 37°C without CO_2 and after incubation the cell sheets were washed three times with PBS. Stained cell sheets were then washed briefly with methanol and allowed to air dry in the dark which enables dried slides to be kept for several months protected from the light. The cells were then checked at 200X magnification for a blue precipitate using a light microscope and the percentage of SA-β gal positive cells was determined in at least 4-5 fields of view/or 200-400 cells (Positive SA-β-gal cells scored/total counted = % of positive SA-β-gal cells). Positive control etoposide treated cells were stained at the same time as normal cells for each experiment.

2.3.2 Irradiation Protocols

2.3.2.1 Preparation of cells for irradiation

Glass microscope slides (Menzel) or coverslips were labelled with pencil for identification and then acid washed with gentle agitation in a 1:10 volume of HCl:dH_2O for 30 minutes, then rinsed with sterile dH_2O before being transferred to 100% Methanol at 4°C until needed. Slides were flamed for sterilization before placement into quadriPERM® dishes (Sigma) or culture dishes/flasks, prepared with 1 ml of warm medium in advance of seeding 8-8.4 x 10^4 cells per slide (maintaining a seeding density of 3333-3500cells/cm^2). Where necessary to maintain cells in culture after IR for longer than one subculture, NHBE cells were also seeded into separate T25 flasks for IR at the seeding density described above, with subsequent dishes/slides prepared from these flasks according to the experiment endpoints required. 5-7 ml of BEBM or complete DMEM (see section 2.2.3), was added to each slide compartment/flask and quadriPERMs were incubated at 37°C in 5% CO_2 for 2-3 days until cells reached 60-80% confluency for irradiation. Medium was refreshed in accordance with 2.2.3.1 and 2.2.3.2. QuadriPERMs, flasks and dishes were prepared separately for shams and each dose, however all conditions were kept the same except that the sham slides were not exposed at the source.

Prior to irradiation of prepared culture vessels, cell confluency was checked under the microscope to ensure that growth was sufficient, including allowance of a degree of cell death that may occur after exposure (dose-dependent).

QuadriPERM dishes and prepared flasks were placed into thermally insulated boxes containing heat packs, and taken down to the relevant irradiation source. Sham slides were always transported with and treated in exactly the same way as the irradiated slides; however they were not irradiated at the source. When possible, a non-gassed 37°C incubator setup in position to keep the cells warm during radiation exposure was used. This was to further reduce the shock/stress of low temperatures in the cells during transportation to and during treatment in the irradiation suite.

2.3.2.2 Low LET Gamma Exposure

Cells were exposed to low-linear energy-transfer (LET) Cobalt-^{60} gamma rays using either the higher activity Co-60 source site (nomimal activity on 24th June 1999=1.9KCi,/70.3 TBq) or the lower activity cobalt-60 source (nominal activity on 27 Jan 2000 = 29.9 Ci/106 GBq) within Brunel University. Half-life ($t_{1/2}$) = 63.24 months. The irradiation source that was used for individual exposures was dependent on the total dose required. The higher activity Co-^{60} was used for exposures between 1-2 Gy (0.0933-0.0944 Gy/min dose rate) and the lower activity Co-^{60} was used for all exposures below 0.5 Gy thus far (0.101-0.111 Gy/min dose rates). The dose rate that all cells were exposed at was as kept as consistent between the two sources. Dose rate, distance from source and exposure times were calculated using a Cobalt-60 Higher or lower activity chart, and dosimetry measurements for low dose exposures were performed by Dr Mark Hill and colleagues (Oxford University). T0 was noted at the time of exposure and irradiated and sham vessels were quickly transferred back to the laboratory and incubated at 37°C in 5% CO_2 for the desired experimental incubation time (30minutes – 33 days, see results for specific experimental details and fixation times) prior to fixation with paraformaldehyde (PFA).

2.4 Immunofluorescent Antibody Staining

2.4.1 Fixation of cells

The cell culture medium was removed and slides were gently washed three times with PBS then fixed by incubation with 4% paraformaldehyde (PFA) for 5-10 minutes at room temperature (RT). The slides further washed 3 times with PBS to remove the PFA, and then transferred to a 50ml tube containing fresh PBS and refrigerated at 4°C until needed for antibody staining.

2.4.2 Permeabilisation of cells

To enable penetration of the antibodies to the intra-cellular environment, cells were permeabilised by incubating with 0.5% Triton X-100 detergent in PBS for 5 minutes at 4°C, followed by three times washes with cold PBS.

2.4.3 Antibody staining

To detect the recruitment of the 53BP1 protein at sites of DNA double strand breaks a mouse anti-human 53BP1 antibody (Clone 19, BD Biosciences) and a secondary goat anti-mouse IgG tagged with the fluorophore Alexafluor568 was used. In addition to incubation with antibodies against 53BP1 proteins, antibodies against a carboxyl terminal segment of Ki-67, a proliferative marker, were sourced. A primary polyclonal rabbit anti-human Ki-67 antibody (Nova Castra) and a secondary goat anti-rabbit IgG tagged with a fluorescin (FITC) (Invitrogen) were used. Antibody containing tubes were centrifuged for 3-6 seconds prior to aliquoting to ensure that any aggregates had been spun down.

Table 2.2 Antibodies used for immunofluorescence

PRIMARY				
Raised in	**To**	**Conjugate**	**Optimal Dilution**	**Antibody against**
Rabbit	Ki-67	-	1:1500	Ki-67
Mouse	53BP1	-	1:200	53BP1
SECONDARY				
Goat	Mouse	AF568	1:200	53BP1
Goat	Rabbit	FITC	1:200	Ki-67

2.4.4 Antibody preparation

100µl of primary and secondary antibody was required per microscope slide, so the total volume of antibody needed was adjusted according to slide number. To prepare an antibody mix that allowed for antibody co-staining against both Ki-67 and 53BP1 antigens, a 1:1500 dilution of primary Ki-67 (2.4.3) in blocking buffer (BB; 5% FBS in PBS) was prepared. 1µl of 53BP1 antibody was then mixed with 199µl of 1:1500 Ki-67 antibody making a 200ul aliquot. Secondary antibodies, goat anti-rabbit FITC (Ki-67) and goat anti-mouse AF568 (53BP1), were both used at a dilution of 1:200 (1µl of each secondary antibody was added to 198µl of blocking buffer).

2.4.5 Blocking and Antibody incubation

After permeabilisation (2.4.2) 200µl of BB was added to each slide, covered with parafilm and incubated at RT for 1hr in a moistened box, to prevent non-specific

antibody binding. 100µl of the primary Ki-67/53BP1 antibody preparation (2.4.3 – 2.4.4), was added to each slide, covered with parafilm and incubated at RT for 1 hour in a moist container. The slides were washed 3 times with cold PBS to remove unbound primary antibody before dipping slides briefly in BB and then addition of 100µl of secondary antibody (section 2.4.3-2.4.4), covering with parafilm and incubation at RT for another hour. After incubation, the slides were further washed 3 times with cold PBS with gentle agitation.

2.4.6 Counterstain

Excess PBS was removed from the antibody stained slides and gently patted dry. Slides were then mounted and chromatin counterstained each with 20-30µl of vectashield containing 4'6-diamidino-2-phenlylindole (DAPI) (VectorLabs), and covered with a glass coverslip. The edges of each slide were sealed with nail varnish to prevent drying out, and the slide stored into a sealed darkened box at 4°C until analysis. Where necessary slides were labelled and coded, to remove bias during analysis.

2.5 Immunofluorescent analysis

Microscope slides for both 1HD and NHBE cell types for all experiments were initially visualised in the same way by manual analysis (2.5.1.1). Later experimental work using irradiated NHBE included manual, as well as automated capture (Metafer v.4) and analysis systems (AutoRIF) (2.5.2-3). Analysis of experimental slides enabled quantification of 53BP1 radiation-induced foci (RIF) number, as well as generation of linear measurements of size by automated analysis for the same manually scored data sets also. Determination of the proliferative status of the cells, and the cell cycle stage was determined by manually classifying the Ki-67 staining of the same nuclei that RIF had been counted in. All immunofluorescently-labelled slides were analysed manually by fluorescence microscopy, and then further analysed using automated capture Metafer v.4 software followed by AutoRIF analysis script (see results for exact experiment details and analysis options). Graphs and tables were generated from raw data using Microsoft Excel and data was normalised to percentage where necessary to account for variations in total nuclei counted across experiments.

2.5.1 Manual analysis

Slides for manual scoring were analysed using an Axioplan 2 –Zeiss 200M Fluorescent Microscope and cells were visualised using oil (Immersol, Carl Zeiss) immersion objectives at 63x and 100x magnification. 85-150 cell nuclei were scored manually per slide, using DAPI to locate cells nuclei. DAPI located nuclei were then scored using TRITC and TR filters for 53BP1 stains, and FITC filter for Ki-67 staining. Images were captured using ISIS software according to the manufacturer's directions.

2.5.1.1 Manual Ki-67 analysis

The Ki-67 staining patterns and their distribution types (type Ia, Ib and II), as described by Dr Joanna Bridger (1998) (Bridger, Kill & Lichter 1998) were used to determine the scoring criteria (Figure 2.4). Ki-67 staining was categorised into Ki-67 negative cells (no visible nuclear FITC staining), type Ia, type Ib and type II Ki-67 positive cells (staining visible under FITC fluorescence as distinct staining patterns related to stage of the cell cycle), and minimal background fluorescence.

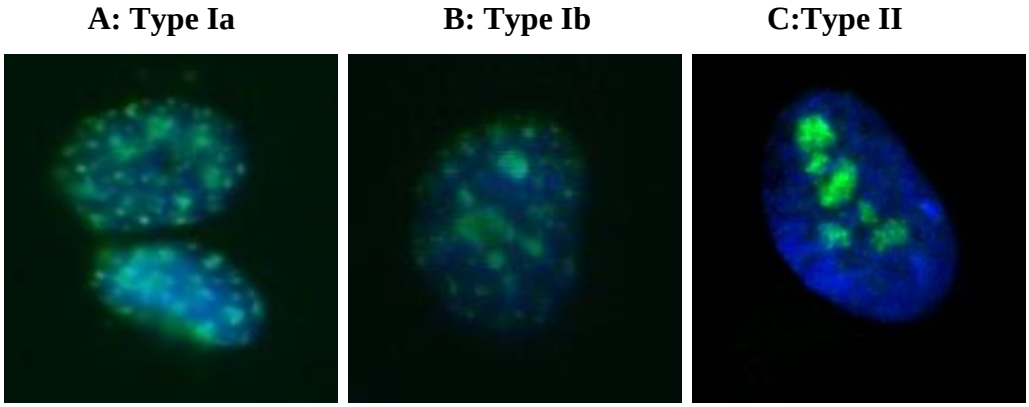

Figure 2.4 Immumofluorescent images of Ki-67 staining patterns in sham NHBE cell nuclei: A, Type Ia, B Type Ib and C Type II as described in Bridger 1998 (Bridger, Kill & Lichter 1998). Nuclei that were in very close proximity to one another were excluded from analysis.

2.5.1.2 Manual 53BP1 foci analysis

53BP1 foci were scored in both Ki-67 positive and negative nuclei. 53BP1 foci were scored directly by eye at 100x magnification in a 3D manner by scrolling through the nuclear focal plane. The total number of foci was recorded per nucleus (100-150 nuclei). Foci were not manually categorised by size due to time

constraints (Figure 2.5) however automated capture and analysis systems (2.7) for later experimental work provided added focus size information.

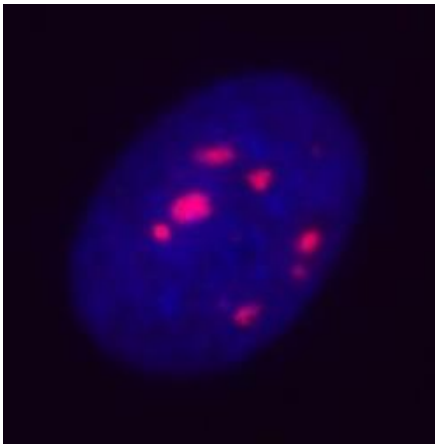

Figure 2.5 Immunofluorescent image of 53BP1 foci in a NHBE cell nucleus: Foci were scored by manually by number and not by size (53BP1=red, chromatin=blue).

2.5.2 Automated image acquisition

Mounted and counter-stained slides as in 2.4.6 were immediately set up onto the Metafer v4 (JAI M4+ 8bit camera) (Metasystems) and this metaphase finder software was utilised to identify cell nuclei coordinates (stored as an MSD file). Once the slides were set up on the stage, the 'MSearch', 'Fluorescence' mode was selected and the correct classifier chosen to allow for scanning of the slide (in this case 'single cells' for finding nuclei). Once an area on the slide had been defined at 10x magnification and the x and y coordinates for the area to be scanned determined, the microscope scanned the defined region and a gallery of all the 'Msearch' DAPI-stained nuclei appears. The 'Msearch' image gallery was checked and all out-of-focus and bad images were deleted for each slide prior to capture. Images of nuclei were then automatically acquired using the 'AutoCap' mode, under the classifier 'ArticleVAL (H2AX-TR-FITC) MIP'. This classifier was set up to enable capturing of images using 3 filters (DAPI for chromatin, TR for 53BP1 foci and FITC for Ki-67), with exposure control as automatic for DAPI, and fixed for TR and FITC channels, where the Max. T integer/second was adjusted accordingly to prevent bleaching or overexposure of slides during image capture. These exposure times were 0.7500, 0.063-0.0167 and 0.1667ms for all experimental slides for DAPI, TR and FITC respectively. The exposure times for TR channel were adjusted to account for variations in fluorescence intensities

across experimental batches. These exposure times for TR were determined by checking the intensity of foci in test images using Image J software and ensuring that foci were not deemed to be overexposed. If this was the case then the exposure time was corrected accordingly and then all of the nuclei were autocaptured. DAPI and FITC were set to 1 focus plane and TR was set to 20 focal planes which allows for 20 z-stacks of 0.5µm step that are then collapsed to form a 2D maximum intensity projection (MIP) image. Approximately 500-1000 images were captured per time point and the saved image thumbnails were then manually scanned and any 'out-of focus'/no nucleus present/poor contrast/dividing cell images were deleted. The number of total images after quality checking varied. The checked black and white images (untick 'merged image' option) were then saved as TIF files for processing using the AutoRIF analysis script. Ki-67 was captured as a potential comparison for manual analysis with larger sample size, but not for automated analysis.

2.5.3 Automated analysis script (AutoRIF)

A java-based AutoRIF software program (McVean *et al*. 2012) was used to analyse each TIF image and count the number and size of 53BP1 foci within each nucleus. In order to determine the optimal filtering iterations to be applied to each experiment, a number of nuclei per time-point and dose were batch tested as described below prior to running the whole experiment. Although the optimal settings for each image will vary, the final filtering steps that were applied across an entire experiment were based on batch tested images and represented those that provided the minimum number of filtering steps without introducing artefacts, and these final settings were applied to all images within an experiment.

2.5.3.1 Calculation of Histograms and analysis of images

In order to process images acquired on the Metafer microscope by AutoRIF, a macro was written that organised each DAPI and TR image file into its own folder in a B/W TIF format. AutoRIF visualises 2 channels where DAPI acts as a mask and the second channel shows the 53BP1 (TR) signal.

A temporary digital folder was created for the histograms and images in advance of the 'two-part' AutoRIF processing. Part 1 of the program was opened as shown in figure 2.6 'start_part1_512m or 1024m' (depending on the speed of the

pc) and the folder with the images to be analysed was selected. A temporary folder was selected to determine the location of the histograms created during Part 1. The 'image with foci' option was selected where 'even' represents the foci channel and odd represents the DAPI channel in this instance. The number of filtering iterations required were selected as determined by the batch test images and these settings were applied to all images within an experiment. As a guide, increasing the Pre-filtering iterations reduce the high frequency noise in the original nucleus by smoothing the image repeatedly, laplasian sensitivity determines the sensitivity to the difference in noise, and post-filtering (Crimmins speckle removal) applies further smoothing to remove noise after the previous filters have been applied.

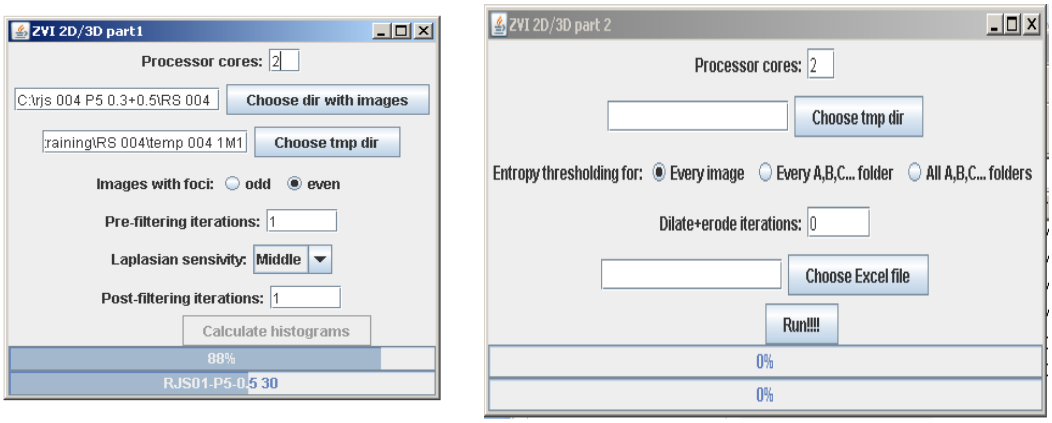

Figure 2.6 Part 1 and 2 AutoRIF analysis script. Part 1: select the directory with the images in 'choose dir with images' and select the temporary directory that has been created 'chose tmp dir'. Select the temporary folder which will determine the location of the histograms. Batch testing a selection of images for each time point was essential to ensure that the settings are correct before running the complete set of images. Filtering iterations need to be optimised for each whole experiment and then the same settings applied to all images within an experiment. **Part 2**: uses histograms generated in part 1 to quantify data as excel output including nucleus number, nucleus area, nucleus height and width, focus number, focus area, focus intensity etc (example output in figure 2.7).

Part 2 of the script converts the histograms and cropped original files into binary images that the data can then be extracted from. To do this, Part 2 was run (start_part2_512m or 1024m), selecting 1 processor core (when running part 2 on the Zoostorm computer), and the temporary folder with the recently generated histograms was selected. A name was generated for the new excel files that are propagated on completion of both parts of the propagated. As the images were

captured as 2D MIP images, the excel output provided focus area information for each focus within a nucleus and x, y, z coordinates for 3D stacks.

2.5.3.2 Automated Excel output

Figure 2.7 shows an example of the excel output generated on completion of AutoRIF Part 2, showing foci intensity and area measurements in pixels for all foci counted within the images of each nuclei processed. In order to confirm AutoRIF identification of a focus, the minimum intensity and size (pixels) thresholds for what is considered to be a focus must be determined and subsequently applied to all time-points within that experiment. These may be different between batches and therefore a number of images were checked and the optimal settings were determined and applied to the whole experiment. Once these were determined a series of IF (AND) equations will return focus area only if it is above both the minimum intensity and size cut-offs. Further equations to group the focus areas into small (<0.5µm = min size-50 pixels), medium (0.5 – 1.0µm = 51-100 pixels), and large (>1.0µm = 100+ pixels) were applied. Calculation of average foci number per nucleus and the proportion of small, medium and large foci were based on nuclei with one or more focus. Finally, only foci that satisfied both the minimum size and intensity requirements described above were included within these calculations.

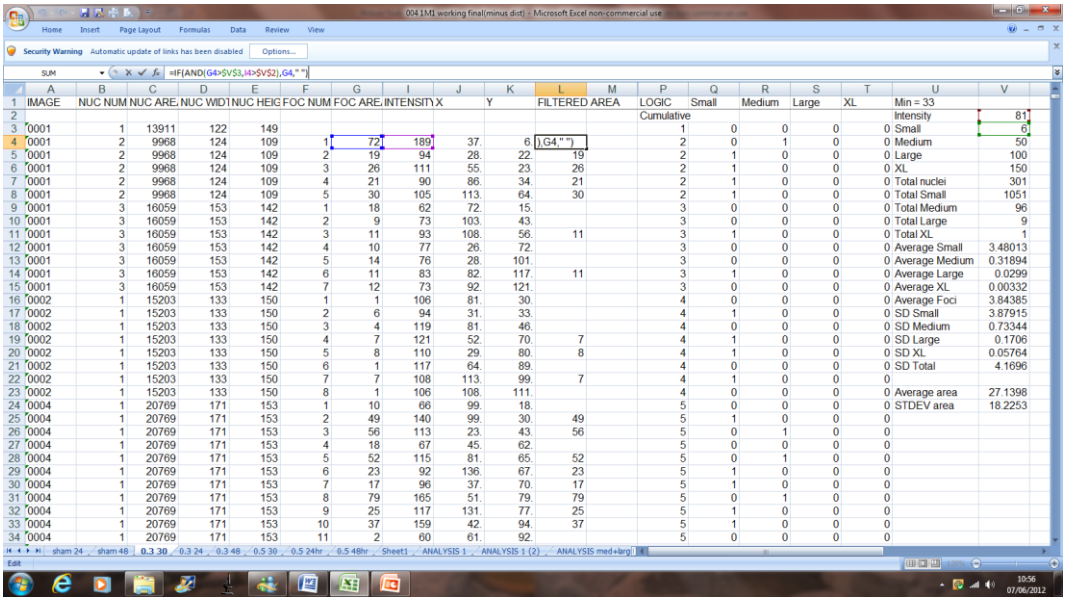

Figure 2.7 Example excel output using AutoRIF analysis script. A different tab is automatically generated for each time point that is analysed within the whole experiment. If focus area (G) and intensity (I) are above minimum intensity cut-off (V1 – determined by user) and size (V3) then filtered area (L) is returned and will be included in calculation

of average area and foci/nucleus. If focus area or intensity does not exceed minimum values, then cell is left blank and categorised as not being a true focus.

2.6 Statistical analysis

Statistical analysis was carried out where possible using a non-paired, two-tailed Student T-test ($P<0.05$ is significant). Statistics were calculated using Microsoft Excel or GraphPad QuickCalcs online statistical calculator.

3 Results

3.1 Cell Culture

3.1.1 NHBE cells in culture

Primary NHBE cells were obtained from Lonza (2.2.1.1) and maintained in NHBE medium (2.2.3.1) at a seeding density of 3500 cells/cm^2. The NHBE cells were maintained for experimental procedures from passage 5 (considered to be mid passage) up to passage 10/11 (late passage) (figure 3.2 A and B). In order to look at the effect of radiation at extended times, NHBE cells were also cultured continuously up to passage 13, which equated to a total of 40 days in culture. Donor 2 (D2) and donor 3 (D3) NHBE were maintained in continuous culture for a period of 17 and 32 days respectively to calculate cumulative cell growth (figure 3.3), while cells from passage 4-13 (D3, n = 2 experiments) were also stained with SA-β-gal (2.3.1.1) to show evidence of an increasing percentage of senescent cells with each passage.

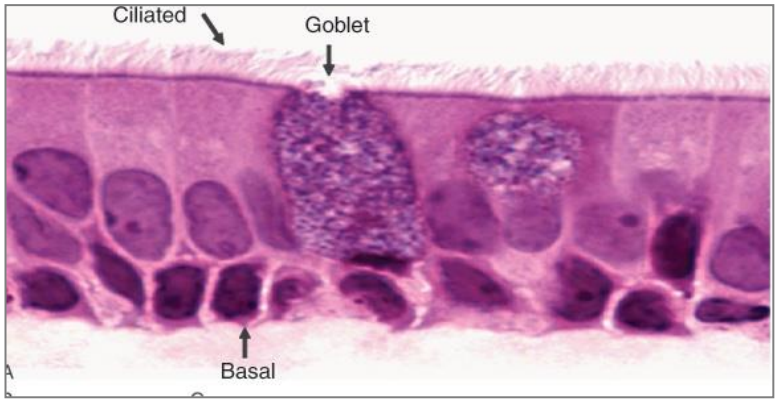

Figure 3.1 Normal human bronchial epithelium. The normal differentiated airway epithelium is made up of three different epithelial cell types including basal, mucous-producing Goblet cells and ciliated epithelial cells (Picture adapted from Vaughan MB, 2006) (Vaughan *et al*. 2006).

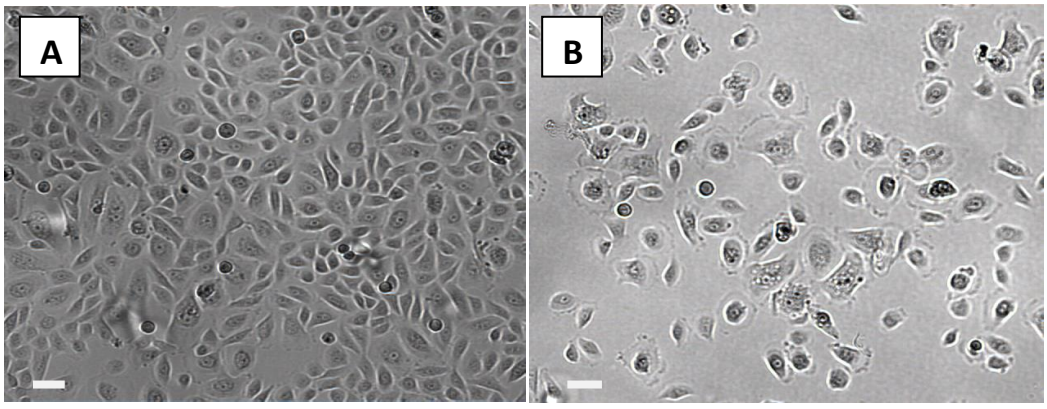

Figure 3.2 NHBE cell morphology in young and ageing cells. Image A = passage 4 NHBE cells with a distinct cobblestone appearance made up predominantly of small basal epithelial types, and image B= passage 10 NHBE cells with a larger proportion of large, goblet cells visible than in younger cultures. Scale bar = 25µm.

The cumulative total growth for D2 NHBE cells was calculated over 17 days and 5 passages, representing a cell population doubling time of 36 hours and ~11 population doublings (PDs). D3 NHBE cells were cultured over 32 days and 6 passages corresponding to ~18 PDs and a population doubling time of ~41 hours. These calculations do not account for plating efficiency and are representative of cumulative population doublings only. Therefore the actual PDs that the NHBE cells will go through during this period observed are considerably less, with Lonza stating that NHBE cells will go through a total of 18 and 15 PDs for D2 and D3 respectively (table 2.1).

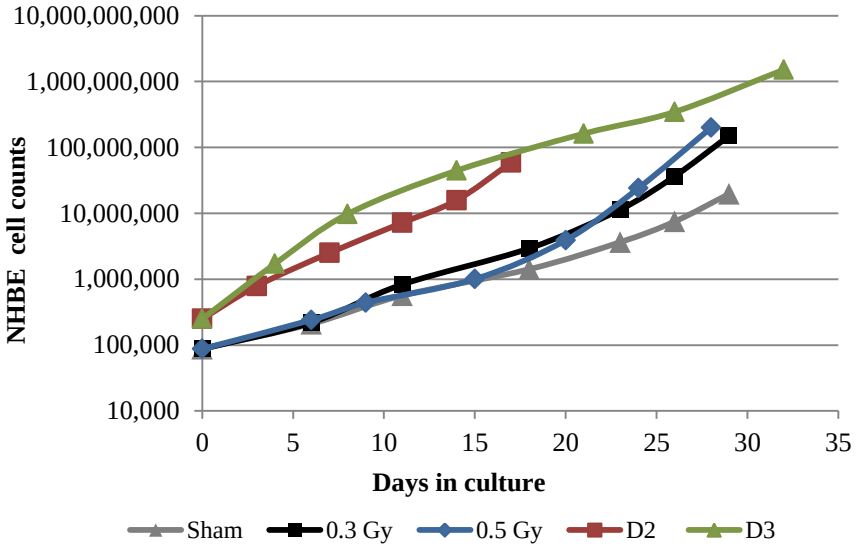

Figure 3.3 Cumulative normalised cell growth curves for NHBE cells in normal monolayer culture and after sham, 0.3 and 0.5 Gy γ-ray exposure. Donor 2 (P4-9; red squares) and Donor 3 (P7-13; grey triangle, black square, blue diamond, and green triangle and P4-P10, green triangle) NHBE cells were maintained in cell culture and counted at each subsequent passage. Cells were stained with Trypan blue and viable cells counted.

To determine the effect of IR on the growth of NHBE cells, cultures at P7 (figure 3.3) were seeded into T25 flasks for exposure to sham, 0.3 and 0.5 Gy γ-rays as described in 2.3.2.1 and 2.3.2.2 for subsequent processing for analysis of 53BP1 foci, Ki-67 proliferative and SA-β gal status at extended times after IR (2.4 and 2.3.1.2). Cell populations were therefore maintained in culture enabling the

generation of cumulative growth curves after radiation exposure. Similar to above, these do not take into account plating efficiency and represent cumulative PDs during culture period only. The cumulative PDs were similar to those seen during normal monolayer culture of both D2 and D3, although it is apparent that the population growth of sham-treated cells appears to slow ~20 days in culture, relative to irradiated populations.

3.1.2 Cellular senescence of NHBE during normal subculture

3.1.2.1 SA β- galactosidase staining of Etoposide treated 1HD fibroblasts

Optimisation of the SA-β galactosidase assay was performed in 1HD fibroblasts (figure 3.4 and 3.5). To act as a positive control, cells were treated with etoposide to induce premature cellular senescence prior to staining for SA-β gal activity (2.3.1-2.3.1.2).

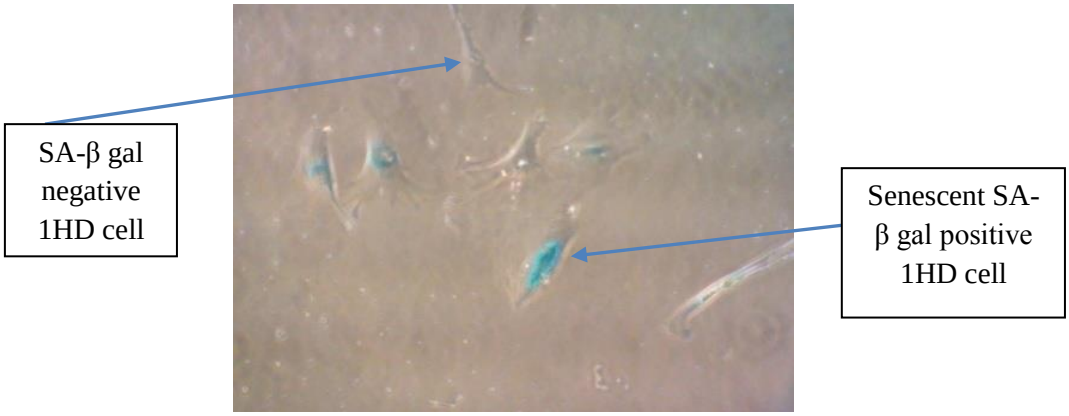

Figure 3.4 SA-β gal staining of etopisode (12.5µM) treated 1HD dermal fibroblasts. Senescent fibroblast shown by the presence of a blue precipate indicating the presence of lysosomal SA-beta-galactosidase activity at pH 6.0.

Figure 3.5 shows that treatment with 12.5µM of etoposide (as suggested by manufacturers) is as effective as treatment with 20µM in our cell type. 16% of non-treated control 1HD cells stained positive for SA-β gal (categorised as senescent), in contrast to 76% of fibroblasts treated with 12.5 or 20µM of etoposide. We therefore concluded that a 24 hour treatment with 12.5µM of etoposide followed by a 4-5 day recovery prior to fixation was sufficient to induce cellular senescence above that of the control treated cells.

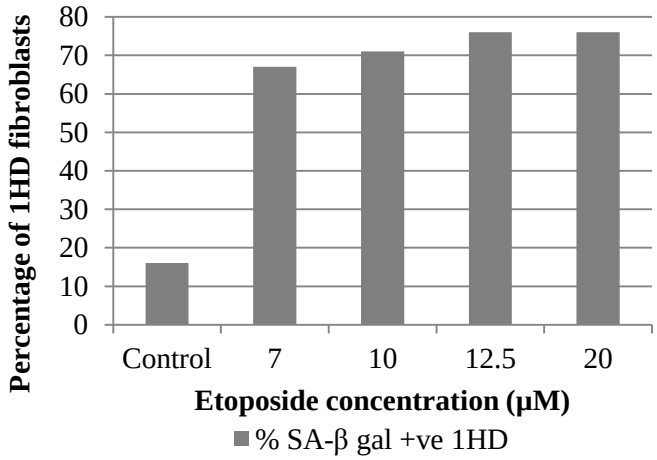

Figure 3.5 Effect of etoposide concentration on the induction of premature senescence in 1HD fibroblasts (P21).

3.1.3.1 SA β-galactosidase staining of normal NHBE cells

In order to determine the baseline level of senescent cells within NHBE cells and to quantify how this fraction of senescent cells changes with each passage, D3 P4-P7 NHBE cells were stained with X-gal to detect SA-β-galactosidase activity at pH 6.0 as described in 2.3.1.1. In addition to determining a baseline senescent fraction within normal NHBE culture, P7 NHBE cells exposed to sham, 0.3 and 0.5 Gy γ-rays were stained for SA-β gal at each passage up to 33 days after IR to determine if there was any indication of premature senescence after our moderate dose exposures (figure 3.6).

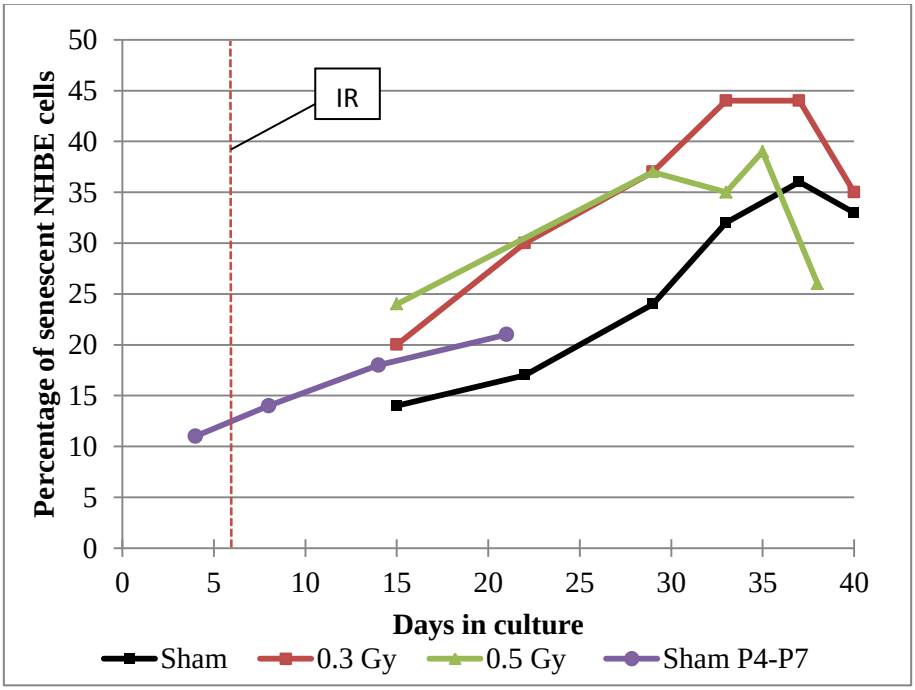

Figure 3.6 SA-β-gal staining of D3 NHBE cells with increasing passage (P4-P13) after sham, 0.3 and 0.5 Gy γ-ray exposure. Cells were irradiated at P7 (red dashed line), and SA-β gal dishes were prepared at each subsequent passage (P8 onwards). Cells were fixed from 8 days after exposure to sham (black lines/squares), 0.3 Gy (red line/squares) and 0.5 Gy (green line/triangles) IR. Sham P4-P7 (purple line/circles) represent the SA-β gal positive fraction of NHBE cells during normal subculture in an independent experiment, and all data points represent one measurement. No SA-β gal measurements were obtained at T0 in P7 NHBE cells due to insufficient cell counts.

11% of P4 NHBE stained positive for SA-β gal activity, which subsequently increased to 21% at P7 (purple lines/circles) (figure 3.6 and 3.7). This increase in SA-β-gal staining was coupled with an enlarged morphology of the blue stained positive cells possibly representing an increasing number of NHBE reaching their finite replicative capacity and entering senescence. Although this method is extremely subjective and therefore requires that large numbers of cells are scored, Ki-67 immunofluorescent staining which is absent in senescent cells, correlates with this. Specifically, 16 - 36% (average 25%) of cells were Ki-67 negative at P6, increasing to ~57% in ageing (P10) shams (range 43-62%) (figure 3.26). Comparatively, 14% of sham NHBE cells at P8 were positive for SA-β gal activity which subsequently increased to 36 % at P12. Figure 3.6 shows that although there is obvious variability in the percentage of senescent cells in P7 and P8 NHBE cell populations (2 separate experiments) in sham and irradiated nuclei, the fraction of senescent cells within both of these populations of cells increases with the same trend (20% and 24% at P8 increasing to 44% and 39% in P12 NHBE cells exposed to 0.3 and 0.5 Gy respectively). The increase in SA-β gal positive NHBE with increasing passage represents an increase in the percentage of senescent cells within the culture, with age, however there does not appear to be any signs of an increasing percentage of senescent cells after a single acute dose of radiation (0.3 or 0.5 Gy). Notably, there is a decrease in the fraction of SA-β gal activity in P13 sham (33%) 0.3 Gy (35%) and 0.5 Gy (26%) exposed cells compared to P12 nuclei (figure 3.6). This may represent a technical loss of SA-β gal positive cells during passage or a loss of the senescent cells from the population by apoptosis. In order to determine whether this decrease/plateau is a result of maintaining the cells in continuous culture and to account for the variation that is seen between cell dishes, it is necessary to increase the number of dishes analysed at each time point, as well as replication of the observations

independently. This effect is also seen in the NHBE cells stained for Ki-67 after continuous culture (section 3.4).

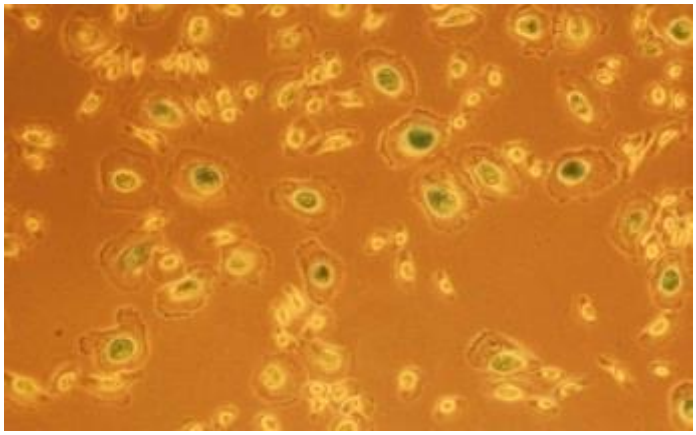

Figure 3.7 SA-β-gal staining in P7 NHBE cells. Magnification x200

3.2 Induction and persistence of 53BP1 foci in NHBE cells of varying passage age after exposure to γ-rays

To determine the frequency of radiation-induced damage in NHBE cells of varying age, cells were exposed to 0 – 2 Gy of Co^{60} γ-rays (~0.1 Gy/min dose rate). Cells were seeded onto acid-washed and flamed microscope slides or T25 flasks for extended culturing as described in 2.3.1 and transported for IR at 70-80% confluency (2.3.2 and 2.3.3). The sham slides were always treated in exactly the same way as the irradiated slides however they were not irradiated at the source. Cells were fixed according to section 2.4.1 at varying times post-irradiation and antibody stained using anti-53BP1 in order to determine the induction and persistence of DNA DSB after exposure.

Table 3.1 Summary of Irradiations performed using donor 3 NHBE cells of varying passage number

Passage at Exposure	Cobalt 60 source used	Total dose (Gy)	Dose rate (Gy/min)	Total exposure time (minutes)	Fixation times (hours)	End points
5	Lower activity	0.3 + 0.5	0.111	2.36 + 4.22	0.5, 24 , 48	53BP1 foci number and size; % Ki-67 – ve cells
6	Lower activity	0.3 + 0.5	0.110	2.40 + 4.29	0.5, 24, 29*	53BP1 foci number and size; % Ki-67 – ve cells
10	Lower activity	0.3 + 0.5	0.105	2.47 + 4.41	0.5, 48, 216	53BP1 foci number and size; % Ki-67 – ve cells
10	Higher activity	2	0.1304	15.34	0.5, 48, 168	53BP1 foci number and Ki-67
7	Lower activity	0.3 +0.5 Gy	0.101-0.104	2.83+4.9 (Quads); 2.83 +4.77 (T25)	0-792 (33 days)	53BP1 foci number and size; % Ki-67 – ve cells; % SA-β gal +ve cells

Table 3.1 summarises the experimental details and end points studied using NHBE cells reported in the results section. * 29 hour fixation taken instead of 48 hrs as cells would be more than 85% confluent at 48 hrs.

3.2.1 Induction of 53BP1 foci in mid passage NHBE cells

In order to determine the effect that IR has on the induction of 53BP1 foci ~100 P5 and 6 NHBE nuclei were manually analysed per dose and timepoint for the number of 53BP1 foci per nucleus after exposure to sham, 0.3 and 0.5 Gy γ-rays and fixed after 0.5, 24 and 48/29 hours for P5/P6 cells.

3.2.1.1 Effect of exposure to 0.3 and 0.5 Gy

In order to check that there was no adverse damage induced in shams as a result of the transportation to the irradiation source, a Time 0 sham was scored giving an average of 1 53BP1focus/nucleus, which was in concordance with the other shams at all timepoints (table 3.2). Exposure of mid passage NHBE cells to 0.3 and 0.5 Gy resulted in a significant induction of DNA DSB as detected by an increase in 53BP1 foci compared to shams (table 3.2 and figure 3.8). Specifically, the number of 53BP1 foci increased from 1.2 foci per nucleus in mid-passage sham nuclei, to 5.3 and 6.5 foci per nucleus after 0.3 and 0.5 Gy respectively at 30 minutes post exposure (graph 3.8). Thus the number of 53BP1 foci induced was similar for cells exposed in P5 and P6 (Table 3.2 and pooled graph 3.8). By 24 hours, the average number of 53BP1 foci had returned to sham levels after 0.5 Gy (1.3 foci/nucleus). However, after 0.3 Gy the average number of 53BP1 foci (1.7 foci/nucleus) was still significantly different to the 24 hour sham (unpaired, two-tailed t test, $p=0.0118$) possibly suggesting a higher number of DSB that have yet to be repaired and resolved. Given this was not seen in cells fixed at 29 hours or at 48 hours, it is more likely that this reflects the variability in foci seen in NHBE cells.

Table 3.2 Average number of 53BP1 foci in mid passage NHBE cells after 0.3 and 0.5 Gy

Age of NHBE	Timepoint (PI) and dose	Average number of 53BP1 foci/nucleus
Passage 5 (n=100)	Sham 30mins	1.22
	Sham 24hr	0.77
	Sham 48hr	1.06
	0.3 Gy 30	5.29
	0.3 Gy 24hr	1.17
	0.3 Gy 48hr	1.00
	0.5 Gy 30 mins	6.76
	0.5 Gy 24hr	0.87
	0.5 Gy 48hr	1.37
Passage 6 (n=100)	T0	1.0
	Sham 30 mins	1.1
	Sham 24hr	1.5
	Sham 29hr	1.3
	0.3 Gy 30m	5.3
	0.3 Gy 24hr	2.2
	0.3 Gy 29hr	1.2
	0.5 Gy 30 mins	6.2
	0.5 Gy 24hr	1.8
	0.5 Gy 29hr	1.2

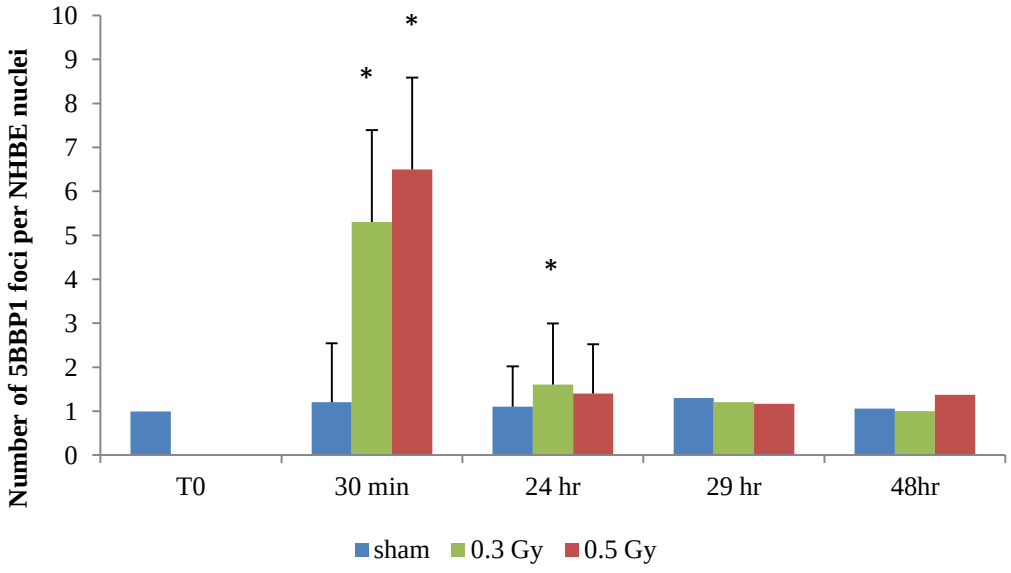

Figure 3.8 Average number of 53BP1 foci in mid passage NHBE cells after 0.3 and 0.5 Gy. 0.5 hr and 24 hour sham, 0.3 and 0.5 Gy are averages calculated from independant experiments (n=2) . 24 hours after exposure to 0.3 Gy, average number of 53BP1 foci counted in 100 nuclei was statistically significant from foci number in sham nuclei after 24 hours (p=0.0118). * = Two-tailed p value = <0.05, statistically significant

compared to sham at same timepoint. Error bars represent SD of the mean based on 2 independent experiments.

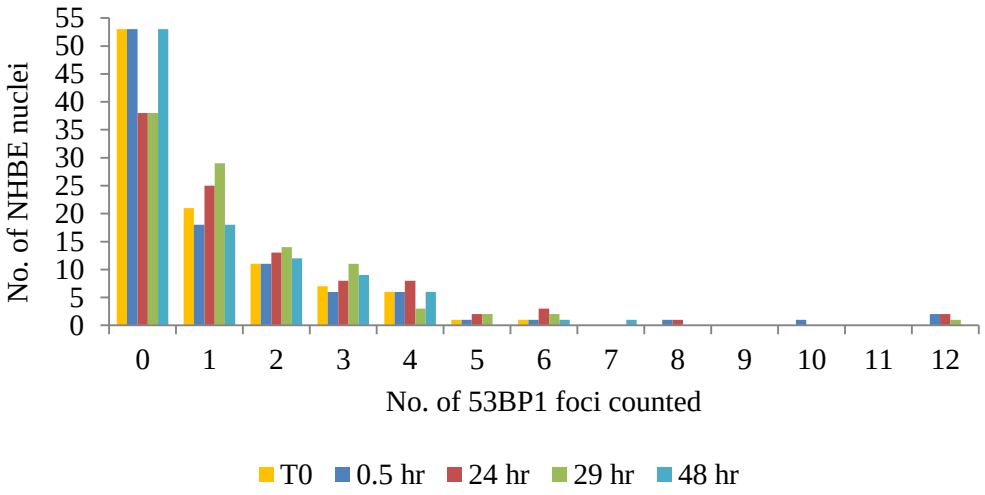

Figure 3.9 Distribution of 53BP1 foci in mid passage sham nuclei. 53BP1 foci distribution is the same in mid passage nuclei (T0-48hr), with the majority of NHBE cells containing between 0-2 foci per cell (38-53% of nuclei contained no 53BP1 foci at all time points). Graph is for comparison between all mid passage shams.

After IR, the induction of DNA damage is shown by the increasing number of nuclei with increasing numbers of 53BP1 foci by 30 minutes and an apparent dose effect which returns to a similar distribution to the shams by 24hrs (Figure 3.9 and 3.10). The elevation of average number of foci (figure 3.10) which was still significant to sham at 24 hours after 0.3 Gy can be accounted for by an increase in nuclei with 2 foci. Nuclei with above 30 foci per nucleus were excluded as they were seen in both irradiated and sham cells and thought to be S phase cells; these accounted for <5% in all experiments.

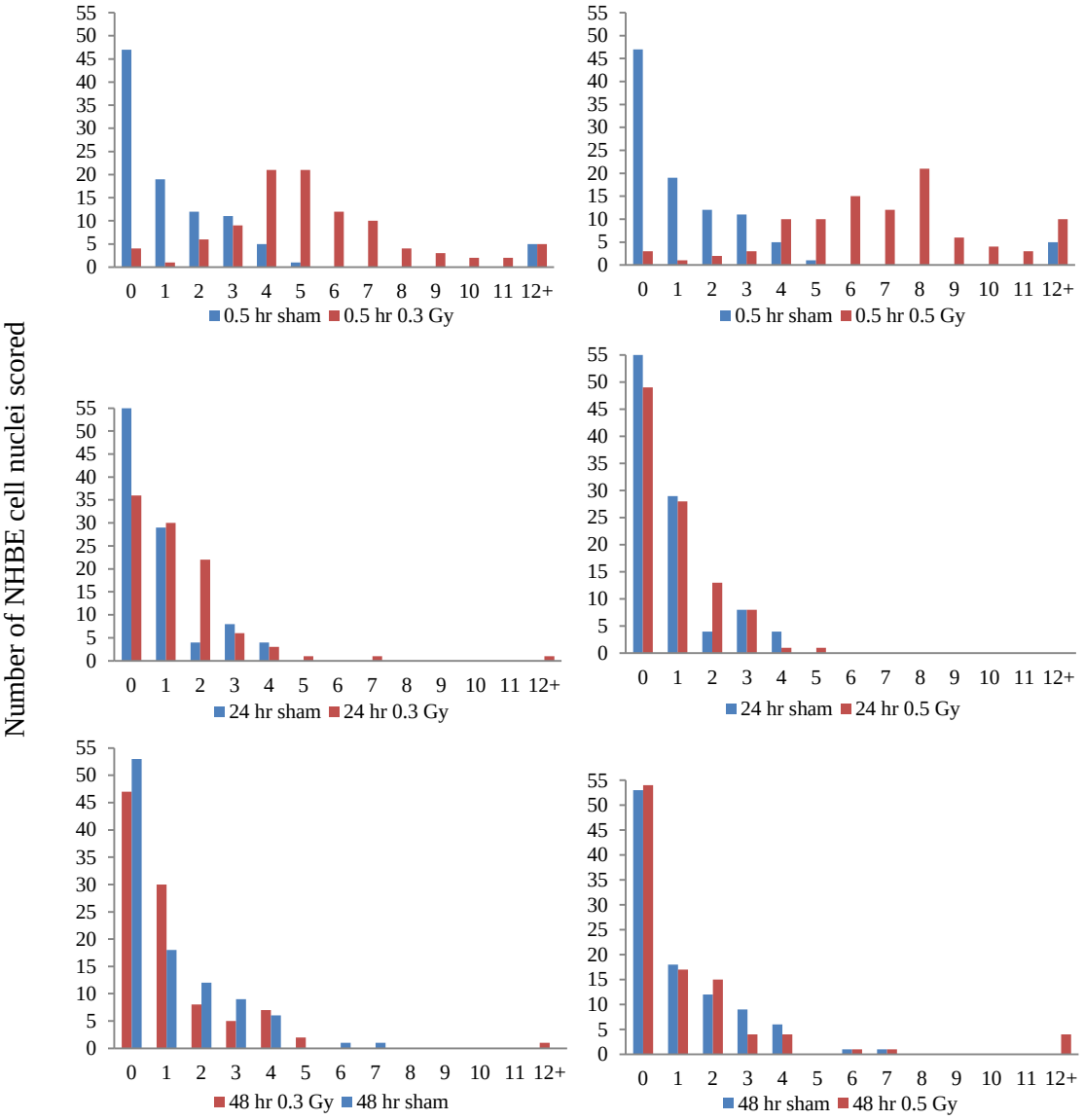

Figure 3.10 Distribution of 53BP1 foci number in mid passage NHBE nuclei after exposure to 0.3 Gy and 0.5 Gy γ-rays. Distribution profiles are from P5 sham and exposed nuclei. P5 distribution profiles are representative of P6 profiles (data not shown).

3.2.2 Induction and persistence of 53BP1 foci in late passage NHBE cells after exposure to γ-rays.

P10 NHBE cells were exposed to sham, 0.3 Gy and 0.5 Gy γ-rays and fixed at varying times (30 minutes-216 hours) after IR and stained for the detection of 53BP1 foci (2.4). 150 nuclei per time-point were analysed by manual scoring methods (2.5.1.2).

The distribution of foci in late passage sham exposed cells was shown to be between 2-4 foci/nucleus (table 3.3 and figure 3.13) compared to 0-2 foci in mid

passage cells (figure 3.10). By 30 minutes post exposure there is evidence of a significant induction of DNA damage (p=0.0001) after 0.3 Gy (6.86 foci/nucleus) and 0.5 Gy (8.21 foci/nucleus) which is also higher than the average foci number seen in mid passage cells (figure 3.8 and 3.11). It is likely that the increase in background foci in the aged cells (P10 at time of IR) accounts for this (figure 3.12). These cells were fixed over a period of 216 hours (9 days), with a cell passage separating the 48 hour and 216 hour time points. Again as seen with younger mid passage cells (P5/6), by 48 hours the average number of 53BP1 foci had returned to sham levels. However interestingly 216 hours after exposure to 0.5 Gy the average foci scored was elevated (4.73 foci/nucleus, p=0.0001) compared to the 216 hour sham (3.31 foci/nucleus), possibly representative of the appearance of new foci. That said, variability was observed between shams at different time points e.g. between 30 minute and 48 hour (p=0.0007) and 30 minute and 216 hour (p=0.0012) shams, meaning such interpretation must be considered with caution.

Table 3.3 Average number of 53BP1 foci in late passage NHBE cells after exposure to 0.3 and 0.5 Gy

Age of NHBE	Timepoint (PI) and dose	Average number of 53BP1 foci/nucleus	Modal average number of 53BP1 foci/nucleus
Passage 10/11 (n=150)	Sham 30 mins	2.44	0
	Sham 48 hr	3.43	2
	Sham 216 hr	3.31	3
	0.3 Gy 30 min	6.86	7
	0.3 Gy 48hr	3.95	3
	0.3 Gy 216 hr	3.57	4
	0.5 Gy 30 min	8.21	7
	0.5 Gy 48 hr	4.03	2
	0.5 Gy 216 hr	4.73	3

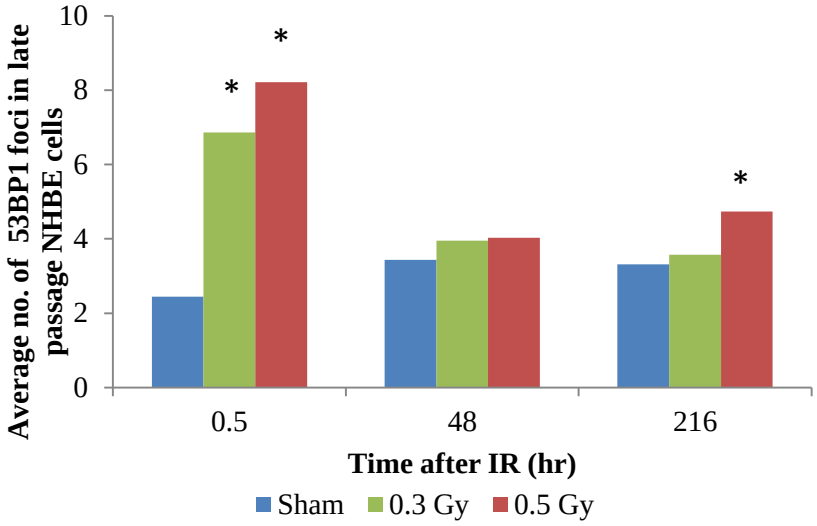

Figure 3.11 Average number of 53BP1 foci in late passage NHBE cells up to 216 hours after γ-ray exposure. n=1.

The distribution of foci in sham and exposed NHBE cells are shown in figure 3.12. The background distribution is fairly consistent for all sample time points, however it is higher compared to mid-passage cells with only ~24% of late-passage sham nuclei having zero foci (15-34%), compared to ~50% of mid passage nuclei (38-55%) (figure 3.10). The increase in the background and broader distribution patterns in later passage cells may make distinction of radiation effects more difficult, particularly at low dose exposures. Again, by 216 hours after 0.5 Gy, it is possible to see a shift in the distribution of NHBE cells with more nuclei with increased numbers of foci compared to sham

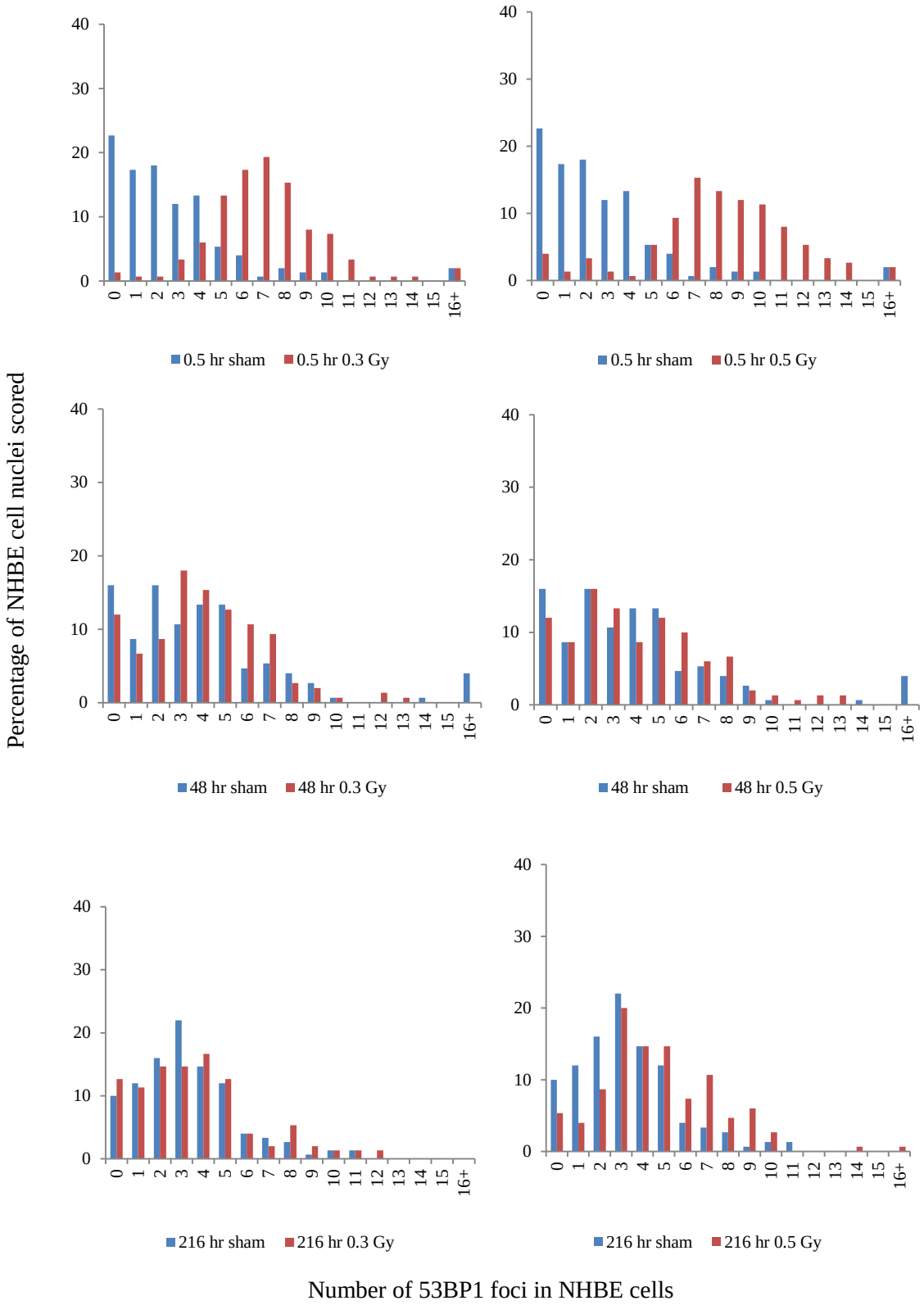

Figure 3.12 Distribution of 53BP1 foci number in late passage NHBE nuclei after exposure to 0.3 Gy and 0.5 Gy γ-rays. Sham is the same sample on both 0.3 and 0.5 Gy graphs. X axis = Number of 53BP1 foci in NHBE nuclei, y axis = percentage of NHBE cells scored (NHBE cells scored = 150 per sample).

3.2.3 Induction and persistence of 53BP1 foci in NHBE cells up to 33 days after irradiation.

In addition to looking at the difference between induction and decline of 53BP1 foci in mid and late passage NHBE cells, it was necessary to determine if there was an increase or persistence in the number of DNA damage foci after irradiation at extended times compared to sham treated NHBE. Passage 7 NHBE cells were exposed to sham, 0.3 and 0.5 Gy γ-rays on either glass slides in Quadriperms (24-48 hr fixation) or in T25 flasks (for continuous culture) and fixed for co-staining for 53BP1 and Ki-67 analysis up to 792 hours after exposure (table 3.4).

The 30 minute-48 hr timepoints in table 3.4 represent the pooled averages from independent analysis of 53BP1 foci in P4-P7 NHBE cells after 0.3 and 0.5 Gy. The average number of 53BP1 foci 48 hours after exposure to 0.3 Gy (1.64 foci/nucleus; pooled 1.32 foci/nucleus) and 0.5 Gy (1.44-1.47 foci/nucleus) are both significant (P=0.0047 and P=0.00277 for 0.3 and 0.5 Gy respectively) compared to sham (1 focus/nucleus). However the average number of 53BP1 foci in sham nuclei 196 hours (1.68 foci/nucleus) after IR is no different to that seen by the same time after 0.3 Gy (1.7 foci/ nucleus) and 0.5 Gy (1.69 foci/nucleus). This further highlights interpretative issues when dealing with very small numbers of foci.

Table 3.4 Average number of 53BP1 foci in NHBE cells up to 792 hours after sham, 0.3 and 0.5 Gy γ-rays.

Cell type	NHBE cells (P7-P13)	
Dose γ-rays	**Time after IR (hrs)**	**Average number of 53BP1 foci per nucleus**
Sham (n=100)	0.5	1.17
	24	1.11
	48	1.00
	196	1.68
	384	1.51
	528	2.17
	624	1.43
	696	1.14
	792	1.23
0.3 Gy (n=100)	0.5	5.27
	24	1.39
	48	1.32
	196	1.70
	384	1.67
	528	1.17
	624	1.28
	672	0.91
	792	0.48
0.5 Gy (n=100)	0.5	6.46
	24	1.36
	48	1.44
	196	1.69
	360	2.00
	480	1.03
	552	0.95
	648	1.14
	720	0.80

Table 3.4 196 – 792 hr timepoints represents manual analysis from one continuous experiment. Averages calculated at 0.5, 24 and 48 hr timepoints represent pooled data from both mid passage NHBE experiments (figure 3.8) and longterm analysis where applicable (n=2-3).

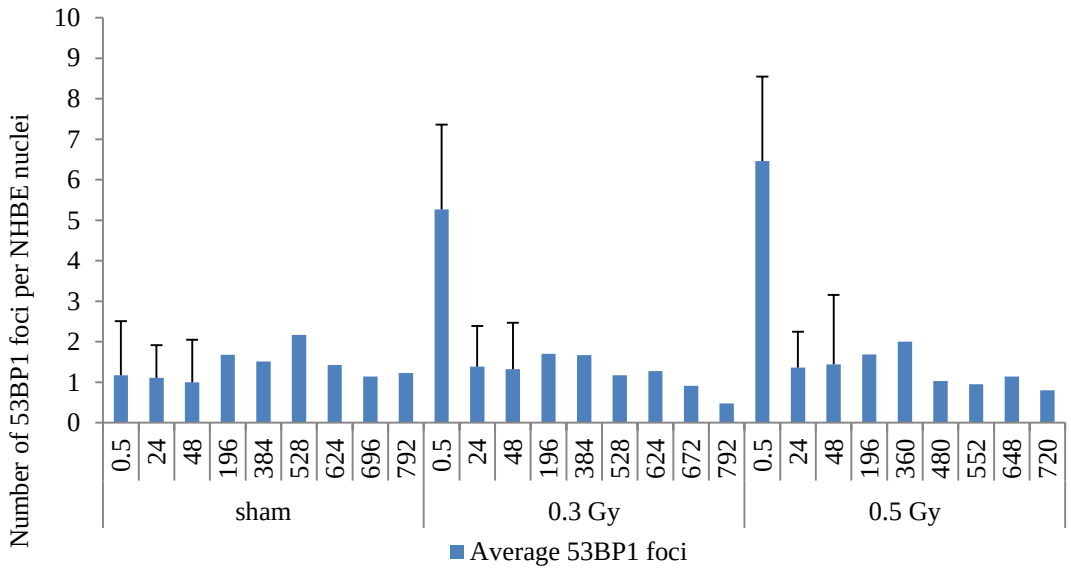

Figure 3.13 Manual analysis of average number of 53BP1 foci in NHBE cells (P5-P13) up to 792 hours after sham, 0.3 and 0.5 Gy exposure. Error bars represent SD of the mean from 2 (0.5 and 48 hour) and 3 (24 hr) independent experiments. Variation is large due to the spread of foci in samples.

Figure 3.13 and figure 3.14 highlight the average number and distribution profiles of 53BP1 foci in NHBE nuclei up to 792 hours (33 days) after exposure to sham, 0.3 and 0.5 Gy. Both the average number and distribution profiles 24 hours after IR are consistent with sham average foci numbers and distribution. Interestingly, there is a clear reduction in the number of foci in all dose groups (sham 1.43-1.23 foci/nucleus, 0.3 Gy 1.17-0.48 foci/nucleus, 0.5 Gy 1.03-0.8 foci/nucleus) from 528 hrs (P10) compared to earlier timepoints. This reduction is not consistent with the increased background foci seen in sham and irradiated late passage nuclei (3.2.2), and thus cells irradiated at P7 and grown to P13 contain significantly less foci than seen in cells IR at late passage. In mid passage NHBE cells, ~ 50% of sham nuclei have zero foci (figure 3.10), which correlates with the number of NHBE cells with zero foci by 24 hours in sham (51%) 0.3 Gy (50%) and 0.5 Gy (35%) P7 exposed nuclei. Comparatively only 23% of late passage NHBE nuclei had zero foci (figure 3.12) and this proportion of cells with zero foci in later passage cells is not seen in the NHBE cells continuosly subcultured to late passage. 528 hours after sham exposure, 17% of nuclei contained 3 foci, compared to 5-11% of nuclei at all other timepoints analysed. The increase in nuclei scored with 3 foci accounts for the average number of foci in sham nuclei (2.17 foci/nucleus) being significantly different to 0.3 Gy 528 hours (1.17

foci/nucleus, P= 0.0013) and 0.5 Gy 480 hours (1.03 foci/nucleus, P=0.0005) after exposure. Thus, although this experiment spans the P10 age of NHBE cells, the data represents observations taken over 6 passages, whereas the earlier experiments were irradiated and fixed within one cell passage. This may indicate that during continued subculture, the cells with an increased background are either removed from the cell population as a result of cell death (possibly apoptosis) or due to continued culture. It is interesting to note that this decline occurred in all three independent cell populations (sham, 0.3 and 0.5 Gy) around the same time and therefore may represent an effect of continued culture on differentiation statuses of the cells. Overall though, there is no evidence of any increase in number of 53BP1 foci up to 33 days after a single exposure of 0.3 and 0.5 Gy γ-rays.

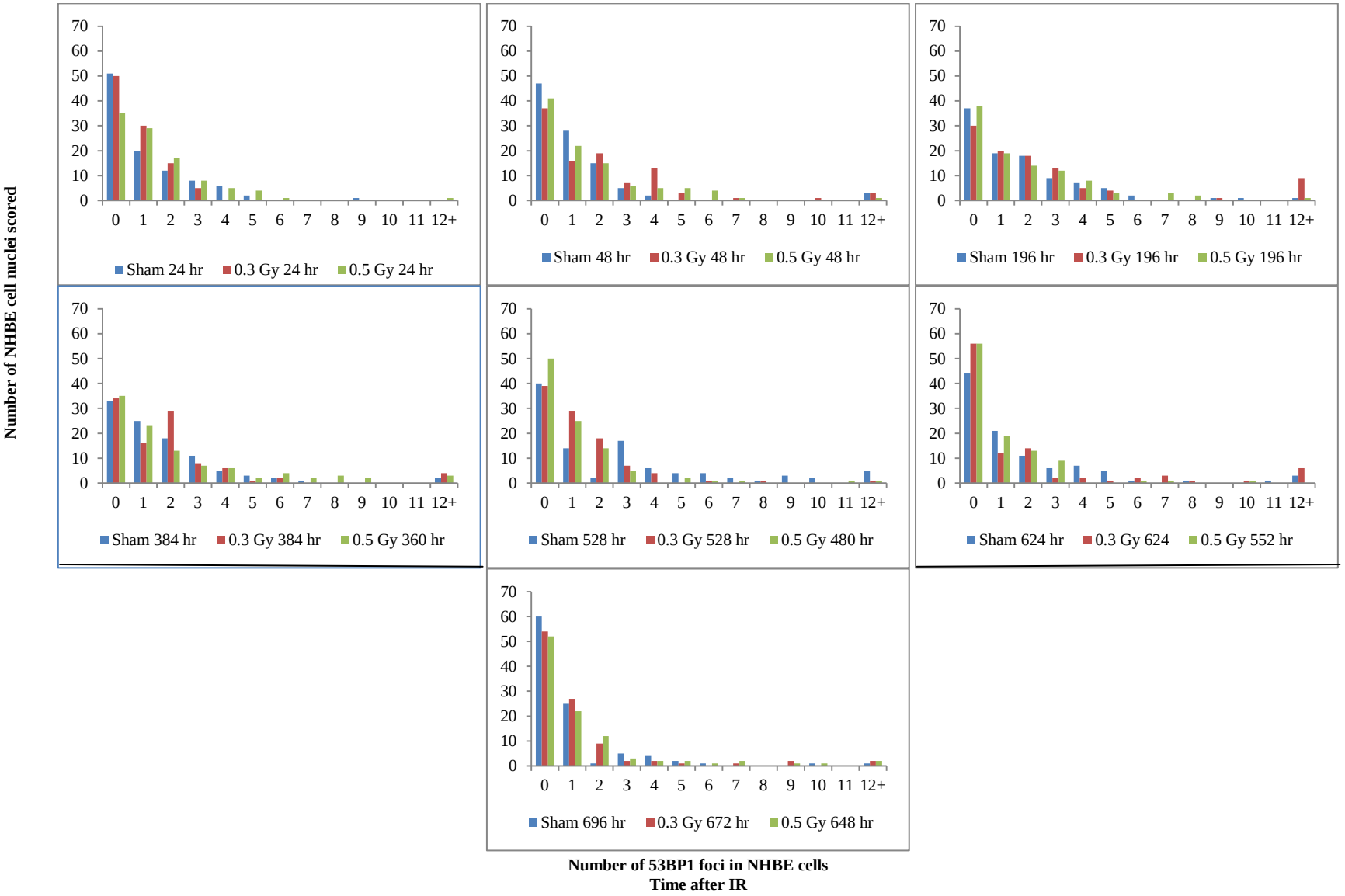

Figure 3.14 Distribution profiles of 53BP1 foci in NHBE cells up to 792 hours after 0.3 and 0.5 Gy γ-ray exposure.
150 NHBE cell nuclei scored per timepoint.

3.2.3 Effect of exposure to 2 Gy

P10 NHBE cells were fixed for indirect-immunofluorescence 0.5, 48 and 168 hours after exposure to sham and 2 Gy γ-rays.

DNA damage can be seen by an increase in 53BP1 foci in NHBE nuclei (11.21 foci/nucleus) 30 minutes after exposure to 2 Gy which is significantly different (P=<0.0001) to sham levels at this time (1.77 foci/nucleus) (figure 3.15). As seen after 0.3 and 0.5 Gy exposures, the number of foci (2.63 foci/nucleus) had returned to sham (2.21 foci/nucleus) after 48 hours in culture. By 168 hours, there is suggestion of a significant increase in the number of 53BP1 foci (3.24 foci/nucleus) (as was seen at 216 hours in late passage cells after a dose of 0.5 Gy), compared to sham (2.4 foci/nucleus, p=0.0108). This can also be seen in the distribution graph (figure 3.16) whereby there is an obvious increase in the number of NHBE cells that still contain 6-8 53BP1 foci compared to sham at 168 hours. However as this experiment would need to be replicated to determine significance (n=1).

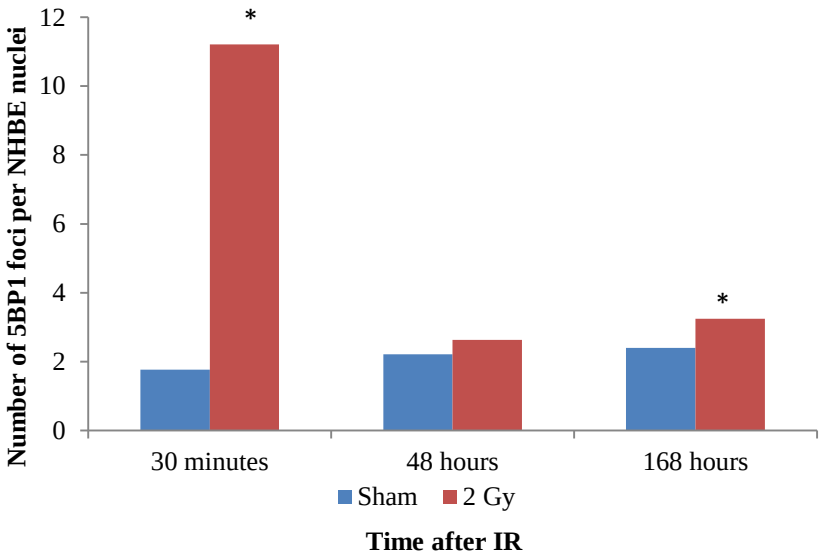

Figure 3.15 Average number of 53BP1 foci in NHBE nuclei up to 168 hours after sham and 2 Gy exposure.

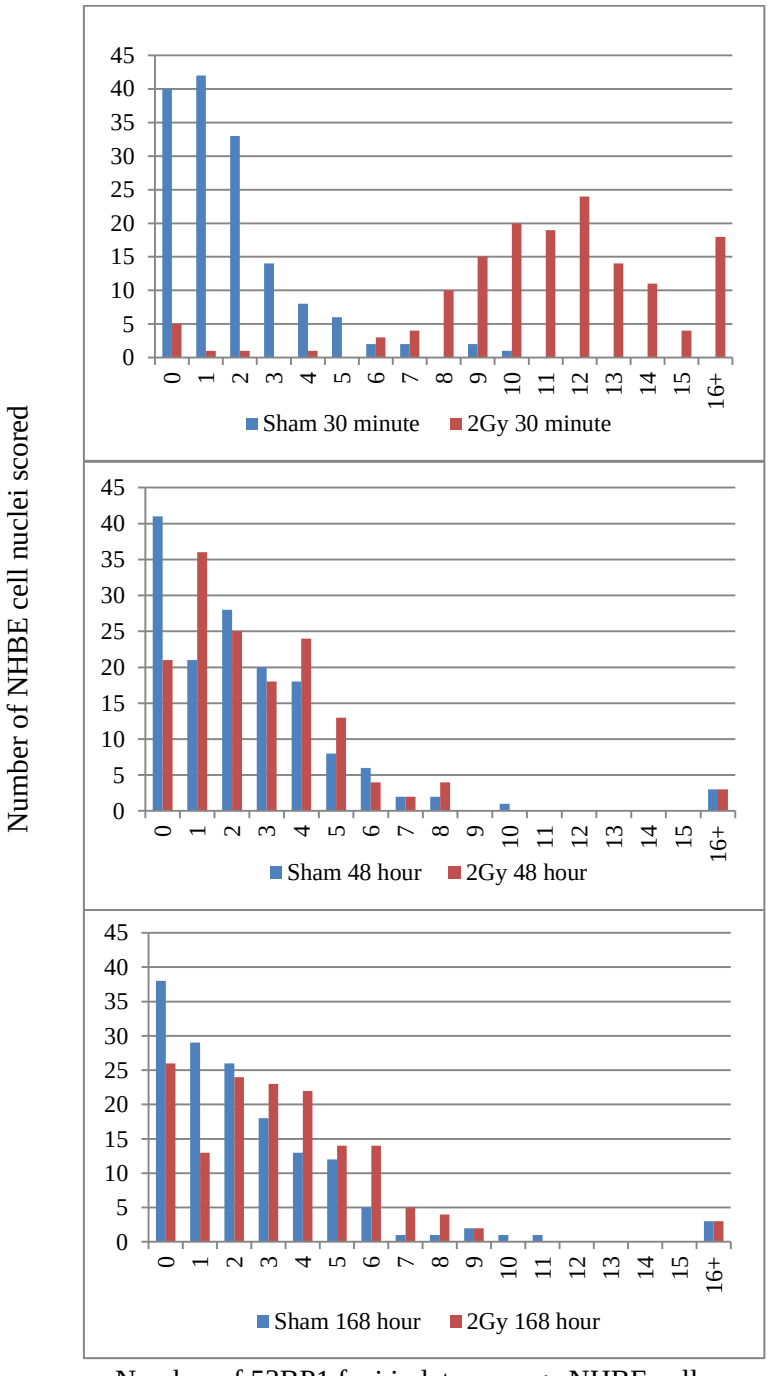

Figure 3.16 Distribution of 53BP1 foci in late passage NHBE cells after exposure to sham and 2 Gy γ-rays.

3.3 AutoRIF analysis of DNA damage in mid and late passage NHBE cells

To increase the number of nuclei analysed and also to gain information on the size of 53BP1 foci, images of nuclei from mid and late passage NHBE (3.2.1 and 3.2.2) were automatically acquired using Metafer v4.0 software (2.5.2), enabling subsequent automated analysis of 210-1000+ images using AutoRIF (McVean *et al*. 2012) (2.5.3-2.5.3.2). A series of pre-processing steps and batch testing of ~10% of images from each time point were performed according to 2.5.3.1 and 2.5.3.2 and the optimum settings were determined and applied to the whole experiment. AutoRIF then generated an excel output that provided statistics on each focus that is filtered to be above the minimum size and intensity thresholds previously set by the user.

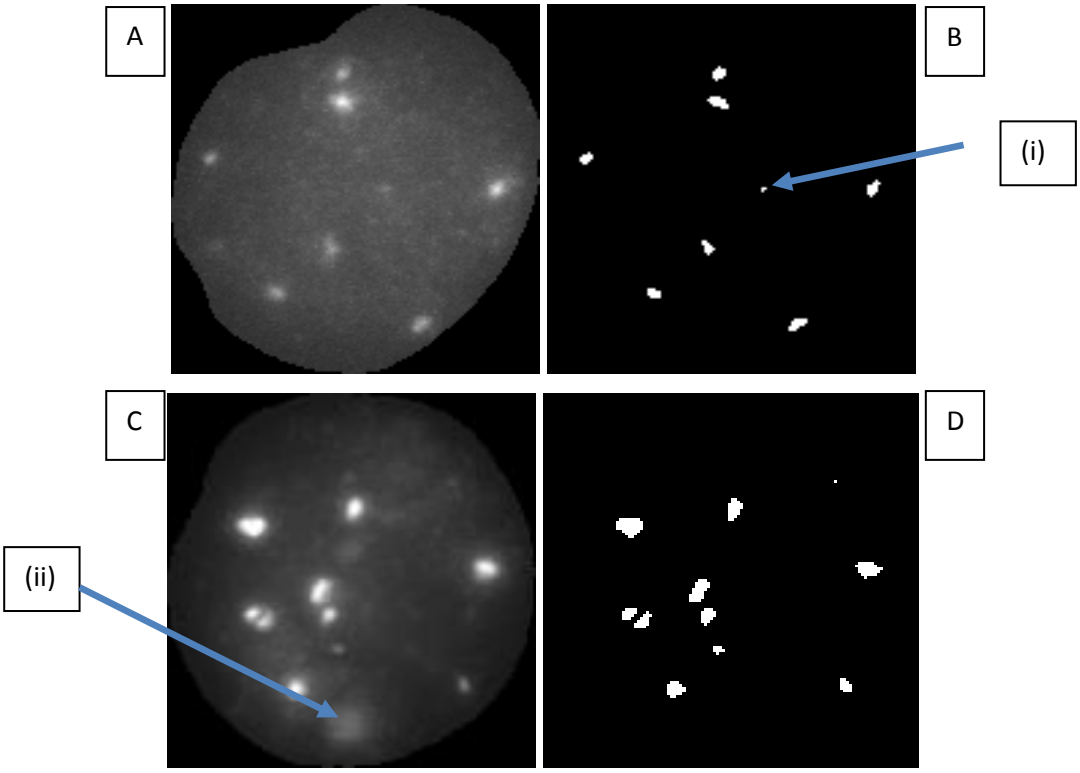

Figure 3.17 Example AutoRIF cropped and threshold images. A+B; Mid passage: 0.3 Gy 30 min example images. Minimum settings determined by batch testing were 1 pre-processing, medium laplasian sensitivity and 1 post filtering iteration. The minimum intensity threshold was determined as 89 and the minimum size was > than 6 pixels in area**. C+D. Late passage: 0.5 Gy 30 min example images.** Minimum settings determined as 2 pre-processing, medium laplasian sensitivity, and 1 post-filtering iteration. These initial settings determine the foci output, and then user defined minimum intensity and size cut-offs further determine what is classified as a focus. Image B highlights a focus that has been included in the threshold image but which will be excluded as it is below the minimum size cut-off (i). Image C shows a focus that would not be quantified by AutoRIF as it is below the required intensity (ii). Cropped image ~ 1320 x 1030 pixels in size.

3.3.1 Quantification of 53BP1 foci in mid passage NHBE cells by AutoRIF analysis

210-598 mid passage NHBE nuclei were analysed by AutoRIF for 53BP1 foci and compared with that previously obtained by manual analysis (table 3.5 and 3.3). A slightly lower average number of 53BP1 foci was seen 30 minutes after 0.3 Gy exposure (4.13 foci/nucleus compared to 5.3 foci/nucleus for AutoRIF and manual analyses respectively), while a significantly higher number was seen 30 minutes after 0.5 Gy (9.2 foci/nucleus compared to 6.8 foci/nucleus, P=0.0145) for AutoRIF and manual analysis respectively). Such differences may be as a result of a far larger population of nuclei being analysed by AutoRIF than by manual analysis and the inclusion of a higher proportion of smaller foci (discussed in section 3.5). Correlation between AutoRIF and manual analysis was seen 24 hours (1.63 foci/nucleus) after 0.3 Gy and 48 hours (1.05 and 0.96 foci/nucleus) after 0.3 and 0.5 Gy respectively, whereby AutoRIF determined that the average number of 53BP1 foci had decreased to sham (1.24 and 1.22 foci/nucleus in 24 and 48 hour sham).

Table 3.5 AutoRIF analysis of mid passage NHBE cells after exposure to 0.3 and 0.5 Gy.

Dose and time of fixation after IR exposure									
Total 53BP1 foci counted by AutoRIF	Sham			IR 0.3 Gy			IR 0.5 Gy		
	30 min	24 hr	48 hr	30 m	24 hr	48 hr	30m	24 hr	48 hr
Total nuclei scored	NA	598	483	301	440	406	516	210	346
Total small foci		689	481	1134	634	385	2863	255	292
Total medium foci		40	81	100	61	30	1397	37	22
Total large foci		14	27	10	21	11	466	11	18
Total foci in all nuclei		743	589	1244	716	426	4726	303	332
Average 53BP1 foci/nucleus									
Average Small foci	NA	1.15	0.99	3.75	1.44	0.95	5.54	1.21	0.84
% Small foci		93	82	91	89	90	61	84	88
Average Medium foci		0.07	0.17	0.33	0.14	0.07	2.71	0.18	0.06
% Medium foci		5	14	8	9	7	30	12	7
Average Large foci		0.02	0.06	0.03	0.05	0.03	0.90	0.05	0.05
% Large foci		2	5	1	3	3	10	4	5
Average Foci/nucleus in all nuclei		1.24	1.22	4.13	1.63	1.05	9.16	1.44	0.96
Average foci/nucleus (manual score)	1.22	0.77	1.06	5.29	1.17	1.00	6.76	0.87	1.37
Average 53BP1 foci in foci positive nuclei only	NA	2.54	2.64	5.00	3.19	2.40	10.48	2.70	1.97
% of foci positive nuclei		49.00	46.58	83.06	51.14	43.84	88.57	53.81	48.84
Average Small foci		2.35	2.15	4.55	2.82	2.17	6.37	2.27	1.73
Average Medium foci		0.14	0.37	0.40	0.27	0.17	3.09	0.33	0.14
Average Large foci		0.05	0.13	0.04	0.09	0.06	1.02	0.10	0.11

Table 3.5 summarises the average number of 53BP1 foci in mid passage NHBE cells as determined by AutoRIF analysis (No 30 minute sample was available for AutoRIF analysis due to slide breakage). The average number of 53BP1 foci determined by manual analysis of the same samples has been show for comparison. Focus size information has been represented here for section 3.5.

As shown in figure 3.18 the number of normal sham mid passage NHBE nuclei with 1 or more focus is 48%, which as expected increases to 83% and 89% 30 minutes after 0.3 and 0.5 Gy respectively, as a result of an increase in the number of nuclei containing damage. 24 hours after exposure this remains elevated at 51% (0.3 Gy) and 54% (0.5 Gy) but by 48 hrs the number of nuclei containing foci has returned to sham levels as damage is resolved to background.

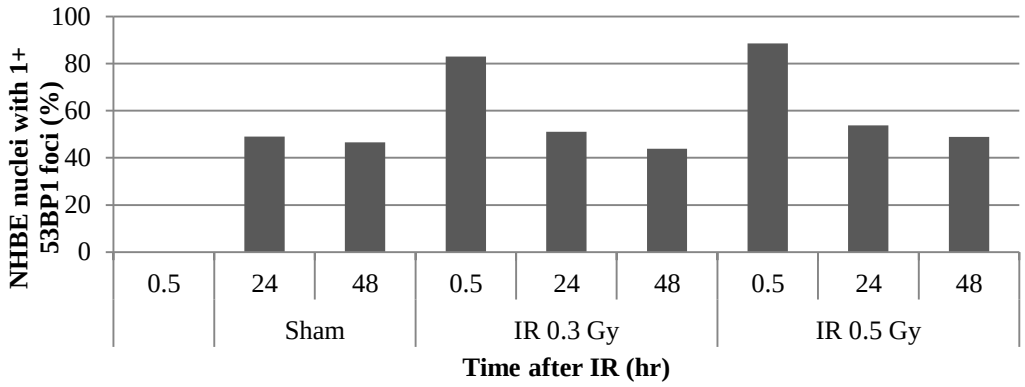

Figure 3.18 Percentage of mid passage NHBE cells with 1+ foci up to 48 hours after sham, 0.3 and 0.5 Gy exposure.

Figure 3.19 shows the distribution profiles of 53BP1 foci in mid-passage NHBE cells whereby 50-60% of sham nuclei have zero foci, and the remaining nuclei contain ~2-4 foci, directly correlating with the distribution of nuclei with zero foci detected by manual analysis (figure 3.10). After the shift in distribution of 53BP1 foci to the right as a result of IR exposure, the irradiated cells appear to have a similar distribution of 53BP1 foci to the sham cells at both 24 hours and 48 hours, supporting the earlier analysis that repair of the induced damage was completed by this time.

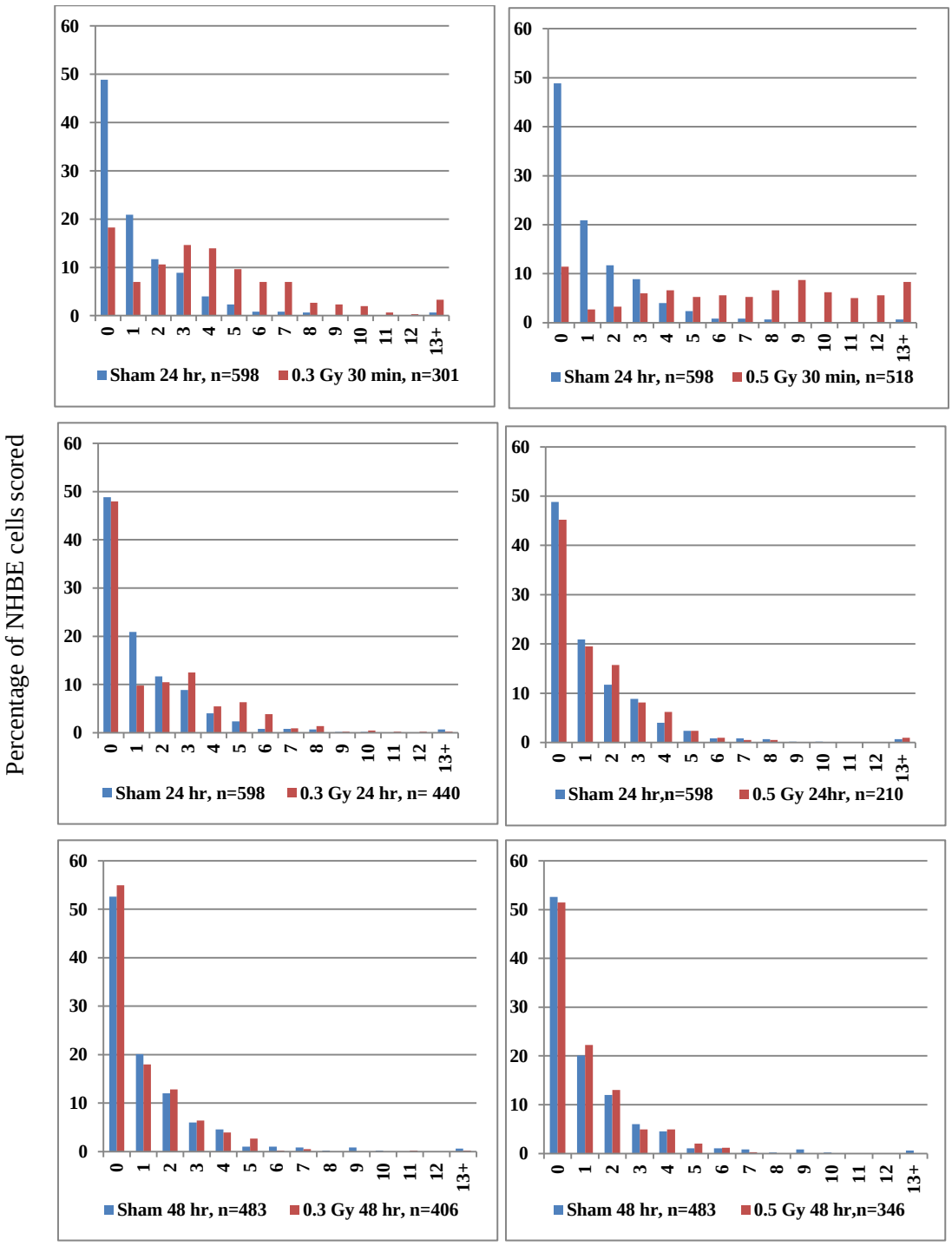

Figure 3.19 Distribution of 53BP1 foci in mid passage NHBE cells (AutoRIF).

3.3.2 Quantification of 53BP1 foci in late passage NHBE cells by AutoRIF analysis

In order to determine if there was an increase in 53BP1 foci background in aged NHBE cells as determined by manual analysis, the same samples were analysed using the automated capture and analysis script (section 2.5.2-2.5.3.2). Late passage NHBE cells analysed by AutoRIF showed a great deal more variation compared to the manual counts obtained in late-passage cells. This could reflect greater statistics for AutoRIF due to the increased numbers of cells and therefore may better reflect the actual amount of damage present or by contrast it may reflect technical issues with AutoRIF. The increased background seen in ageing sham nuclei may test the limits of the analysis program after lower dose exposures. Specifically, the average number of foci per nucleus at 30 minutes was 6.31 and 9.75 after 0.3 and 0.5 Gy respectively for AutoRIF (table 3.7) compared to 6.86 and 8.21 foci/nucleus scored manually (table 3.3 and figure 3.11). The average number of foci scored at 48 hours (4.13 foci/nucleus) and 216 hours (5.57 foci/nucleus) after 0.3 Gy, and 48 hours (5.23 foci/nucleus) after 0.5 Gy remains elevated compared to shams. However there is greater variation in sham background foci at all sampling times (range 2.55-4.29 foci/nucleus) compared to manual analysis (range 2.44-3.31 foci/nucleus).

Table 3.6 AutoRIF analysis of late passage NHBE after exposure to 0.3 and 0.5 Gy.

AutoRIF analysis of late passage NHBE cells									
Dose and time of fixation after exposure									
Total 53BP1 foci counted by AutoRIF	**Sham**			**IR 0.3 Gy**			**IR 0.5 Gy**		
	30 min	**48 hr**	**216 hr**	**30 m**	**48 hr**	**216 hr**	**30m**	**48 hr**	**216 hr**
Total nuclei scored	367	496	511	529	372	418	460	545	306
Total small foci	1302	969	1613	2607	1200	1886	3336	2398	843
Total medium foci	183	217	399	584	224	296	896	313	192
Total large foci	78	80	180	149	114	146	254	138	107
Total foci in all nuclei	1563	1266	2192	3340	1538	2328	4486	2849	1142
Average 53BP1 foci/nucleus									
Average Small foci	3.54	1.95	3.15	4.92	3.22	4.50	7.24	4.39	2.75
% Small foci	83	77	74	78	78	81	74	84	74
Average Medium foci	0.50	0.44	0.78	1.10	0.60	0.71	1.95	0.57	0.63
% Medium foci	12	17	18	17	15	13	20	11	17
Average Large foci	0.11	0.05	0.21	0.11	0.17	0.14	0.21	0.12	0.14
% Large foci	5	6	8	4	7	6	6	5	9
Average Foci/nucleus in all nuclei	4.26	2.55	4.29	6.31	4.13	5.57	9.75	5.23	3.73
Average foci/nucleus (manual score)	2.44	3.24	3.31	6.86	3.95	3.75	8.21	4.03	4.73
Average 53BP1 foci in foci positive nuclei only	4.98	3.19	4.87	6.85	4.64	6.00	10.61	5.75	4.33
% of foci positive nuclei	86.10	80.65	88.65	93.01	89.78	93.54	93.04	91.38	86.60
Average Small foci	4.15	2.44	3.59	5.35	3.63	4.86	7.90	4.84	3.19
Average Medium foci	0.58	0.55	0.88	1.19	0.67	0.77	2.11	0.63	0.73
Average Large foci	0.25	0.20	0.40	0.31	0.34	0.37	0.60	0.28	0.40

Table 3.6 summarises the average number of 53BP1 foci in late passage NHBE cells as determined by AutoRIF analysis. The average number of 53BP1 foci determined by manual analysis of the same samples has been show for comparison. Focus size information has been represented here for section 3.5.

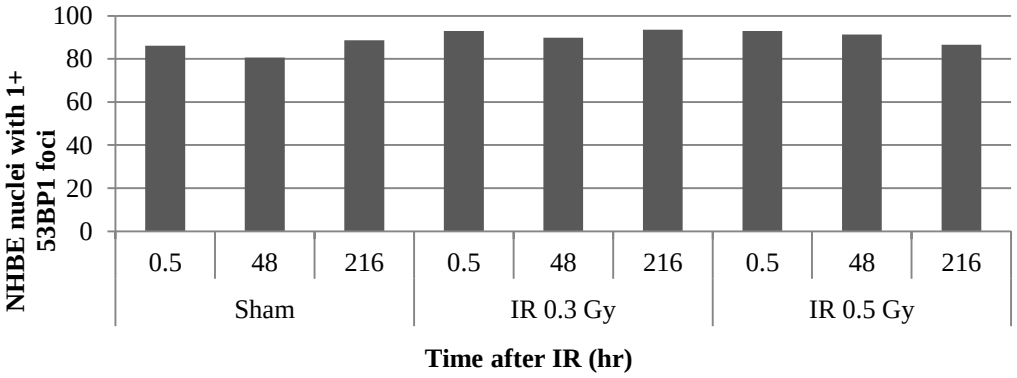

Figure 3.20 Percentage of late passage NHBE cell nuclei with more than one focus up to 216 hrs after 0.3 and 0.5 Gy exposure.

Interestingly, the percentage of late passage NHBE cells (figure 3.20) with more than 1 focus present does not change as markedly as with the mid passage cells (figure 3.18) after exposure to 0.3 or 0.5 Gy. 80-88% of late passage sham nuclei contain more than 1 focus, compared to 47-49% in mid passage sham nuclei. This again highlights the increased background level of 53BP1 foci in the late passage NHBE nuclei and also suggests that these radiation doses do not necessarily induce damage foci in all nuclei or the damage may be repaired in a proportion of nuclei prior to our earliest observation at 30 minutes.

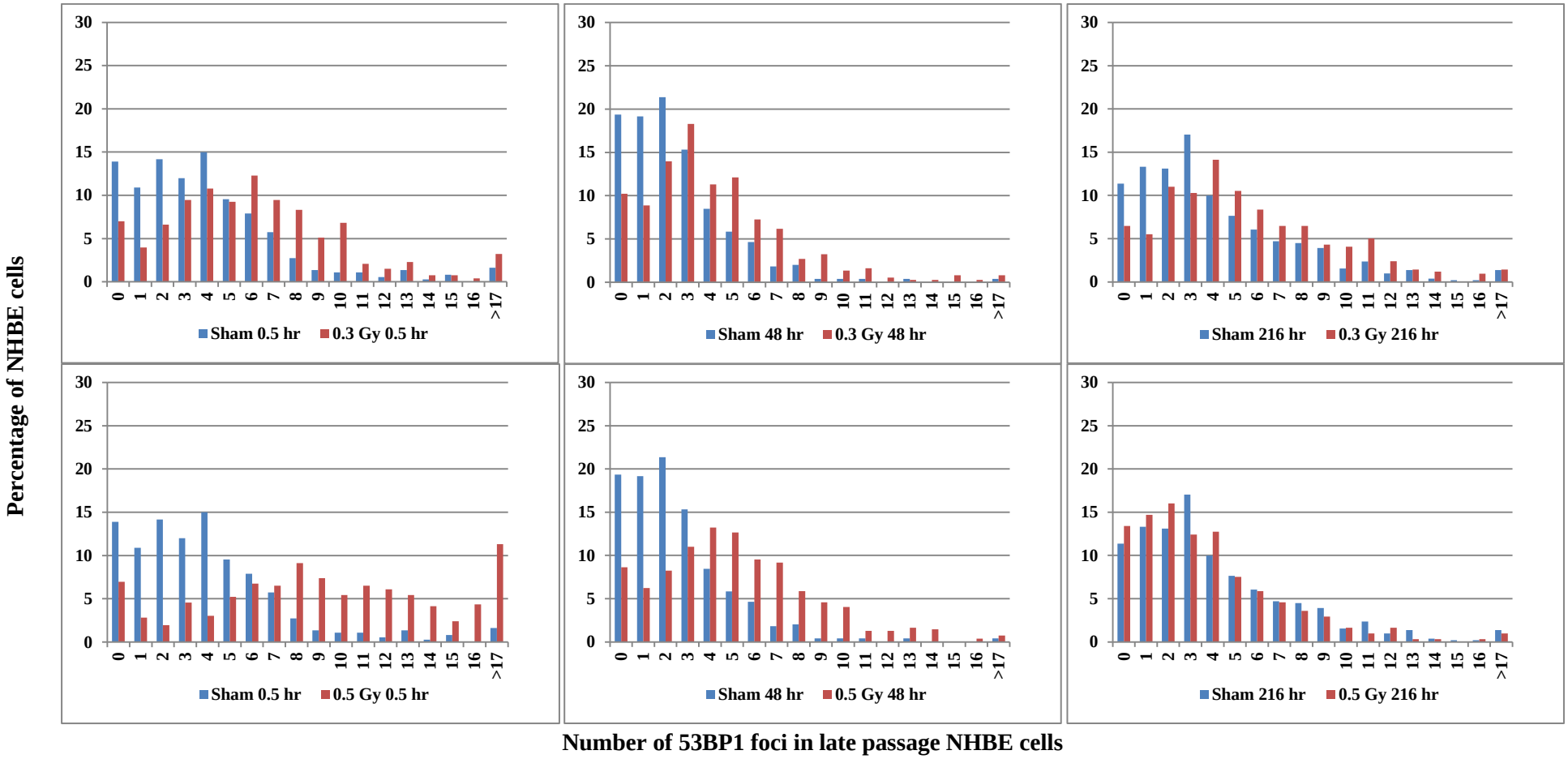

Figure 3.21 Distribution of 53BP1 foci in late passage NHBE cells after exposure to 0.3 Gy and 0.5 Gy (AutoRIF).

The frequency distribution graphs (3.21) of 53BP1 foci in ageing late-passage NHBE cells up to 216 hours after exposure to 0.3 and 0.5 Gy show an increase in the number of cells with increased 53BP1 foci in both sham and irradiated cells, compared to mid-passage NHBE exposed to the same dose. In late-passage sham nuclei there is a decrease in nuclei with zero foci compared to mid passage cells. This increase in background damage foci in late passage cells is shown by only 14, 19 and 11% of sham nuclei containing zero foci. In concordance with manual analysis however, 52, 64 and 53% of sham nuclei at 30 minutes, 48 hours and 216 hours respectively had between 2-4 foci. The initial induction of DNA damage after 0.5 Gy as determined by AutoRIF analysis shows a flattened distribution of foci with NHBE nuclei, therefore the NHBE cell nuclei contain a large variation of foci number. At 30 minutes, the majority of nuclei (53%) contained between 6-12 foci, and 29% contained between 12-16 foci which is comparable to manual analysis. Interestingly, it is clear from the graphs that 48 hours after exposure to 0.5 Gy, the distribution profile has not yet returned to sham, with 45% of the nuclei still containing between 4-7 foci and the trend appears similar to that seen 30 minutes after 0.3 Gy exposure. However, after 216 hours 56% of nuclei contained between 2-4 foci which is representative of sham.

3.3.3 Quantification of 53BP1 foci in NHBE cells up to 792 hours after exposure by AutoRIF analysis

In order to quantify 53BP1 foci number and size at extended times after IR exposure, ~500-2000 cell nuclei were analysed per timepoint by AutoRIF up to the extended time of 33 days after IR, with the exception of ~200 nuclei captured at 24 hr due to available cell numbers (see table 3.5 and 3.6 for exact numbers for each timepoint). As shown in table 3.7 AutoRIF analysis has shown no further increase in 53BP1 foci number up to 792 hrs after 0.3 Gy and 0.5 Gy exposure. By 24 hours after IR, P7 NHBE cells show generally good concordance with manual analysis after sham (1.23 foci/nucleus) compared to 1.10 foci/nucleus, and after 0.5 Gy (1.06 foci/nucleus) compared to 1.34 foci/nucleus for AutoRIF and manual analyses respectively). The average number of 53BP1 foci 24 hr after 0.3 Gy was slightly higher (1.28 foci/nucleus) than manual (0.75 foci/nucleus) but this is more than likely due to the smaller cell sample size at this time which will impact on the average foci numbers scored when not all nuclei will contain foci. AutoRIF analysis also determined that there was a reduction in average number of

53BP1 foci approximately 360 hours (P9) after exposure to all doses, which was seen during manual analysis also.

Table 3.7 AutoRIF analysis of NHBE cells cultured for up to 792 hours after 0.3 and 0.5 Gy exposure

Dose and time of fixation after exposure																							
Total 53BP1 foci counted by AutoRIF	**Sham**								**0.3 Gy**								0.5 Gy						
	24 hr	**48 hr**	**196 hr**	**384 hr**	**528 hr**	**624 hr**	**696 hr**	**792 hr**	**24 hr**	**48 hr**	**196 hr**	**384 hr**	**528 hr**	**624 hr**	**672 hr**	**792 hr**	**24 hr**	**48 hr**	**196 hr**	**360 hr**	**480 hr**	**648 hr**	**720 hr**
Total nuclei scored	190	567	405	1302	1040	964	1578	1870	120	410	767	734	2173	1963	1081	1324	249	453	631	1000	2336	1158	1458
Total small foci	204	445	407	1372	757	515	760	855	138	383	990	700	1472	1284	397	653	213	538	778	832	1319	813	844
Total medium foci	26	92	87	273	106	87	118	140	11	68	164	111	193	148	61	103	33	75	147	158	228	110	86
Total large foci	5	27	19	92	38	54	71	88	5	18	31	32	105	86	38	43	17	23	40	55	117	45	55
Total foci in all nuclei	235	564	513	1737	901	656	949	1083	154	469	1185	843	1770	1518	496	799	263	636	965	1045	1664	968	985
Average Small foci	1.06	0.78	1.00	1.05	0.73	0.53	0.48	0.46	1.14	0.93	1.29	0.95	0.68	0.65	0.37	0.49	0.85	1.19	1.23	0.83	0.56	0.70	0.58
% Small foci	87	79	79	79	84	79	80	79	90	82	84	83	83	85	80	82	81	85	81	80	79	84	86
Average Medium foci	0.14	0.16	0.21	0.21	0.10	0.09	0.07	0.07	0.09	0.17	0.21	0.15	0.09	0.08	0.06	0.08	0.13	0.17	0.23	0.16	0.10	0.09	0.06
% Medium foci	11	16	17	16	12	13	12	13	7	14	14	13	11	10	12	13	13	12	15	15	14	11	9
Average Large foci	0.03	0.05	0.05	0.07	0.04	0.06	0.04	0.05	0.04	0.04	0.04	0.04	0.05	0.04	0.04	0.03	0.07	0.05	0.06	0.06	0.05	0.04	0.04
% Large foci	2	5	4	5	4	8	7	8	3	4	3	4	6	6	8	5	6	4	4	5	7	5	6
Average Foci/nucleus in all nuclei	1.23	0.99	1.27	1.33	0.87	0.68	0.60	0.58	1.28	1.14	1.54	1.15	0.81	0.77	0.46	0.60	1.06	1.40	1.53	1.05	0.71	0.84	0.68
Average foci/nucleus (manual score)	1.10	0.95	1.68	1.51	2.17	1.43	1.14	1.23	0.75	1.64	1.70	1.67	1.17	1.28	0.91	0.48	1.34	1.47	1.69	2.00	1.03	1.14	0.80

Table 3.7 continued:

Dose and time of fixation after exposure																							
Total 53BP1 foci counted by AutoRIF	**Sham**								**0.3 Gy**								0.5 Gy						
	24hr	**48 hr**	**196 hr**	**384 hr**	**528 hr**	**624 hr**	**696 hr**	**792hr**	**24 hr**	**48hr**	**196 hr**	**384 hr**	**528 hr**	**624 hr**	**672 hr**	**792 hr**	**24 hr**	**48 hr**	**196 hr**	**360 hr**	**480 hr**	**648 hr**	**720 hr**
Average 53BP1 foci in foci positive nuclei only	2.13	1.93	2.15	2.21	1.95	1.77	1.62	1.69	2.31	2.06	2.30	2.02	1.93	1.98	1.46	1.68	1.77	2.31	2.36	1.94	1.80	2.01	1.86
% of foci positive nuclei	58.12	51.85	59.01	60.98	44.52	38.59	37.52	34.44	55.83	56.10	67.54	57.08	42.29	39.33	31.64	36.03	59.84	61.37	65.45	54.40	39.77	41.71	36.69
Average Small foci	1.85	1.52	1.71	1.74	1.64	1.39	1.29	1.34	2.06	1.68	1.92	1.68	1.60	1.67	1.16	1.38	1.43	1.95	1.90	1.54	1.43	1.69	1.59
Average Medium foci	0.23	0.32	0.36	0.35	0.23	0.23	0.20	0.22	0.18	0.30	0.32	0.27	0.21	0.20	0.18	0.22	0.22	0.27	0.36	0.30	0.25	0.23	0.16
Average Large foci	0.05	0.09	0.08	0.12	0.08	0.15	0.12	0.14	0.07	0.08	0.06	0.08	0.12	0.11	0.11	0.09	0.11	0.08	0.10	0.10	0.13	0.09	0.10

Table 3.7 shows the average number and size of 53BP1 foci in NHBE cells after exposure to 0.3 and 0.5 Gy and fixed between 24-720 hours.

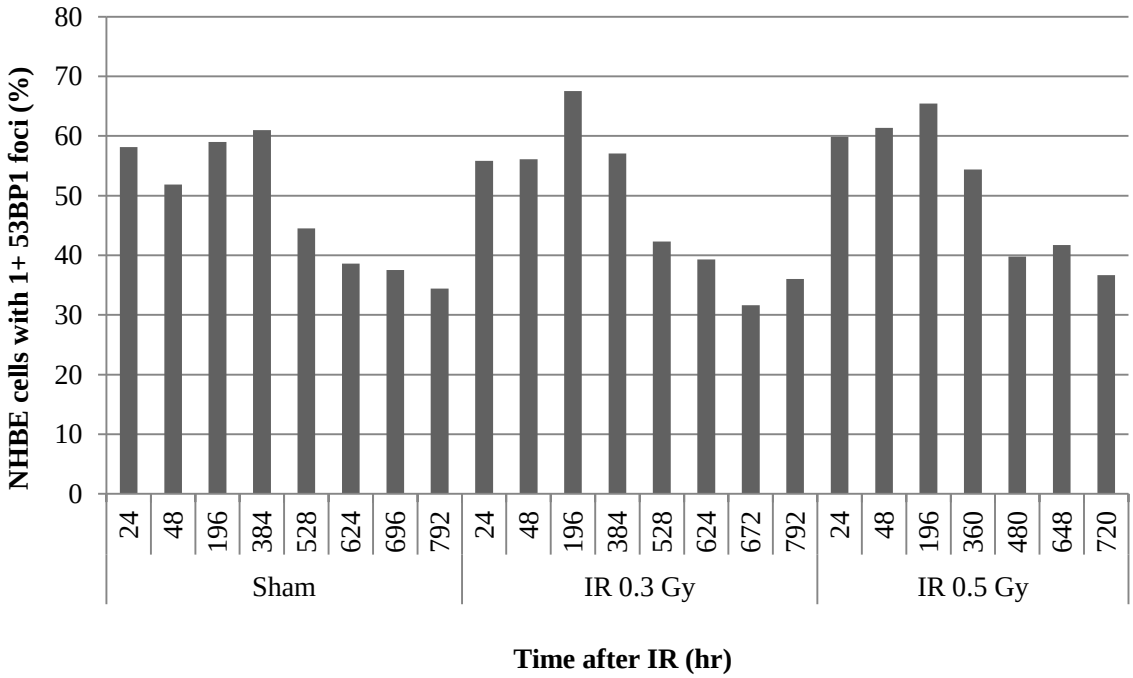

Figure 3.22 Percentage of NHBE cells with more than one focus up to 792 hrs after 0.3 and 0.5 Gy exposure.

The percentage of NHBE nuclei with 1+ foci 24-384 hours (P7-P9) after sham (range 52-61%), 0.3 Gy (56-67%) and 0.5 Gy (60-65%) (figure 3.22) was seen to be higher than the percentage of mid passage sham (47-49%), 0.3 Gy (44-51%) and 0.5 Gy (49-54%) that contained 1 + foci (3.18). This may be as a result of an age related increase in the number of nuclei that contain foci. However, as also described previously by manual analysis, there is a reduction in the number of NHBE cells with more than one focus from 528 hours onward at all doses which may be as a result of loss of the cells which contain 1+ foci or resolution of these foci. This can also be seen in the distribution plots, whereby the distribution of foci in consistent with sham, with the number of nuclei with foci decreasing even at extended times. This may represent ongoing repair, or the removal of the nuclei with foci from the proliferating population.

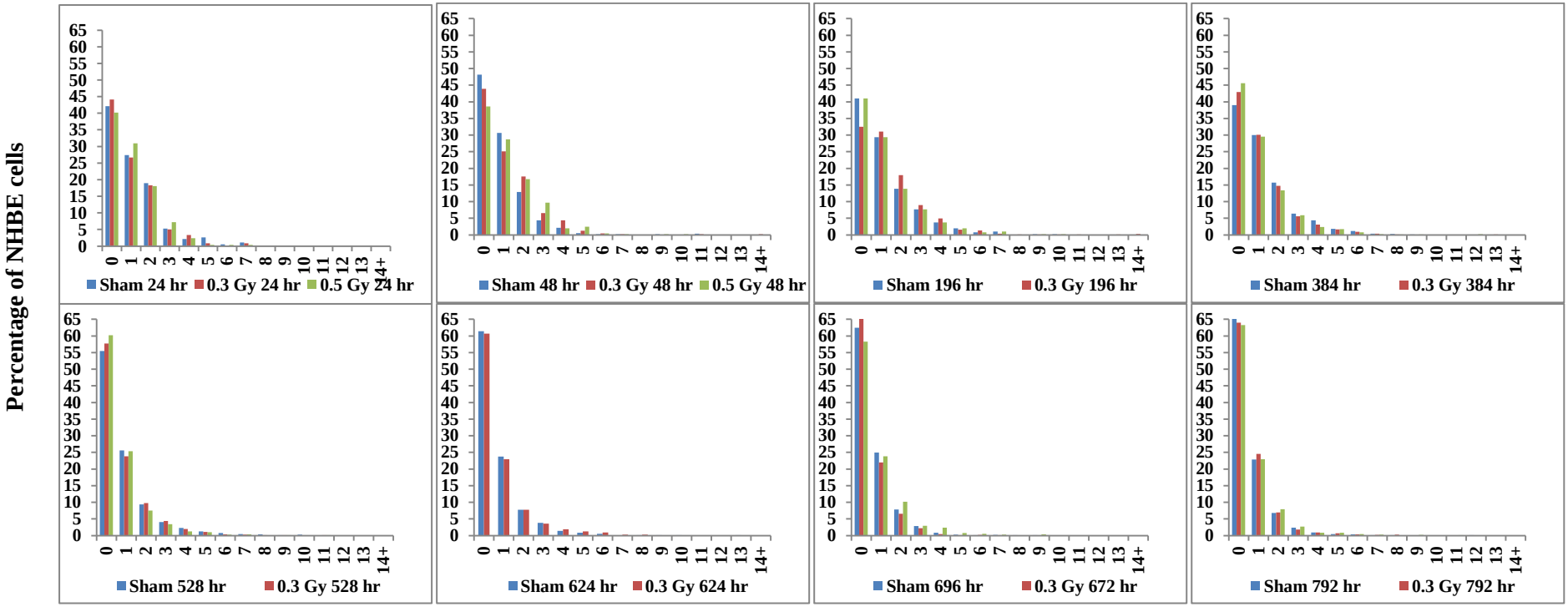

Figure 3.23 Distribution profiles of NHBE cells up to 792 hours after exposure to sham, 0.3 and 0.5 Gy.

No 0.5 Gy sample at P11 analysed by AutoRIF due to slide breakage (~624 hr),

3.4 Influence of ionising radiation exposure on cellular proliferation

In order to determine whether exposure to moderate to low doses of IR had any effect on the proliferative status of NHBE, and further to classify and visualise any trend in proliferative status with DNA DSB burden, 100-150 NHBE nuclei of varying passage were stained with primary antibodies rabbit anti human (Ki-67) or in combination with mouse anti human (53BP1) as described in 2.4.1. Secondary antibodies for the co-stain, goat anti rabbit (FITC) and goat anti-mouse AF568 were also prepared as a single aliquot. The visualised cells were then manually scored for their Ki-67 staining patterns using the FITC filter, and positive Ki-67 cells further categorised into type Ia, type Ib, or type II staining patterns as described by Bridger (Bridger, Kill & Lichter 1998). 53BP1 nuclear foci were manually scored as described in 2.6.2, by scrolling through the focal plane in a 3D manner for the same nuclei as scored for Ki-67 staining. Ki-67 proliferative staining and the number of 53BP1 foci per nuclei were classified in NHBE 0- 792 hours after exposure to 0 - 2 Gy γ-rays.

3.4.1 Ki-67 Staining in NHBE cells

Table 3.7 shows the Ki-67 negative and positive cells scored for mid passage (P5-P6) and late passage (P10/11) NHBE after sham and γ-ray exposure. The fraction of Ki-67 negative (non-proliferating cells, NP) in mid-passage nuclei is 25% (range 16-36%) (figure 3.25) compared to an average of 57% in late passage cells (range 43-62%) (table 3.8 and figure 3.26), highlighting the increase in the number of Ki-67 negative cells in cultures of increasing passage age. There appears to be no difference between the fraction of Ki-67 negative and positive cells at T0 compared to 30 minute shams, as well as by 30 minutes after exposure to 0.3, 0.5 and 2 Gy compared to sham, highlighting that there is no immediate change in the fraction of NP cells after exposure.

216 hours after exposure of late passage NHBE cells to 0.3 Gy, the Ki-67 negative fraction is shown to be 73% compared to 61% in sham, which may represent an increase in the NP fraction of cells at later times after 0.3 Gy exposure. This is not seen 216 hours after 0.5 Gy, which is consistent with sham fractions scored (61%). Therefore, although the fraction of NP cells increases with age as expected, there is no clear evidence of an increase in NP cells after IR for the duration of analysis as visualised by Ki-67 at the sampling times thus far examined. This is also the case after exposure to a higher dose of 2 Gy visualised over 168 hours where the fractions of Ki-

67 negative cells were the same for both sham and irradiated nuclei, with the exception of a contrasting increase in the Ki-67 positive fraction 30 minutes after exposure (55% Ki-67 negative) compared to sham (43% Ki-67 negative) (table 3.8 and figure 3.27).

Although NHBE cells grow as a non-synchronous culture, which may also account for the slight variation between samples in sham nuclei for Ki-67 scoring, ~70-90% of the total proliferating cells were scored as being of type II distribution (where Ki-67 is restricted to the nucleoli in late G_1, G_2 and S phases of the cell cycle, data not shown), irrespective of passage age or radiation exposure. This may correspond with FACS data from our group that showed ~80% of cells to be in G1 phase during normal subculture. The remaining small fraction of proliferative cells were stained predominately as type Ib cells, and a consistently small fraction of cells were scored with type Ia distribution representative of very early G_1, again irrespective of passage age in sham and irradiated nuclei.

Table 3.7 Proliferative status of mid passage NHBE cells after exposure to 0.3 and 0.5 Gy.

Age of NHBE	Timepoint (PI) and dose	Number of Nuclei scored (%)	
		Ki-67 negative	Total Ki-67 positive
Passage 5 (n=100)	Sham 30mins	26	74
	Sham 24hr	16	84
	Sham 48hr	21	79
	0.3 Gy 30	38	62
	0.3 Gy 24hr	23	77
	0.3 Gy 48hr	27	73
	0.5 Gy 30 mins	30	70
	0.5 Gy 24hr	39	61
	0.5 Gy 48hr	33	67
Passage 6 (n=100)	T0	32	68
	Sham 30 mins	36	64
	Sham 24hr	18	82
	Sham 29hr	23	77
	0.3 Gy 30m	35	65
	0.3 Gy 24hr	22	78
	0.3 Gy 29hr	46	54
	0.5 Gy 30 mins	37	63
	0.5 Gy 24hr	30	70
	0.5 Gy 29hr	23	77

Table 3.8 Proliferative status of late passage NHBE cells after exposure to 0.3, 0.5 and 2 Gy.

Age of NHBE	Timepoint (PI) and dose	Number of Nuclei scored (%)	
		Ki-67 negative	Total Ki-67 positive
Passage 10 (n = 150)	Sham 30 mins	43	57
	Sham 48 hr	59	41
	Sham 168 hr	61	39
	2 Gy 30 mins	55	45
	2 Gy 48 hr	60	40
	2 Gy 168 hr	57	43
Passage 10/11 (n=150)	Sham 30 mins	56	44
	Sham 48 hr	62	38
	Sham 216 hr	61	39
	0.3 Gy 30 min	51	49
	0.3 Gy 48hr	63	37
	0.3 Gy 216 hr	73	27
	0.5 Gy 30 min	46	54
	0.5 Gy 48 hr	62	38
	0.5 Gy 216 hr	61	39

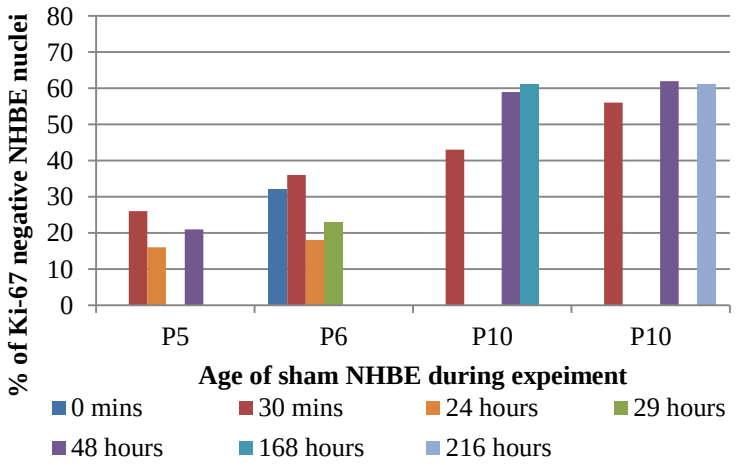

Figure 3.24 Fraction of Ki-67 negative NHBE cells in sham nuclei of varying passage age.

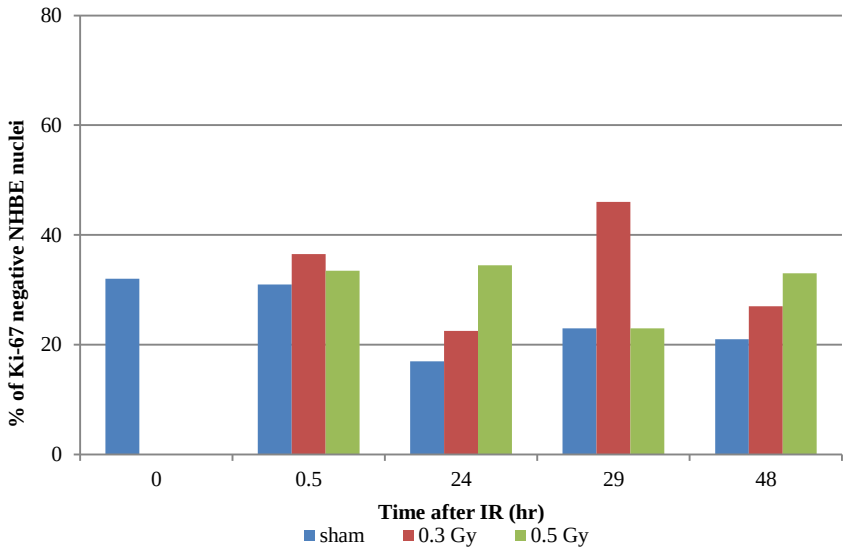

Figure 3.25 Senescent fraction (Ki-67 negative) of mid passage NHBE cells up to 48 hours after 0.3 and 0.5 Gy exposure. Sham 0-48 based on average of n=2.

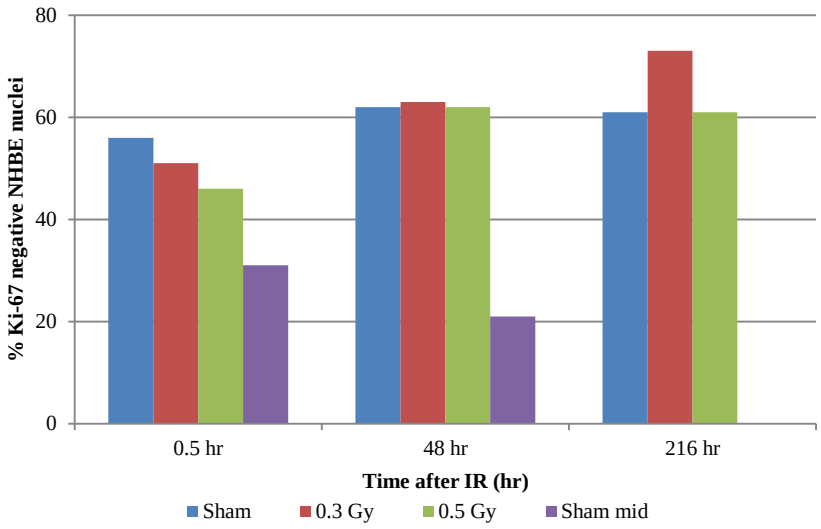

Figure 3.26 Senescent fraction (Ki-67 negative) in late passage NHBE cells up to 216 hours after 0.3 and 0.5 Gy exposure. N=1.

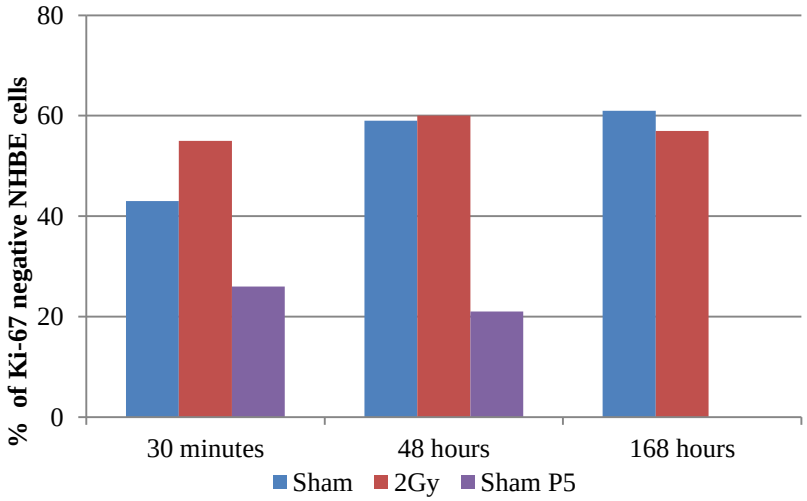

Figure 3.27 Senescent fraction (Ki-67 negative) of late passage NHBE cells up to 168 hours after 2 Gy exposure. N=1.

The Ki-67 negative fraction of NHBE cells during continued subculture for up to 792 hours after sham, 0.3 and 0.5 Gy exposure is shown in table 3.9 and figure 3.28. Cells were irradiated at P7 and then cultured to P13 and stained for Ki-67 as described in 2.5.1 and 2.5.1.1. The fraction of Ki-67 negative nuclei at P7 after sham (39%), 0.3 Gy (33%) and 0.5 Gy (39%) appears to correlate with the range seen in previous Ki-67 stained mid passage cells (table 3.7; range = 16-46%) and is therefore suggestive of a gradual increase as expected. These observed fractions appear to remain relatively unchanged up to approximately 384 hours (corresponding to P9) after sham, 0.3 and 0.5 Gy exposure, albeit the variation that is clearly seen (range 33-53% Ki-67 negative) up to this time. However, most notably after this point there does not appear to be any further evidence of an increase in the number of Ki-67 negative cells with increasing passage, and as such, the late passage P10 Ki-67 fractions (range 28-37%) do not reflect those seen previously in cells of similar passage age (table 3.8; range = 43-73%). Instead the fraction of Ki-67 negative cells in P10-P13 NHBE cells appears to remain almost constant before dropping to 18-30% Ki-67 negative by 792 hours (P13). These later results are therefore not representative of what has been previously shown and suggests that differences in the culture duration of the NHBE may impact on the preservation of NHBE (namely non-proliferating Ki-67 negative) cells within culture.

Table 3.9 Proliferative status of P7 NHBE cells exposed to 0.3 and 0.5 Gy and cultured to P13.

Dose	Time after IR	Percentage Ki-67 negative
Sham	24	39
	48	50
	196	30
	384	41
	528	28
	624	35
	686	27
	792	18
0.3 Gy	24	33
	48	37
	196	34
	384	53
	528	37
	624	34
	672	33
	792	30
0.5 Gy	24	39
	48	39
	196	51
	360	40
	460	29
	552	27
	648	31
	720	19

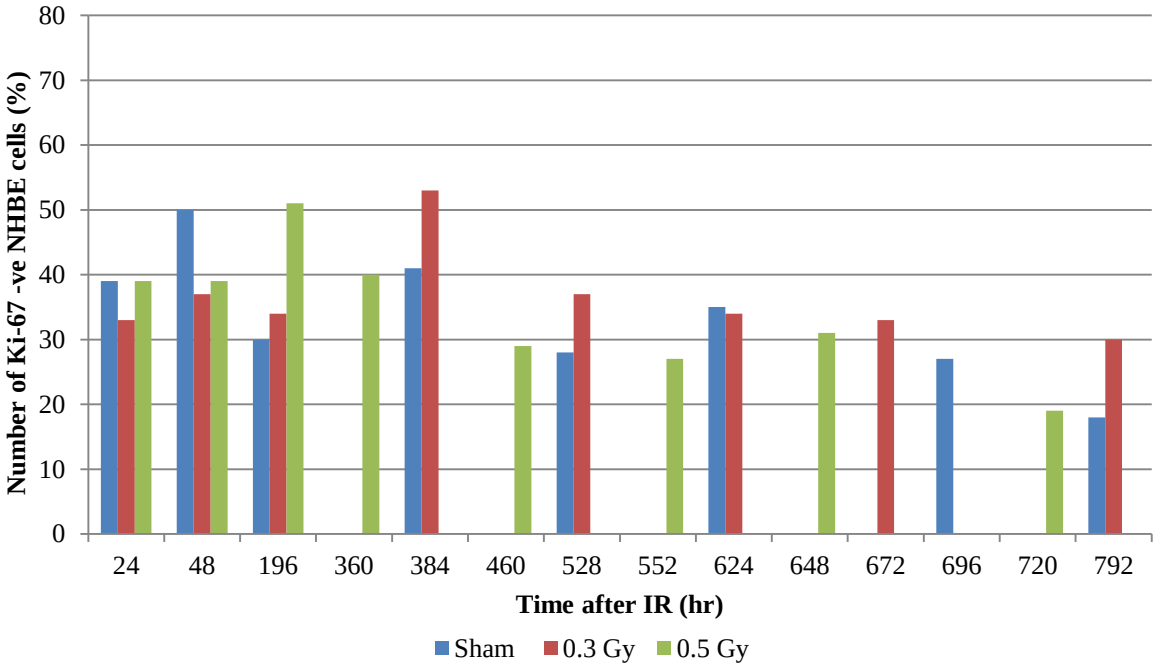

Figure 3.28 Senescent fraction (Ki-67 negative) of NHBE cells up to 792 hours after 0.3 and 0.5 Gy exposure.

3.4.2 Distribution of 53BP1 foci in proliferating and non-proliferating NHBE cells.

Co-staining NHBE with antibodies against Ki-67 and 53BP1 as described in 2.4 allowed us to further classify cells with DSB burden into their proliferative status and to determine if there was any trend between cells with increased or persisting DSB burden, and the stage of the cell cycle they were in.

In mid (figure 3.29), late (figure 3.30), and mid-late (figure 3.32A-C) passage NHBE cells that were exposed to sham, 0.3 and 0.5 Gy, and late passage NHBE exposed to 2 Gy (figure 3.31), it is possible to visualise the distribution of 53BP1 DNA damage foci in both proliferative (Ki-67 positive, green line) and non-proliferative (Ki-67 negative, blue line) cells and see how this changes over time. Irrespective of passage age and dose, the induction of 53BP1 DNA damage foci was shown to be the same in both proliferating and non-proliferating (senescent) NHBE cells showing that damage is induced to the same efficiency irrespective of proliferative status. The trends shown in figure 3.29 alter according to cell passage whereby Ki-67 positive cells dominate in mid-passage cells while Ki-67 negative cells dominate in late passage cells (figure 3.30 and 3.31). This therefore correlates with negative cells containing the majority of the foci by late passage. According to the graphs, there is no obvious difference in the processing of 53BP1 foci in mid passage cells however there is a suggestion that processing of foci and DSB may be altered between proliferating and senescent cells in late passage cells. Specifically, up to 216 hours after 0.5 Gy, the number of senescent NHBE cells that contain >6 foci per nucleus, remains higher than in sham nuclei.

In order to determine if there was any increase in DNA damage burden in either Ki-67 negative or positive cells at later times after IR, NHBE were observed up to 792 hours after IR. The distribution of 53BP1 foci in both Ki-67 negative and positive NHBE (P7 onwards) shows the same distribution as seen in NHBE irradiated at mid passage (P5). However, approximately 384 hours (P9) after all dose exposures the number of Ki-67 negative cells actually decreases at each passage rather than increases, as shown before. As a result of the Ki-67 negative data not being consistent with previous experimental results it is difficult to determine if this is a real effect of the cells being removed from the population by apoptosis, or due to technical design. As previously shown by our data and the literature, the fraction of Ki-67 negative cells within an ageing culture will

increase as the culture becomes senescent and therefore it is probable that a technical error in passage has meant that the whole cell populations have not been removed from the flasks at passage and their numbers decreased with each passage, or that senescent Ki-67 negative NHBE cells do not continue to adhere during frequent subculture. As a result, NHBE cells at the later observation times represent the Ki-67 positive population containing foci. As with NHBE cells exposed at mid passage and late passage, the distribution of 53BP1 foci is the same in both senescent (Ki-67 negative) and proliferating (Ki-67 positive) NHBE up to 792 hours after IR (figure 3.32A-C), and there is no increase in Ki-67 negative NHBE with increased damage burden up to 792 hours after 0.3 Gy (figure 3.32B) and 0.5 Gy (figure 3.32C) compared to sham (figure 3.32A).

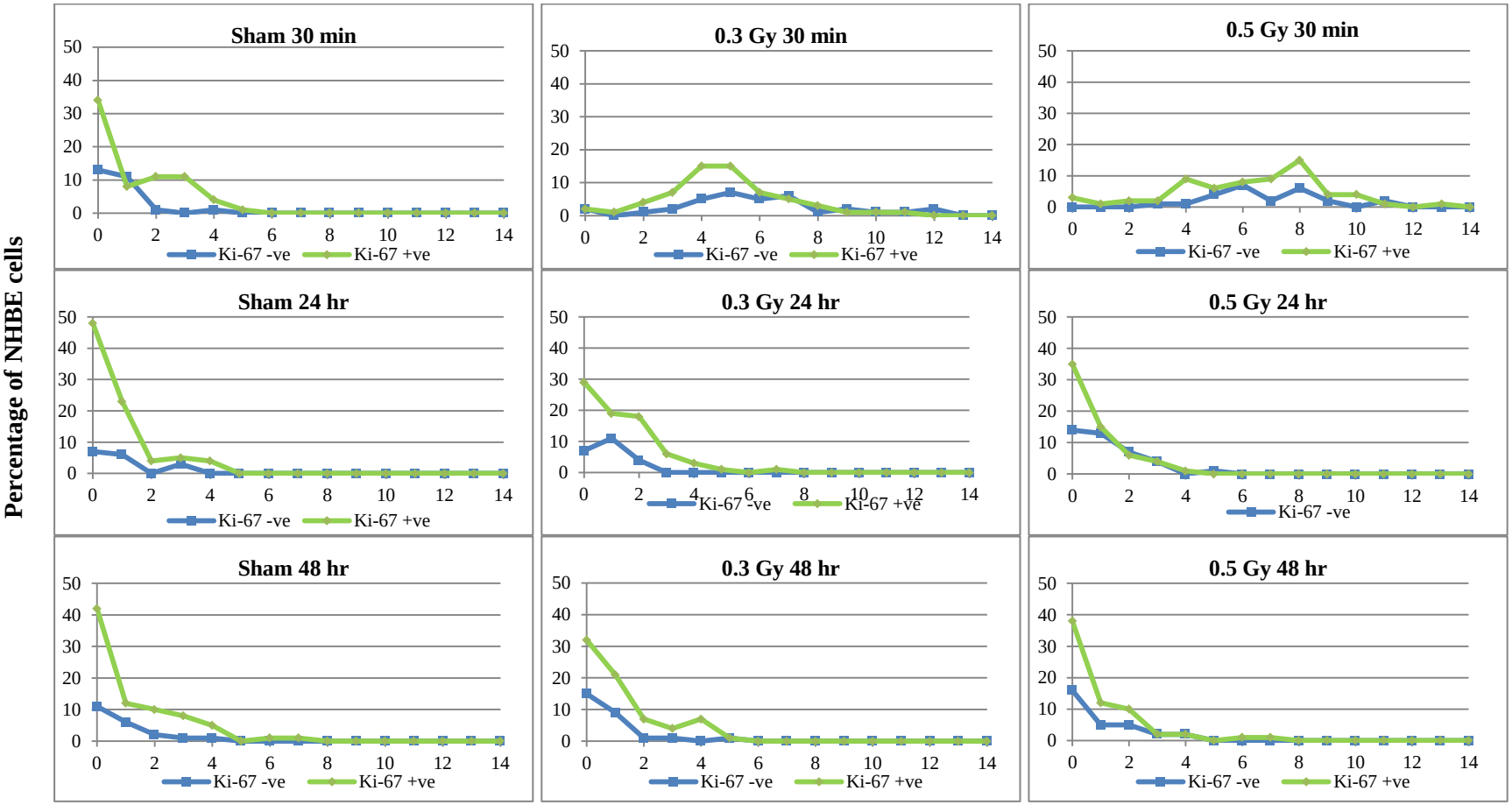

Figure 3.29 Mid passage Ki-67 and 53BP1 co-stained NHBE nuclei after 0.3 and 0.5 Gy.

Blue line represents Ki-67 –ve nuclei and green line represents Ki-67 + nuclei.

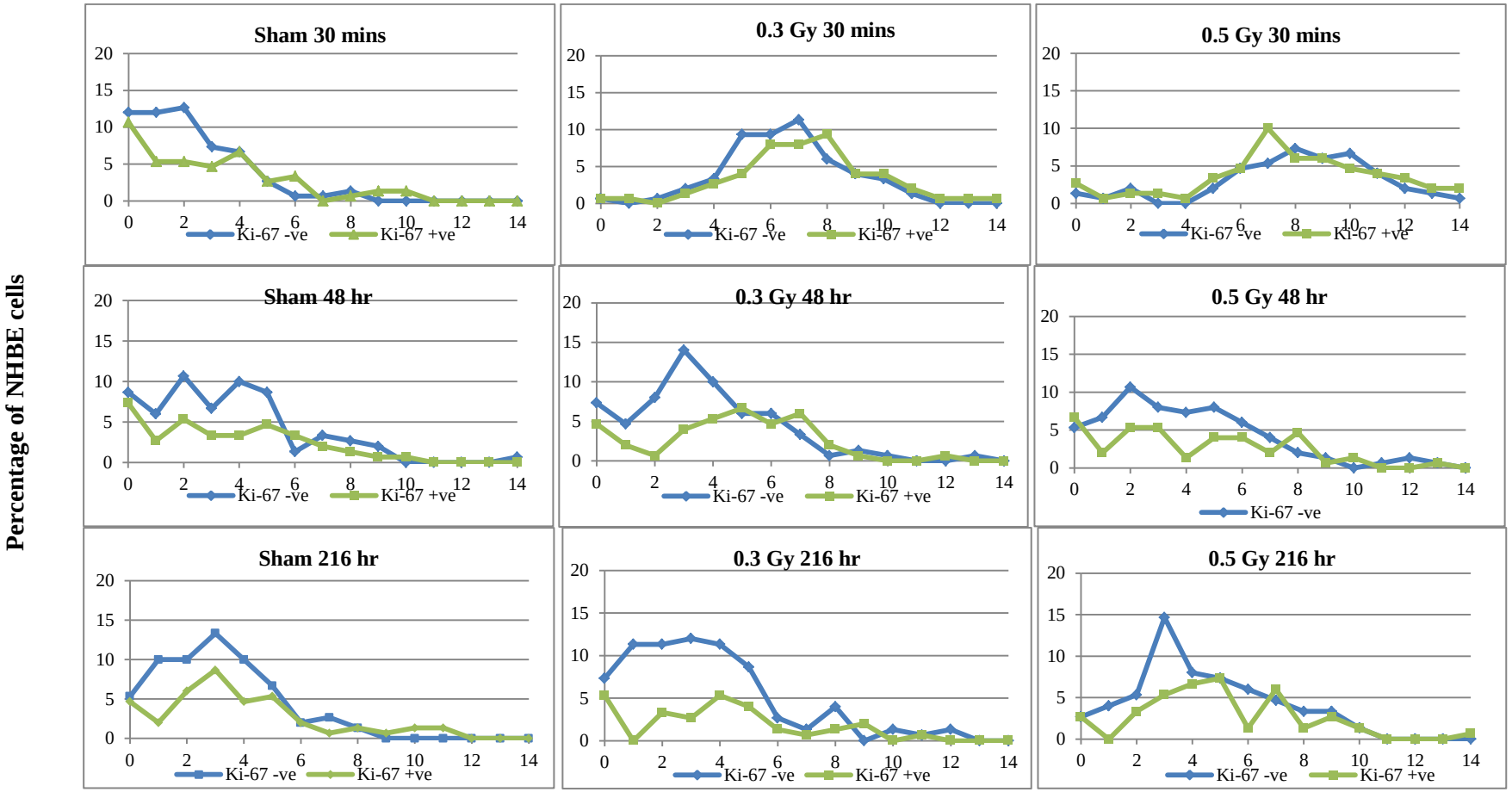

Figure 3.30 Late passage Ki-67 and 53BP1 co-stained NHBE nuclei after 0.3 and 0.5 Gy.

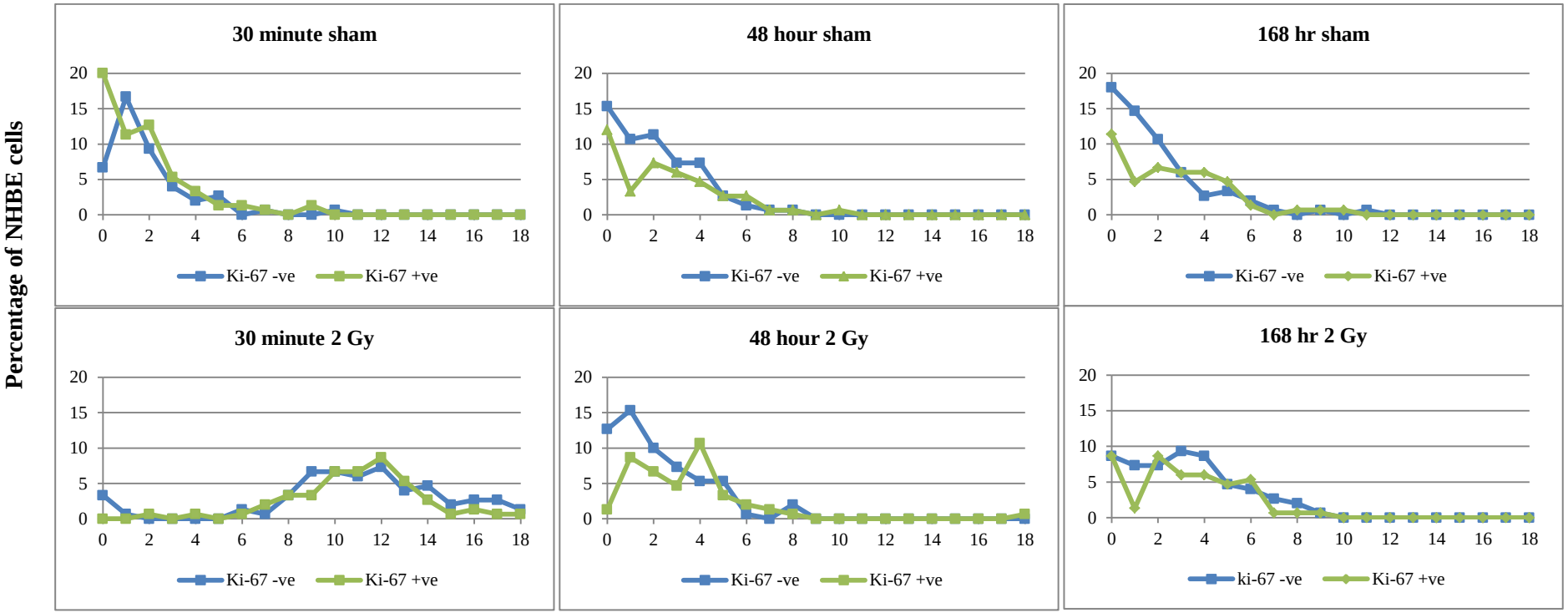

Figure 3.31 Late passage Ki-67 and 53BP1 co-stained NHBE nuclei after 2 Gy.

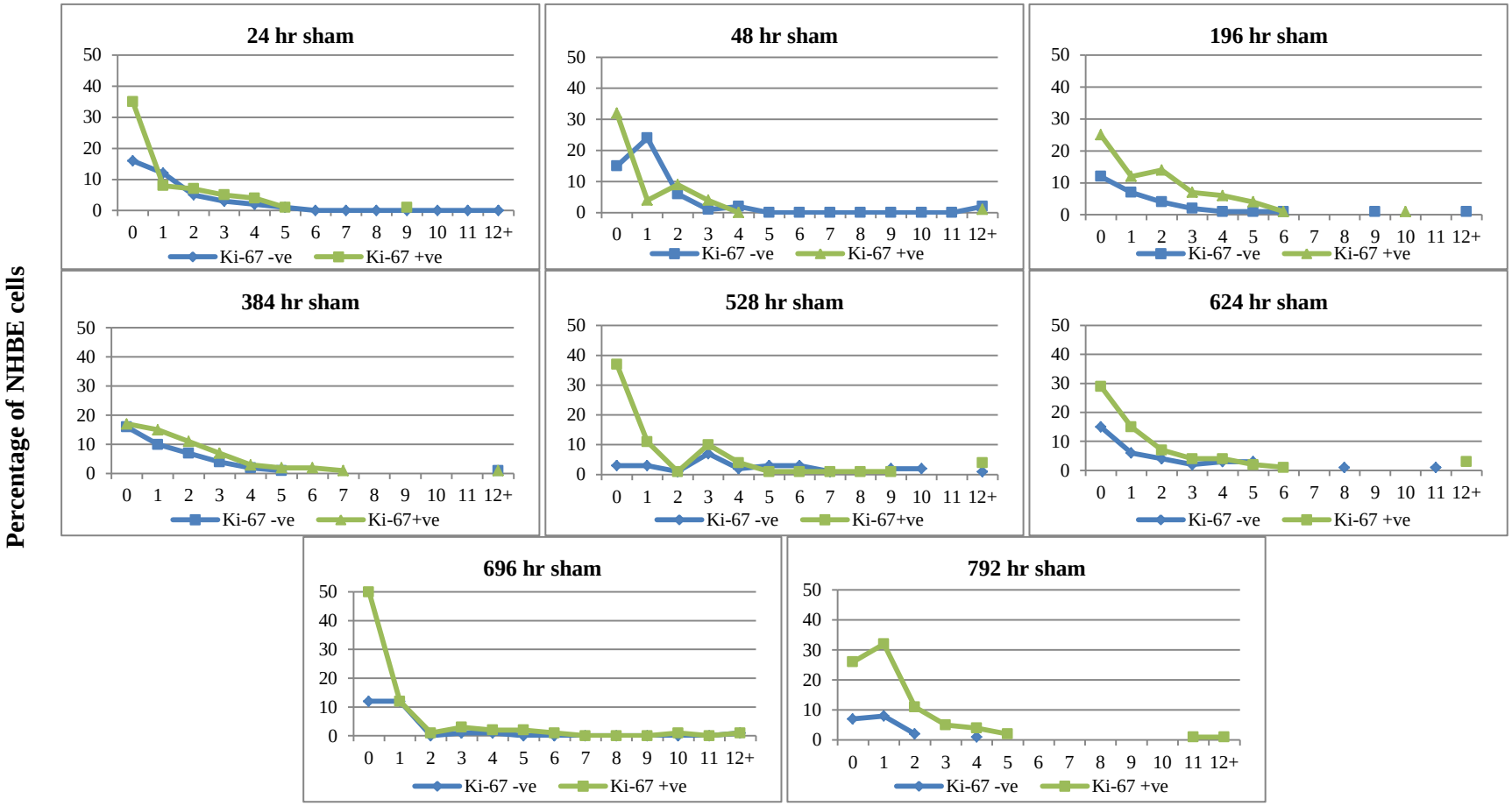

Figure 3.32A Long-term analysis of Ki-67 and 53BP1 co-stained sham NHBE nuclei.

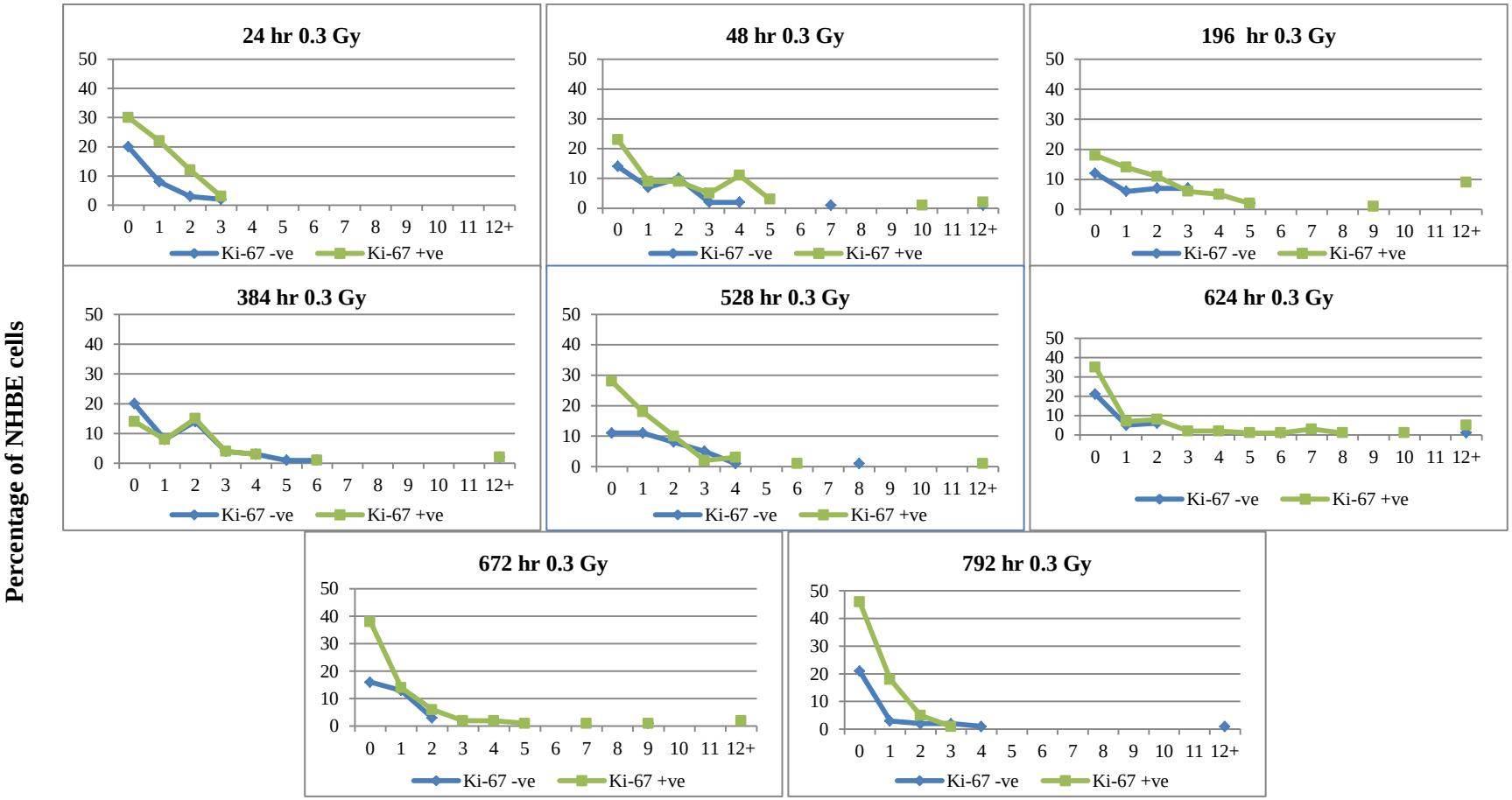

Figure 3.32B Long-term analysis of Ki-67 and 53BP1 co-stained NHBE nuclei after 0.3 Gy.

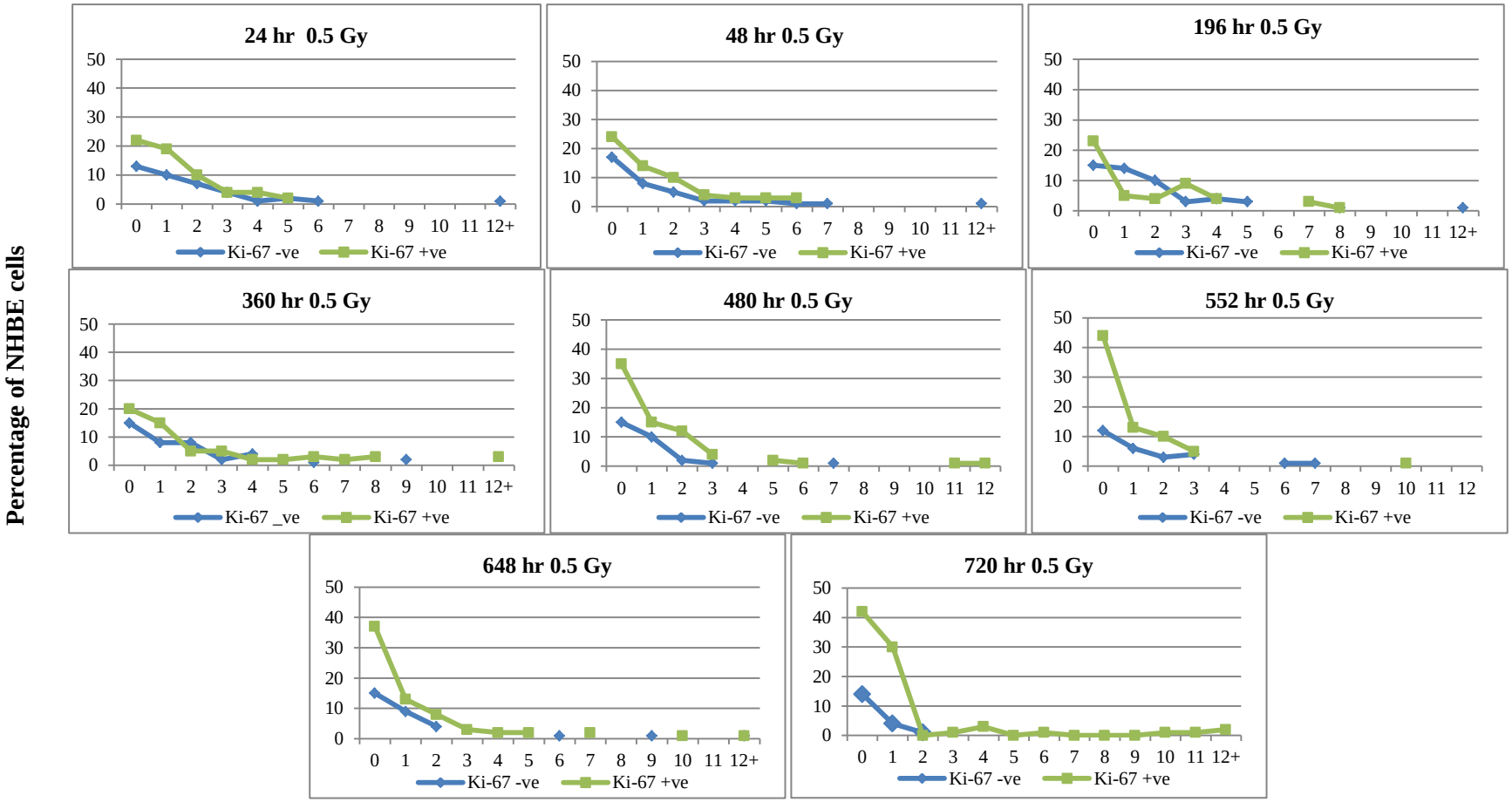

Figure 3.32C Long-term analysis of Ki-67 and 53BP1 co-stained NHBE nuclei after 0.5 Gy.

3.5 Average size of 53BP1 foci in mid and late passage NHBE determined by AutoRIF analysis.

As well as looking at the increase in DSB burden in NHBE cells after exposure to ionising radiation, the AutoRIF analysis system also allowed calculation of focus size (represented here in pixel size). This therefore allowed us to further classify foci into size integers and determine if there is a dose or time-related increase in focus size, or persistence of larger 53BP1 foci after exposure to 0.3 and 0.5 Gy. This will also allow us to see if there is any difference between the focus size in young and aged cells so far.

In order to categorise focus area which were generated within an excel output sheet from running part 2 of the AutoRIF analysis script, the focus sizes were categorised into small (6-50 pixels = <0.5µm), medium (51-100 = 0.5-1.0µm) and large (100+ = >1.0µm) categories as described in 2.5.3.2. The size categories, along with the minimum intensity and minimum size thresholds that are determined for each experiment by the user, allow for any foci that are not above the minimum thresholds to be excluded. Anything above these thresholds is then grouped into the categories according to size.

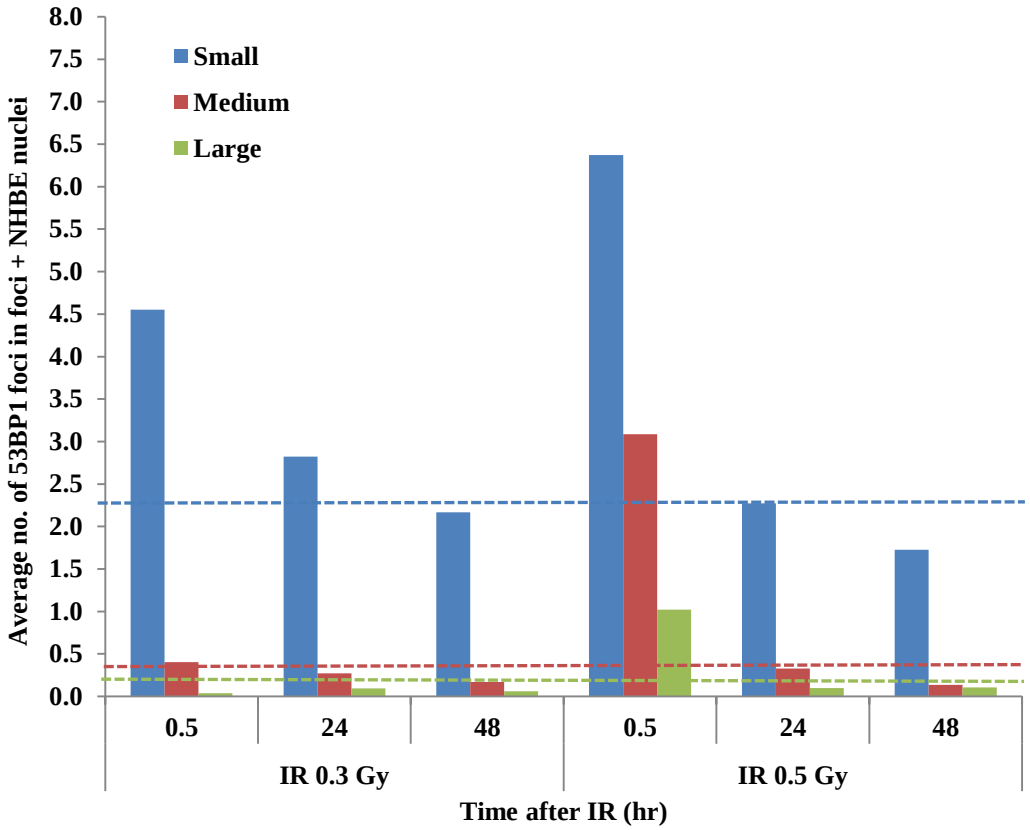

Figure 3.33 AutoRIF analysis of average 53BP1 foci number in foci positive mid passage NHBE cells up to 48 hours after 0.3 and 0.5 Gy exposure. Average number of small,

medium and large foci counted in mid passage (P5) foci positive NHBE cells by AutoRIF. Dashed lines represent average number of small (blue line; 2.25), medium (red line; 0.25) and large (green line; 0.09) 53BP1 foci in mid passage foci positive sham NHBE nuclei only. NB: there is no 30 minute sham for AutoRIF of mid-passage NHBE (due to slide breakage); the 24 hour sham shall be used.

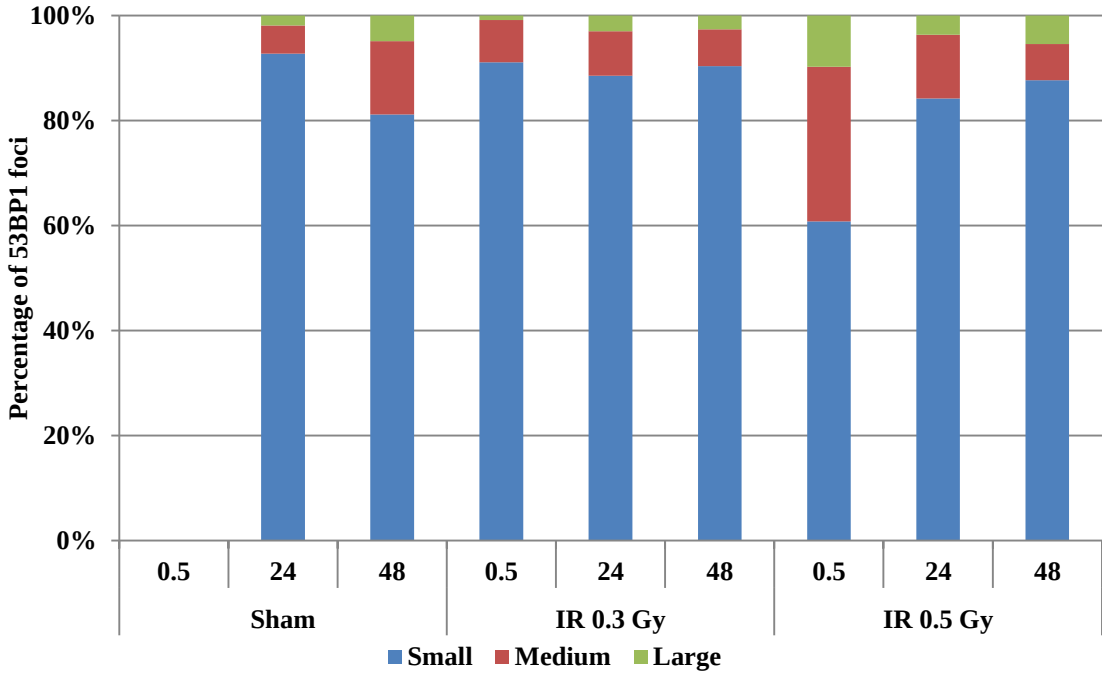

Figure 3.34 AutoRIF analysis of 53BP1 foci size in foci positive mid NHBE cells up to 48 hours after exposure to 0.3 and 0.5 Gy.

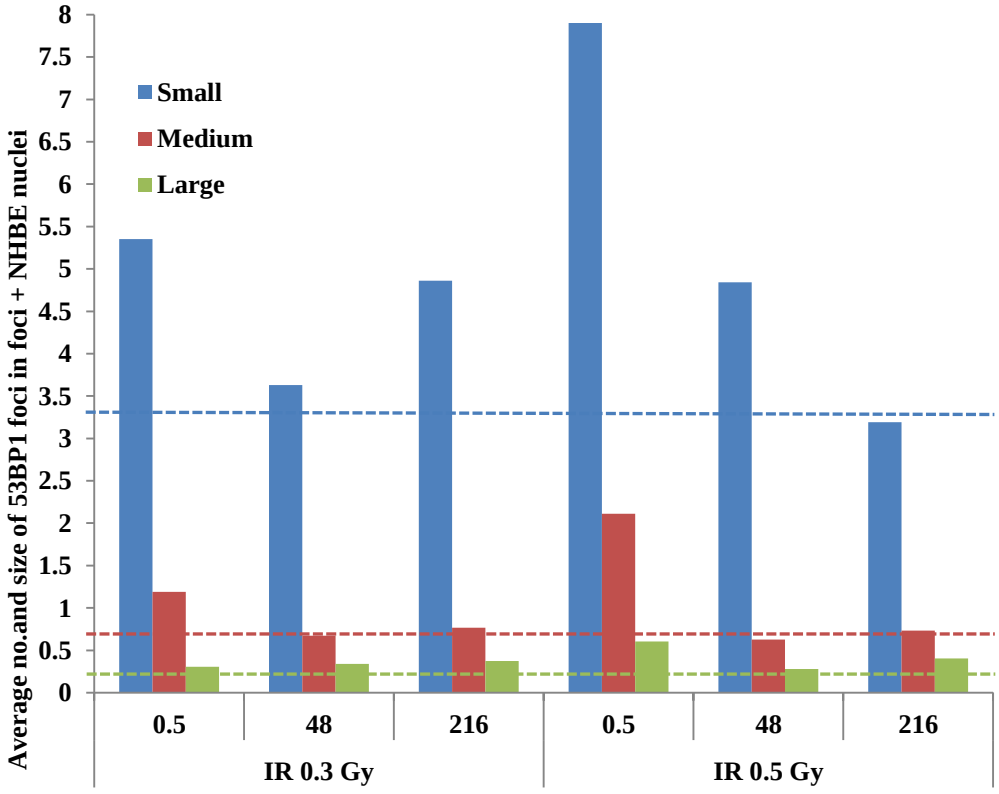

Figure 3.35 AutoRIF analysis of average 53BP1 foci number in foci positive late passage NHBE cells up to 216 hours after 0.3 and 0.5 Gy exposure. Average number of small, medium and large foci counted in late passage (P10) foci positive NHBE cells by AutoRIF. Average number of small (blue line; 3.39), medium (red line; 0.67) and large (green line; 0.28) 53BP1 foci in late passage foci positive, sham NHBE nuclei.

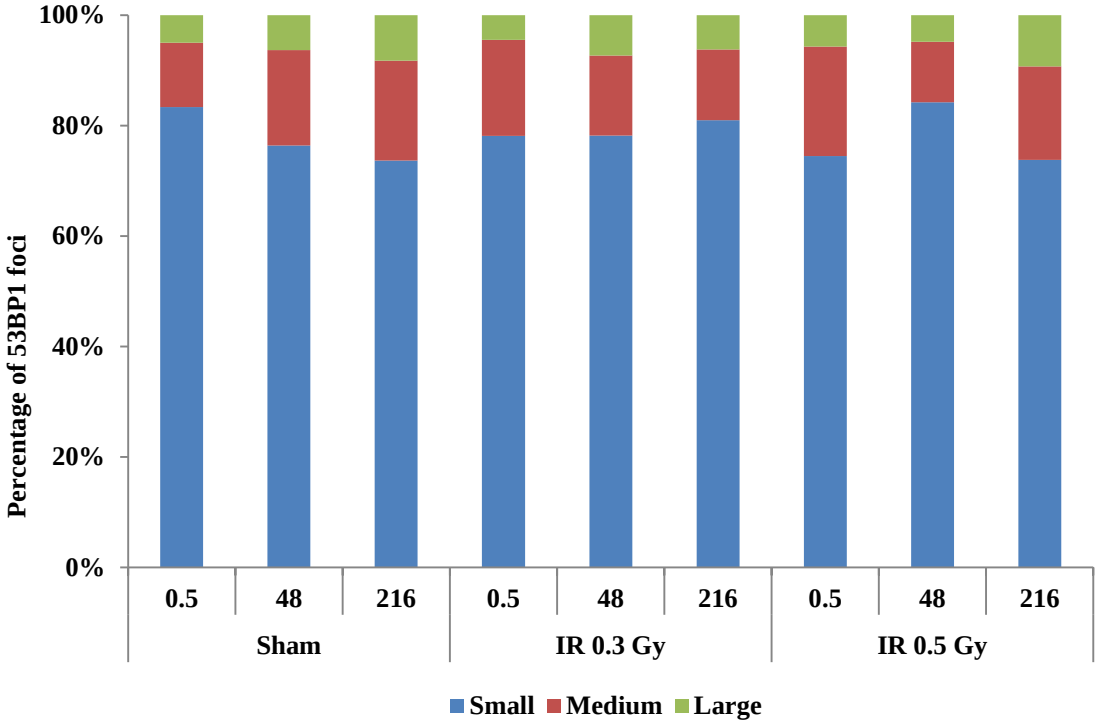

Figure 3.36 AutoRIF analysis of 53BP1 foci size in foci positive mid NHBE cells up to 216 hours after exposure to 0.3 and 0.5 Gy.

As represented by figure 3.39A the average focus area (pixels) is 22 and 33 pixels in mid passage 24 hour and 48 hour shams, compared to 34, 40, and 44 pixels in late passage 30 minute, 48 hr and 216 hour shams (table 3.6 and figure 3.39B). This therefore represents a high proportion of small foci that are less than 0.5µm in size. The average foci area after 0.5 Gy exposure in young cells is significantly higher than all other shams and irradiated cells over the 48 hour observation period. There does not appear to be any increase in the average number of large foci at all timepoints although there is an increase in medium and large foci in P5 nuclei 30 minutes after 0.5 Gy compared to sham (average 10.48 foci in foci positive nuclei, of which, 3.09 were medium and 1.02 large after 0.5 Gy compared to 0.05 large foci in an average 2.54 foci/nucleus) in shams. This is also the case in ageing P10 cells after 0.3 Gy (1.2 medium foci/nucleus), and 0.5 Gy (2.11 medium foci/nucleus) compared to sham (0.25 foci). It is possible to determine from figure 3.34 that there is an increase number of foci of larger size in the late passage nuclei compared to mid passage (figure 3.36)

which is shown by an increase in the fraction of foci being of medium and large (>0.5 μm) size. It is difficult to interpret whether there is a radiation-induced change in focus size over time, and whether or not there is an increase in focus size in later passage cells. However, although there appears to be no distinct radiation-induced difference in foci size over time, there is an obvious increase in the average focus size in sham and irradiated P10 nuclei, and the fraction of 53BP1 foci that are of a medium and large size, is greater than seen in younger mid passage cells In mid passage NHBE cells there is a visibly increased fraction of large foci (>1.0 μm and 100+ pixels in size) at 30 minutes after exposure to 0.5 Gy, which is not shown by 24 hours whereby approximately 80% of foci scored are of a small size (<0.5 μm and ~6-50 pixels). However at 48 hours after exposure to 0.5 Gy, there is an increase in the number of large foci which is seen to be different from the exposed cells at 24 hours, and also different from both the 24 hour and 48 hour shams. The difference between the composition of these large foci seen at early and later times would need to be investigated further by extending observation times. The data thus far shows no evidence of a radiation-induced increase in foci size in NHBE cells up to 216 hours after irradiation. In order to determine if there was any change in foci size or evidence of persisting foci that are different to shams beyond 216 hours, foci size was quantified up to 792 hours after 0.3 and 0.5 Gy exposure.

Due to the majority of damage being repaired in NHBE cells by 24 hours and therefore a high proportion of nuclei will contain zero foci, the average focus size will be discussed for foci positive cells only. Table 3.7 and figure 3.37 and 3.38 shows the average number and size of 53BP1 foci in NHBE cells over a period of 33 days after IR. Based on average alone the average number of foci in foci positive nuclei remains fairly constant from 24 – 792 hours after sham (range = 1.6-2.1 foci/nucleus), 0.3 Gy (range =1.4-2.3 foci/ nucleus) and 0.5 Gy (range =1.7-2.3 foci/nucleus). Of these foci, small foci (<0.5μm) account for ~80% (sham), 83% (0.3 Gy) and 81% (0.5 Gy) of the foci per foci positive nuclei. Medium foci (0.5-1.0 μm) account for ~13% foci (sham), ~12% foci (0.3 Gy) and ~13% foci (0.5 Gy) which is consistent with an increasing proportion of medium foci seen in ageing late passage cells previously (~16%, ~15% and 16% in late passage sham, 0.3 and 0.5 Gy exposed NHBE respectively). Interestingly, the proportion of large foci in sham nuclei increases from 2.12 % (24 hrs) to 8 % (792 hrs). The total proportion of large foci after 0.3 Gy exposure follows a similar trend to sham nuclei (3.23% at 24hrs and 5.35% at 792 hrs) suggesting that there is an age-associated

increase in the proportion of large foci during the culture period and not a radiation-effect. So although there is no radiation-induced increase in size or number, the proportion of large and medium foci in P7-P13 nuclei are consistently higher than in mid passage P5 nuclei again providing a baseline for the proportion of large and medium foci within ageing cultures

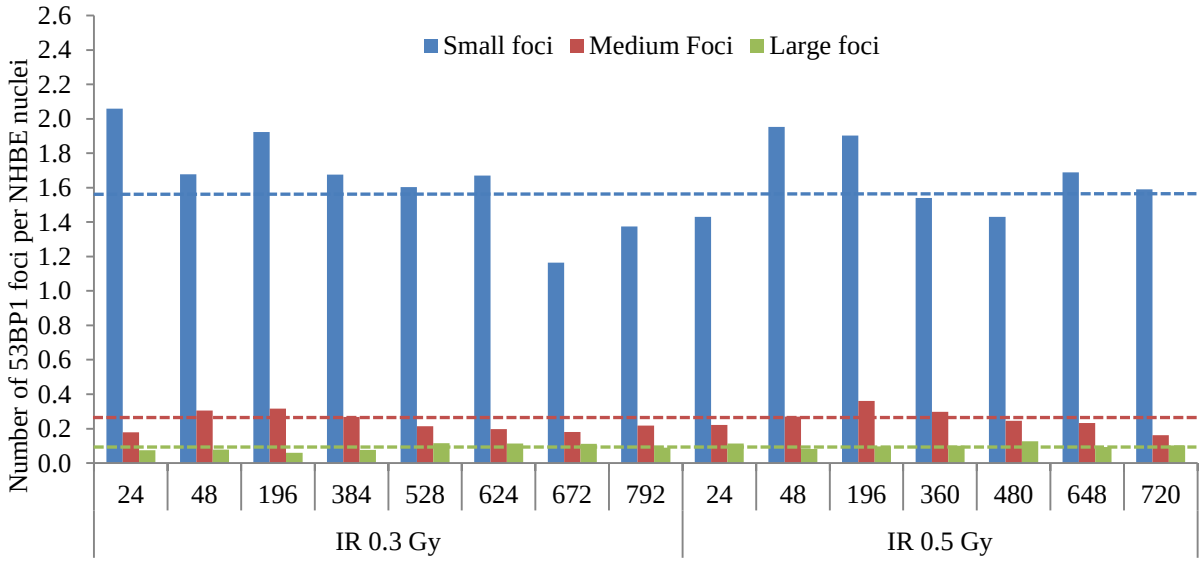

Figure 3.37 AutoRIF analysis of average size and number of 53BP1 foci in foci positive NHBE nuclei only, up to 792 hours after 0.3 and 0.5 Gy. Dashed lines represent average number of small (blue line; 1.56), medium (red line; 0.27) and large (green line; 0.1) 53BP1 foci in mid passage foci positive sham NHBE nuclei only.

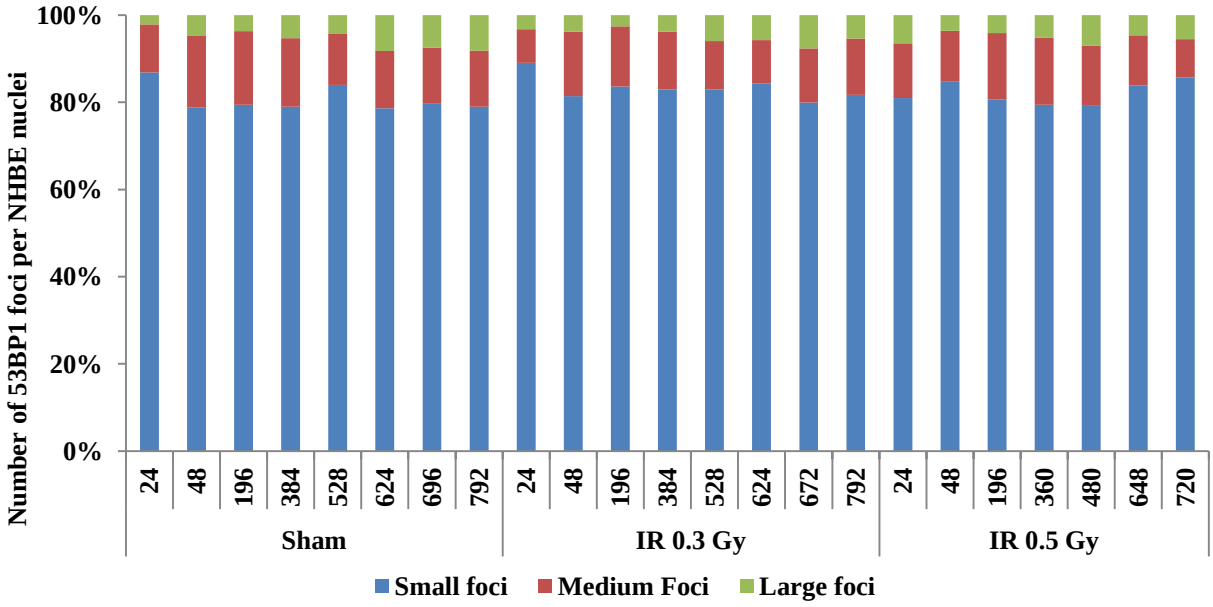

Figure 3.38 AutoRIF analysis of 53BP1 foci size in foci positive NHBE cells up to 792 hours after 0.3 and 0.5 Gy exposure.

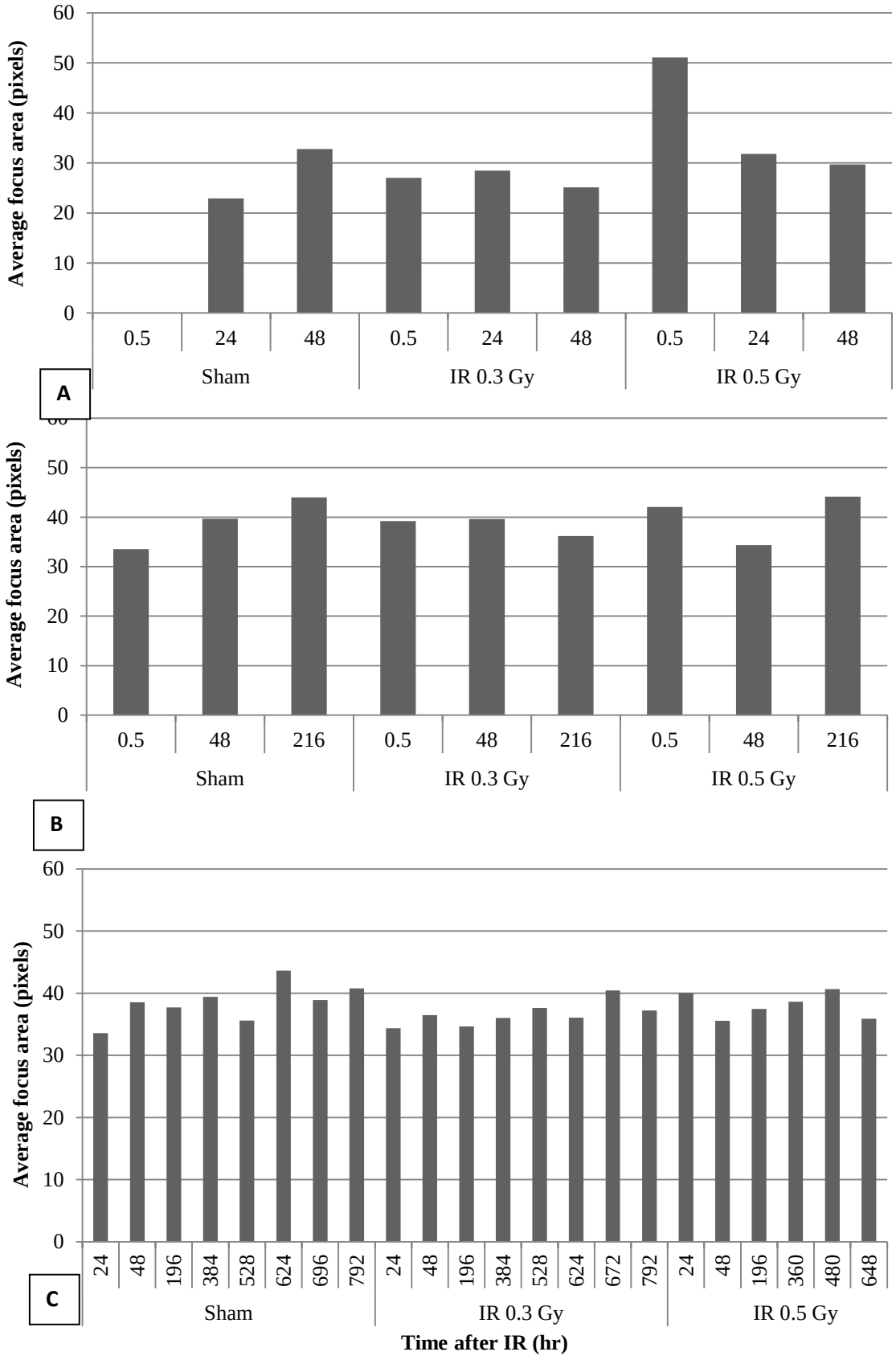

Figure 3.39 Average area of 53BP1 foci in mid (A) late (B) passage NHBE cells. C represents cells exposed at P7 and maintained in culture (area in pixels).

4 Discussion

The rationale of this study is based on the recent suggestion that exposure to ionising radiation (IR) may initiate a stress-induced premature cellular senescence (SIPS) in cells with intact signalling pathways (Ben-Porath, Weinberg 2005, Suzuki *et al*. 2001, Suzuki, Boothman 2008, Rave-Fränk *et al*. 2001) . The overall aim was to examine the effect of moderate to low dose exposures of IR on DNA damage induction and persistence, and the effect, if any, that this may have on the proliferative status of primary normal human bronchial epithelial (NHBE) cells. To do this, we irradiated sub-confluent NHBE cells with gamma IR and fixed at varying times for immunofluorescent staining. Specifically, these cells were then fixed and stained for indirect immunofluorecence for detection of the Ki-67 protein, which is a proliferation marker exclusively linked with the active phases of the cell cycle (Bridger, Kill & Lichter 1998, Gerdes *et al*. 1984) and for the DNA damage protein 53BP1, which is recruited to DSB sites and like phosphorylated histone H2AX (γ-H2AX), is a useful marker of DSB damage. Both Ki-67 and 53BP1 were analysed over time to determine if, after a single acute dose, we saw any radiation-modifying effects that may suggest the induction of a stress–induced premature senescence phenotype.

NHBE cells were used in this study as they represent a clinically relevant target cell for studying low dose ionising radiation effects, including those received during diagnostic procedures (i.e. CT scans and chest X-rays), the usage of which are increasing. In addition NHBE cells have been shown to act as immune effector cells (Nakamura *et al*. 1991, Kaufman *et al*. 2001) meaning they are a useful cell type for studying possible inflammatory responses as a result of IR and stress-induced premature senescence (SIPS). Furthermore, NHBE cells are reported to be more resistant to the DNA-damaging effects of IR compared to lung fibroblasts, and have shorter G_1 and G_2 cell cycle delay responses potentially as a result of higher basal levels of p53 (Gadbois, Lehnert 1997). Given that lung epithelial cells are almost continuously exposed to DNA-damaging agents, a limited checkpoint response in these epithelial cells may increase the chance of unrepaired lesions being transmitted to future progeny.

In this study, NHBE cells grew exponentially in culture to ~80% confluency at each passage, being classified as early, mid or late passage depending on their time to reach confluency, morphological appearance and passage age. For example, NHBE cells grown beyond passage 10 were categorised as late passage cells due to an observed reduction in cell counts at each passage, increased time to reach confluency and reduced cell viability. The total culture period of our NHBE cells represented between 9-18 population doublings (PDs) with Lonza guaranteeing the viability of D2 and D3 NHBE cells to approximately 18 and 15 PDs respectively. After this, a higher rate of cell death is observed, encompassing reduced viability, change of cell morphology and altered gene expression. This suggests that extended culture will result in the classical changes seen with cells becoming senescent and this is consistent with our calculations of mid and late passage cells and the growth and morphological observations we made of the cells in culture. Cumulative cell growth curves (figure 3.3) for 0.3 Gy and 0.5 Gy irradiated NHBE cultures showed no clear difference in growth rates to those seen in sham irradiated cells during the observed culture period, suggesting that there is no radiation effect on growth rates after a single acute dose.

In order to determine the proliferative status of our NHBE cells after exposure to IR, we employed an immune-fluorescent co-stain method whereby cells were stained against both Ki-67 and 53BP1. The nuclear antigen Ki-67 is associated with cellular proliferation but even 30 years after its discovery by Gerdes and colleagues (1983), its exact function still remains unknown (Endl, Gerdes 2000, Starborg *et al*. 1996, Gerdes *et al*. 1983). They showed expression of a nuclear antigen that was only found to be associated with proliferating cells and thus the active phases of the cell cycle, but which was absent in non-proliferating, quiescent and senescent cells (Gerdes *et al*. 1984, Gerdes *et al*. 1983). Schluter (1993) also showed that pKi-67 was necessary for cell cycle progression by incubating IM-9 cells with synthetic antisense deoxyoligonucleotides complementary to the translation start site of pKi-67 (Schlüter *et al*. 1993). This removal of pKi-67 resulted in the prevention of [^{3}H] thymidine-incorporation and the prevention of cellular proliferation. In addition to this, the confined nuclear distribution of Ki-67 is cell cycle dependant and is associated with the nucleoli of proliferating cells where it stains regions surrounding the fibrillar centres,

suggesting that Ki-67 plays a role in regulation of nucleolar metabolism and the rate of ribosome synthesis (Kill 1996, Gerdes *et al*. 1983, Schlüter *et al*. 1993, Verheijen *et al*. 1989) . However, as Ki-67 negative cells are still viable, it suggests that pKi-67 is not specifically needed for nucleolar function but is important for structural maintenance at different stages of the cell cycle. Moreover, Ki-67 positive staining patterns can differentiate cells into different phases of the cell cycle. For instance, cells displaying small, numerous foci throughout the nucleoplasm, are classified as type I distribution, corresponding to G_1 (Bridger, Kill & Lichter 1998, Kill 1996). Ki-67 staining is associated with the dense fibrillar components of reforming nucleoli and restricted to the nucleoli in type II distribution, which encompasses late G_1, S phase and G_2 cells where localisation is maintained in this manner until the middle of G_2 phase (Kill 1996). We therefore exploited these features of Ki-67 staining to enable us to distinguish between proliferating and non-proliferating cells within the NHBE population.

We found ~25% of mid passage NHBE cells (~passage 5-6) were Ki-67 negative (range 16-36%) compared to 57% Ki-67 negative (range 43-62%) in later passage cells (figure 3.25 and 3.26). This showed a clear increase in the non-proliferating fraction of NHBE cells, thought to be senescent, with increasing cellular passage. Irrespective of passage age, ~83% of the Ki-67 positive fraction (range 76-97%, data not shown) were of type II staining distribution, representative of being in late G_1, S, G_2 (Bridger, Kill & Lichter 1998), and exposure to 0.3 and 0.5 Gy did not appear to modify this relative to sham during the initial observed period of up to 216 hours. Similarly, 44% of passage 7 1HD (data not shown) cells were Ki-67 positive and 86% of this fraction exhibited a type II staining distribution, while Kill (1996) showed that 84% of human dermal fibroblasts (HDFs) stained with a type II distribution (Kill 1996). Thus a similar proportion of our non-synchronised NHBE cells are in late G1 onwards at all times analysed. It is expected that the fraction of Ki-67 positive cells will decrease with passage as shown by Kill (1996) and Thomas (1997) (Kill 1996, Thomas *et al*. 1997) which is representative of an increasing number of the cells reaching their maximum replicative age and becoming senescent. The NHBE cells used in this study are grown in serum-defined BEBM (section 2.2.3.1) and therefore are under conditions whereby Ki-67 negative staining is representative of the senescent fraction of a culture, in contrast to quiescent cells (also Ki-67 negative) (Kill

1996). In concordance with mid and late passage Ki-67 fractions observed in NHBE cells, 39% (sham), 33% (0.3 Gy) and 39% (0.5 Gy) of NHBE cells at P7 were Ki-67 negative suggesting a steady increase in the non-proliferative fraction with passage age. However in contrast to this, when we continued subculture of NHBE beyond approximately 360-384 hours up to 792 hours we did not observe a linear expected increase in Ki-67 negative fraction (table 3.9). Instead we observed that the fraction of Ki-67 negative cells remained constant or reduced in both sham and irradiated samples approximately 15-20 days into the long-term culture (figure 3.28). A possible explanation for this
is given later in this Discussion.

The application of Ki-67 analysis for determination of senescent cells was corroborated by parallel staining for senescence-associated beta-galactosidase (SA-β gal) activity at pH 6. Cells irradiated at Passage 7 and grown for a total of 33 days were also stained for SA-β gal to determine if there was any evidence of premature-radiation-induced senescence comparative to shams. We showed that the SA-β gal positive fraction of NHBE increased from 11% at passage 4 to 21 % by passage 7 representing an increasing number of cells that were senescing in culture. Similarly, SA-β gal staining of P8-P13 NHBE cells showed a correlating trend in both sham and irradiated samples (figure 3.6) however similar to that observed with Ki-67, we did not see the expected increase in cells IR at P7 and cultured beyond P10-P11 (figure 3.6). Although the percentage of SA-β gal positive cells subsequently dropped after P10-P11, this increase was seen in culture for a longer period than was seen by Ki-67 analysis of cells of the same passage age (P9 onwards). It must always be noted that the accuracy of using β-galactosidase activity to detect the presence of senescent cells *in vitro* and *in vivo* has long been debated. For instance, SA-β gal activity at pH 6.0 has also been shown in adult melanocytes (Dimri 1995), as well as in quiescent serum-starved or heparin-treated murine fibroblast cells, leukemic cells that have undergone differentiation, or in cells held at confluence (Yegorov *et al*. 1998, Severino *et al*. 2000, Krishna *et al*. 1999). As a result of the variation that is seen across sample dishes often as a result of user subjectivity and non-specificity of the assay under different culture conditions, the detection of senescent/non-proliferating cells should not be determined by SA-β gal activity alone, and should always be used in conjunction with other detection methods. For both SA-β gal activity and Ki-

67 staining the reproducibility of analysis was excellent in this study meaning such technical considerations may not account for the observation that the percentage of SA-β gal positive nuclei and Ki-67 negative at P13 decreased compared to earlier cultures. Instead this may suggest that a fraction of senescent cells are being lost at each passage such that we are not identifying a true accumulation of senescent cells. This highlights a possible issue with studies designed to observe the late effects after IR exposure, where the long-term maintenance of NHBE cells by continued subculture may impact on the growth characteristics of these primary cells past P10 or by the continual loss of senescent cells due to technical reasons. In addition, although the BEBM medium contains supplements to ensure that the NHBE cells do not become differentiated during subculture, we cannot exclude this as a possibility since no markers to distinguish between cells that have become terminally differentiated were used. Overall though, we measured an age-associated increase in SA-β gal staining however we did not observe any enhancement of this after exposure to a single acute dose of 0.3 and 0.5 Gy.

IR-induced 53BP1 foci have been shown to form within minutes peaking around 30 minutes post-irradiation, in a dose-dependent manner (Anderson, Henderson & Adachi 2001). Our findings correlate with the literature, showing the induction of 53BP1 foci in mid-passage NHBE cells 30 minutes after exposure to both 0.3 Gy (average 5.3 foci/nucleus) and 0.5 Gy (6.5 foci/nucleus) to be elevated compared to sham (1.16 foci/nucleus) (figure 3.8). In late-passage cells exposed under the same conditions, 53BP1 foci were induced to the same efficiency as in mid-passage cells after exposure to 0.3 Gy (6.86 foci/nucleus) and 0.5 Gy (8.21 foci/nucleus) compared to sham (2.44 foci/nucleus) (figure 3.11). However average foci numbers were higher due to the increased background of foci that is seen in ageing NHBE cells. An increase in background DNA damage foci in ageing cultures is also well documented in other cell types, specifically early passage fibroblast cultures showed 0.2-0.3 γ-H2AX foci/cell increasing to 2.2-4.1 foci/cell in senescent cultures (Sedelnikova 2004), with senescing human and mice cells in other studies also showing an increasing accumulation of foci (Paull *et al*. 2000, Sedelnikova 2004, Rothkamm, Löbrich 2003, Sedelnikova *et al*. 2002). This increasing trend was further seen by the distribution of foci in NHBE cells of differing passage age, with only 23% of late passage (P10) sham nuclei

containing zero foci (range 15-34%), compared to ~50% in mid passage (P5/6) cultures (range 38-55%) (figure 3.9 and 3.12). Interestingly for all cultures in the extended population (figure 3.13), a decline in the average number of foci and an increase in nuclei that had zero foci was observed at later times, suggesting that cells are lost from continued culture (beyond P9 in this study). We saw a high background of 53BP1 foci in P10 sham nuclei however we did not see this in the P10 nuclei of cells that had been sham irradiated at P7 and maintained in culture. Therefore it would be advisable to observe whether the average background level of foci would decline and would suggest that the cells are being removed from the population during long-term culture as a result of apoptosis or an aspect of the technical design.

The recruitment of foci to the sites of DSBs and repair of damage is thought to be equivalent at high and low doses of IR (Asaithamby, Chen 2009) however groups have also shown that foci are not resolved after exposure to very low doses of ionising radiation (<10mGy) (Grudzenski *et al*. 2010). 53BP1 and γ-H2AX foci numbers rapidly decrease in the time after challenge due to an elimination of the cells that carry unrepaired DSBs, either by induction of apoptosis as a consequence of un-repairable damage, or through the sufficient implementation of cellular repair mechanisms (Rothkamm, Löbrich 2003). Although still controversial, the rate that 53BP1 foci are resolved show similar kinetics to DSB repair and therefore their disappearance is thought to correlate with DNA repair (Rappold *et al*. 2001, Schultz *et al*. 2000a). Such a decline in foci number was seen in both mid and late passage NHBE cells 48 hours after IR, whereby foci numbers had returned to sham levels (figure 3.8 and 3.11). Interestingly though, manual analysis determined that 216 hours after exposure to 0.5 Gy, the average foci number (4.73 foci/nucleus) remained elevated compared to sham (3.31 foci/nucleus, P=<0.0001) which was also accompanied by a broader distribution of damage foci compared to sham in late passage NHBE cells. However, AutoRIF analysis of a higher number of nuclei highlighted that there is a broader distribution of 53BP1 foci in late passage NHBE cells up to 48 hours after 0.3 and 0.5 Gy, and relative to sham by 216 hours. The slight variation seen in the distribution of DNA damage foci after IR by different analysis methods highlights

the potential effect that individual nuclei variation will have on small sample sizes.

There is also evidence to support the hypothesis that persisting foci are of increased size at extended times after exposure to IR (McVean *et al*. 2012, Suzuki *et al*. 2006, Suzuki *et al*. 2012, Leatherbarrow *et al*. 2006, Staaf *et al*. 2012). We also observed this during manual observation in this study whereby IR induced foci (RIF) at later times were larger and more intensely stained than the small endogenous foci seen in un-irradiated cycling cell nuclei (Ichijima *et al*. 2005). To quantify these larger foci at extended times after IR we employed AutoRIF (McVean *et al*. 2012) to quantify foci of categorised sizes in both mid and late passage cells. Foci were classified as small (<0.5μm), medium (0.5 – 1.0μm) and large (>1.0μm). Specifically, our results showed that there was a distinction between the proportion of medium and large foci in mid and late passage cells (figure 3.33 and 3.35). In addition, NHBE cells irradiated at P7 and cultured continuously for up to 33 days after exposure also contained a higher proportion of medium and large foci compared to NHBE cells that were IR and fixed at mid passage. Specifically the proportion of medium foci scored in sham NHBE nuclei appears to be higher in later passage nuclei (16%) compared to mid passage nuclei (10%), with a further increase in the proportion of large foci seen in P7-P13 nuclei (range=2% at 24 hours and 8% large by 792 hours) (figure 3.37) suggesting that there is indeed an age-related increase of persistent foci size in NHBE cells of increasing passage, allowing distinction between young and ageing NHBE cells in culture. However, no difference in the size of 53BP1 foci was observed relative to sham (figure 3.34, 3.36 and 3.38). Therefore of the doses and dose regimes studied so far, we found no evidence of a radiation-induced increase in foci size over a period of 33 days which suggests that a single acute dose of 0.3 Gy or 0.5 Gy is not sufficient to induce any radiation effects above that of baseline changes in the ageing culture, in NHBE cells.

Given the relationship between persisting foci and the trend that they are of a relative increased size in ageing cell populations and also, that the fraction of Ki-67 negative and SA β-gal positive cells increase with replicative age, we were interested in whether there was any evidence of persisting foci predominantly occurring in Ki-67 negative cells. We saw no difference in the efficiency of

induction of 53BP1 foci and no increased sensitivity to damage in either Ki-67 positive (proliferating) or Ki-67 negative (senescent) mid passage NHBE cells at 30mins (figure 3.29). This was also shown in 1HD cells whereby we saw no difference in the average number of foci in either Ki-67 positive or negative cells (data not shown) within 30mins of IR. However there does appear to be a difference in how the damage is processed between proliferating and senescent cells in late passage cells (figure 3.30 and 3.31). Although the co-stain graphs are difficult to interpret due to the spread of foci number, the number of Ki-67 negative nuclei with >6 foci appears to be altered relative to sham (5.9%), 216 hours after exposure to 0.3 Gy (11%) and 0.5 Gy (19%). This may suggest that at extended times after exposure, there may be increasing numbers of NHBE cells with an increased foci number relative to sham in Ki-67 negative cells as you might predict. However similar to our previous findings, we did not observe any influence of a single acute dose of 0.3 or 0.5 Gy up to 792 hours after irradiation. As discussed previously, the discrepancies in the Ki-67 fraction of cells observed at later times suggests that there may have been a loss of Ki-67 negative cells which may or may not have contained elevated foci (of increased size) as a result of the effect of long-term culture of these primary cells. Senescent cells are thought to be more adherent to flasks than exponentially growing cells, and this may mean that during continued subculture, a fraction of these senescent cells are left behind at each passage and as a result do not contribute to the new fraction that may have become senescent by the next observation period. This may explain why the Ki-67 negative fractions of NHBE did not increase with subsequent passage and with the age of culture as expected. Previous analysis of the fraction of Ki-67 negative mid passage cells showed good correlation with the fraction of SA-β gal positive cells in cultures of similar age, allowing the conclusion that these 2 markers are indeed identifying the same proportion of cells within culture. It is expected, according to Kill, Thomas (Kill 1996, Thomas *et al*. 1997) and previous work, that the relationship between Ki-67 negative cells and SA-β gal positive cells should be relatively inversely proportional. Co-staining nuclei with Ki-67 and the fluorogenic substrate for β-galactosidase known as 5-dodecanoylaminofluorescin di-β-D-galactopyranoside (C_{12}FDG) (Debacq-Chainiaux *et al*. 2009) would allow identification of both proliferative status and quantification of SA-β gal activity within each cell. Further parallel staining of

these CD_{12}FDG stained nuclei for 53BP1 foci would provide a good model to directly distinguish between SA-β gal positive cells (Ki-67 negative) with foci.

Future recommendations for AutoRIF analysis over extended periods of time after moderate to low doses of radiation, must take into account the high background that is seen in both sham and irradiated ageing nuclei. After 24 hours when repair is thought to have been completed the background intensity is at risk of being over-enhanced during image capture resulting in a false increase in the number of small foci detected by AutoRIF which are actually characterised as 'salt and pepper'. The software however allows a huge number of nuclei to be imaged and analysed and shows generally good correlation with smaller manual analyses. An awareness of the advantages and caveats of the system that have been discussed throughout will allow the user to ensure that the optimal settings are used according to experimental design to determine both foci number and size. Further modifications that could be made during analysis of AutoRIF output, would be to modify excel formulas to disregard nuclei with high number of foci in and therefore apply a maximum cut-off for foci number also. This would allow exclusion of those nuclei with high numbers of small endogenous foci that may be as a result of S phase or dividing cells, as were excluded by manual analysis. ,It is therefore necessary that steps are taken to ensure that this small population of cells are either excluded from the population or they are identified and accounted for. As it is not possible to synchronise the growth of NHBE cells, the use of PCNA antibodies would be of great benefit here to estimate the fraction of S phase cells. Additionally, the development of antibodies that are aimed against irreparable IRIF would potentially alleviate the impact that ambiguous foci have on the data. Future analysis should also be less focussed on the presence of foci that are less than 0.5µm in size, and capture settings adjusted to focus on medium and large foci which are of greater importance in this project at later times after IR.

In conclusion, senescence and ageing have been inexplicably linked in a number of pathologies, including cancer possibly as a result of genomic instability and low fidelity repair of DNA damage. A direct link between *in vivo* and cellular ageing and senescence has not yet been conclusively determined although the recent work by Baker and colleagues (2011) provided evidence of a direct link

between senescent cells and age-related pathologies in mice (Baker *et al*. 2011). Of particular importance in this project was whether NHBE cells underwent stress-induced premature senescence in response to single acute doses of IR and if so, future considerations should focus on whether such responses may modify the effects of low dose exposures. In particular the impact of persisting inflammatory or DNA damage responses, either by release of inflammatory products from NHBE cells themselves, or as a result of senescent cells being associated with a secretory phenotype.

Although our current data has shown that a single acute dose of either 0.3 or 0.5 Gy Cobalt^{60} γ-rays does not result in any obvious modifying effects above the levels seen in sham NHBE cells of mid and late passage, the endpoints that were analysed have shown a clear distinction between mid and late passage cells. This provides an excellent model for comparing young and older NHBE cells, which could be applied to study more elaborate radiation strategies. It has well documented that senescence has been induced after exposure to both high (Suzuki *et al*. 2001) and chronic low doses (Tsai *et al*. 2005, Tsai *et al*. 2009) of radiation and although exposure to a single acute moderate dose of 0.3 and 0.5 Gy has shown no effect relative to sham, it is essential that the impact of chronic low and fractionated dose exposures are investigated in this cell type.

In order to further investigate the effect of low dose exposures on the initiation of a stress-induced senescence phenotype in NHBE cells, extended observation of these cells in culture would need to be optimised to ensure that senescent cells within the culture are maintained, or the fate of cells with increased foci are determined. Alongside detailed analysis of the endpoints discussed in this project, molecular assays to assess changes in gene (qtPCR) and protein expression (western blots and ELISA) should form a key element to future analysis of the late effects of ionising radiation. Sampling of NHBE medium for the detection of inflammatory cytokines/chemokines such as IL-8 and IL-6, which are known to be secreted by NHBE epithelial cells after damage, and ICAM-1 expression which is found to be up-regulated on NHBE epithelial cell membranes (Martin *et al*. 1997) would also allow us to determine if there are any radiation-induced responses over time.

Further optimisation of an air-liquid interface 3D (ALI) model would allow differentiation of NHBE cells into a pseudostratified epithelial layer containing basal epithelial cells, mucus producing goblet and ciliated columnar cells, which is more representative of an *in vivo* tissue model. This tissue model is also commercially available from MatTek and has successfully been used by other groups to study radiation effects (Sedelnikova *et al*. 2007). Exploration of culturing these 3D tissue models with (matched) fibroblasts, or immune cells would also allow us to determine the importance of the stromal matrix and immune cell interaction after radiation exposure.

5 References

Abraham, R. 2002, "Checkpoint signalling: focusing on 53BP1", *Nature Cell Biology*, vol. 4, no. 12, pp. 277-279.

Acosta, J., *et al*. 2008, "Control of senescence by CXCR2 and its ligands", *Cell Cycle*, vol. 7, no. 19, pp. 2956-2959.

Anderson, R., *et al*. 2000, "Complex chromosome aberrations in peripheral blood lymphocytes as a potential biomarker of exposure to high-LET alpha-particles", *International Journal of Radiation Biology*, vol. 76, no. 1, pp. 31-42.

Anderson, L., Henderson, C. & Adachi, Y. 2001, "Phosphorylation and Rapid Relocalization of 53BP1 to Nuclear Foci upon DNA Damage", *Molecular and Cellular Biology*, vol. 21, no. 5, pp. 1719-1729.

Anderson, R.M., Stevens, D.L. & Goodhead, D.T. 2002, "M-FISH analysis shows that complex chromosome aberrations induced by α-particle tracks are cumulative products of localized rearrangements", *Proceedings of the National Academy of Sciences*, vol. 99, no. 19, pp. 12167-12172.

Ansieau, S., *et al*. 2008, "Induction of EMT by Twist Proteins as a Collateral Effect of Tumor-Promoting Inactivation of Premature Senescence", *Cancer Cell*, vol. 14, no. 1, pp. 79-89.

Artandi, S., *et al*. 2000, "Telomere dysfunction promotes non-reciprocal translocations and epithelial cancers in mice", *Nature*, vol. 406, no. 6796, pp. 641-645.

Asaithamby, A. & Chen, D.J. 2011, "Mechanism of cluster DNA damage repair in response to high-atomic number and energy particles radiation", *Mutation Research/Fundamental and Molecular Mechanisms of Mutagenesis*, vol. 711, no. 1–2, pp. 87-99.

Asaithamby, A. & Chen, D.J. 2009, "Cellular responses to DNA double-strand breaks after low-dose γ-irradiation", *Nucleic Acids Research*, vol. 37, no. 12, pp. 3912-3923.

Azzam, E.I., de Toledo, S.M. & Little, J.B. 2001, "Direct evidence for the participation of gap junction-mediated intercellular communication in the transmission of damage signals from α-particle irradiated to nonirradiated cells", *Proceedings of the National Academy of Sciences of the United States of America*, vol. 98, no. 2, pp. 473-478.

Baker, D., Jin, F. & van Deursen, J. 2008, "The yin and yang of the Cdkn2a locus in senescence and aging", *Cell Cycle*, vol. 7, no. 18, pp. 2795-2802.

Baker, D., *et al*. 2011, "Clearance of p16Ink4a-positive senescent cells delays ageing-associated disorders", *Nature,* vol. 479, no. 7372, pp. 232-236.

Bakkenist, C.J., *et al*. 2004, "Disappearance of the Telomere Dysfunction-Induced Stress Response in Fully Senescent Cells", *Cancer Research,* vol. 64, no. 11, pp. 3748-3752.

Bassi, P. & Sacco, E. 2009, "Cancer and aging: The molecular pathways", *Urologic Oncology: Seminars and Original Investigations,* vol. 27, no. 6, pp. 620-627.

Beghe, C. & Balducci, L. 2005, "Biological basis of cancer in the older person", *Cancer Treatment and Research,* vol. 124, pp. 189-221.

Bekker-Jensen, S., *et al*. 2005, "Dynamic assembly and sustained retention of 53BP1 at the sites of DNA damage are controlled by Mdc1/NFBD1", *The Journal of Cell Biology,* vol. 170, no. 2, pp. 201-211.

Belyakov, O.V., *et al*. 2005, "Biological effects in unirradiated human tissue induced by radiation damage up to 1 mm away", *Proceedings of the National Academy of Sciences of the United States of America,* vol. 102, no. 40, pp. 14203-14208.

Ben-Porath, I. & Weinberg, R.A. 2005, "The signals and pathways activating cellular senescence", *The International Journal of Biochemistry & Cell Biology,* vol. 37, no. 5, pp. 961-976.

Ben-Porath, I. & Weinberg, R.A. 2004, "When cells get stressed: an integrative view of cellular senescence", *American Society for Clinical Investigation,* vol. 113, pp. 8-13.

Berthois, Y., Katzenellenbogen, J. & Katzenellenbogen, B. 1986, "Phenol red in tissue culture media is a weak estrogen: implications concerning the study of estrogen-responsive cells in culture.", *Proceedings of the National Academy of Sciences of the United States of America,* vol. 83, no. 8, pp. 2496-2500.

Birchmeier, W. & Birchmeier, C. 1995, "Epithelial-mesenchymal transitions in development and tumour progression", *EXS,* vol. 74, pp. 1-15.

Blagosklonny, M.V. 2003, "Cell senescence and hypermitogenic arrest", *European Molecular Biology Organization,* vol. 4, no. 4, pp. 358-362.

Brenner, D., *et al*. 2000, "Second malignancies in prostate carcinoma patients after radiotherapy compared with surgery", *Cancer,* vol. 88, no. 2, pp. 398-406.

Brenner, D. & Ward, J. 1992, "Constraints on energy deposition and target size of multiply damaged sites associated with DNA double-strand breaks", *International Journal of Radiation Biology,* vol. 61, no. 6, pp. 737-48.

Bridger, J., Kill, I. & Lichter, P. 1998, "Association of pKi-67 with satellite DNA of the human genome in early G_1 cells", *Chromosome Research,* vol. 6, pp. 13-24.

Bridger, J.M., *et al*. 2000, "Re-modelling of nuclear architecture in quiescent and senescent human fibroblasts", *Current Biology,* vol. 10, no. 3, pp. 149-152.

Bridger, J.M., *et al*. 1998, "Identification of an interchromosomal compartment by polymerization of nuclear-targeted vimentin", *Journal of Cell Science,* vol. 111, no. 9, pp. 1241-1253.

Burma, S., *et al*. 2001, "ATM Phosphorylates Histone H2AX in Response to DNA Double-strand Breaks", *Journal of Biological Chemistry,* vol. 276, no. 45, pp. 42462-42467.

Campisi, J. 2000, "Cancer, aging and cellular senescence", *In Vivo,* vol. 14, no. 1, pp. 183-188.

Campisi, J. & d'Adda di Fagagna, F. 2007, "Cellular senescence: when bad things happen to good cells", *Nature Reviews. Molecular Cell Biology,* vol. 8, no. 9, pp. 729-740.

Campisi, J. 2007, "Aging and cancer cell biology, 2007", *Aging Cell,* vol. 6, no. 3, pp. 261-263.

Campisi, J. 2005, "Senescent Cells, Tumor Suppression, and Organismal Aging: Good Citizens, Bad Neighbors", *Cell,* vol. 120, no. 4, pp. 513-522.

Campisi, J. 2001, "Cellular senescence as a tumor-suppressor mechanism", *Trends in Cell Biology,* vol. 11, no. 11, pp. S27-S31.

Chaturvedi, V., *et al*. 2004, "Proliferating cultured human keratinocytes are more susceptible to apoptosis compared with mouse keratinocytes", *The Journal of Investigative Dermatology,* vol. 123, no. 6, pp. 1200-1203.

Chen, J. 2004, "Senescence and functional failure in hematopoietic stem cells", *Experimental Hematology,* vol. 32, no. 11, pp. 1025-1032.

Coates, P.J., Lorimore, S.A. & Wright, E.G. 2004, "Damaging and protective cell signalling in the untargeted effects of ionizing radiation", *Mutation Research/Fundamental and Molecular Mechanisms of Mutagenesis,* vol. 568, no. 1, pp. 5-20.

Coates, P., *et al*. 2008, "Ongoing activation of p53 pathway responses is a long-term consequence of radiation exposure in vivo and associates with altered macrophage activities", *The Journal of Pathology,* vol. 214, no. 5, pp. 610-616.

Collins, C.J. & Sedivy, J.M. 2003, "Involvement of the INK4a/Arf gene locus in senescence", *Aging Cell,* vol. 2, no. 3, pp. 145-150.

Coppé, J., *et al*. 2010, "The Senescence-Associated Secretory Phenotype: The Dark Side of Tumor Suppression", *Annual Review of Pathology: Mechanisms of Disease,* vol. 5, no. 1, pp. 99-118.

Coppe, J., *et al*. 2008, "Senescence-associated secretory phenotypes reveal cell-nonautonomous functions of oncogenic RAS and the P53 tumour supressor", *PLoS Biology,* vol. 6, no. 12, pp. 2853-2868.

Coppé, J., *et al*. 2006, "Secretion of Vascular Endothelial Growth Factor by Primary Human Fibroblasts at Senescence", *Journal of Biological Chemistry,* vol. 281, no. 40, pp. 29568-29574.

d'Adda di Fagagna, F., *et al*. 2003, "A DNA damage checkpoint response in telomere-initiated senescence", *Nature,* vol. 426, no. 6963, pp. 194-198.

Danahay, H., *et al*. 2002, "Interleukin-13 induces a hypersectomy ion transport phenotype in human bronchial epithelial cells", *American Journal of Physiology. Lung Cell and Molecular Physiology*, vol 282, no 2, pp. 226-236

Darby, S., *et al*. 2005, "Radon in homes and risk of lung cancer: collaborative analysis of individual data from 13 European case-control studies", *British Medical Journal,* vol. 330, no. 7485, pp. 223-229.

Darby, S., *et al*. 2006, "Residential radon and lung cancer--detailed results of a collaborative analysis of individual data on 7148 persons with lung cancer and 14,208 persons without lung cancer from 13 epidemiologic studies in Europe.", *Scandinavian Journal of Work, Environment and Health,* vol. 32, no. Suppl 1, pp. 1-83.

Davalos, A.R., *et al*. 2010, "Senenscent cells as a source of inflammatory factors for tunour progression", *Cancer Metastasis Review,* vol. 29, pp. 273-283.

De Martinis, M., *et al*. 2007, "Apoptosis remodeling in immunosenescence: implications for strategies to delay ageing", *Current Medicinal Chemistry,* vol. 14, no. 13, pp. 1389-1397.

Debacq-Chainiaux, F., *et al*. 2009, "Protocols to detect senescence-associated beta-galactosidase (SA-beta gal) activity, a biomarker of senescent cells in culture and in vivo.", *Nature Protocols,* vol. 4, no. 12, pp. 1798-806.

DePinho, R. 2000, "The age of cancer", *Nature,* vol. 408, no. 6809, pp. 248-254.

Dickey, J.S., *et al*. 2009, "Intercellular communication of cellular stress monitored by γ-H2AX induction", *Carcinogenesis,* vol. 30, no. 10, pp. 1686-1695.

Dieriks, B., *et al*. 2010, "Medium-mediated DNA repair response after ionizing radiation is correlated with the increase of specific cytokines in human fibroblasts", *Mutation Research/Fundamental and Molecular Mechanisms of Mutagenesis,* vol. 687, no. 1-2, pp. 40-48.

Dimri, G.P. 1995, "A biomarker that identifies senescent human cells in culture and in ageing skin *in vivo*", *Proceedings of the National Academy of Sciences of the United States of America,* , no. 92, pp. 9363-9367.

Dirac, A.M.G. & Bernards, R. 2003, "Reversal of Senescence in Mouse Fibroblasts through Lentiviral Suppression of p53 ,", *Journal of Biological Chemistry*, vol. 278, no. 14, pp. 11731-11734.

Endl, E. & Gerdes, J. 2000, "The Ki-67 Protein: Fascinating Forms and an Unknown Function", *Experimental Cell Research*, vol. 257, no. 2, pp. 231-237.

Erusalimsky, J.D. 2009, "Vascular endothelial senescence: from mechanisms to pathophysiology", *Journal of Applied Physiology*, vol. 106, no. 1, pp. 326-332.

Erusalimsky, J.D. & Kurz, D.J. 2005, "Cellular senescence in vivo: Its relevance in ageing and cardiovascular disease", *Experimental Gerontology*, vol. 40, no. 8-9, pp. 634-642.

Evan, G.I. & d'Adda di Fagagna, F. 2009, "Cellular senescence: hot or what?", *Current Opinion in Genetics & Development*, vol. 19, no. 1, pp. 25-31.

Feinendegen, L., Pollycove, M. & Neumann, R. 2009, "Low-dose cancer risk modeling must recognize up-regulation of protection", *Dose Response: A Publication of International Hormesis Society*, vol. 8, no. 2, pp. 227-252.

Finkel, T., Serrano, M. & Blasco, M. 2007, "The common biology of cancer and ageing", *Nature*, vol. 448, no. 7155, pp. 767-774.

Franke, A., *et al*. 2000, "Long-term efficacy of radon spa therapy in rheumatoid arthritis—a randomized, sham-controlled study and follow-up", *Rheumatology*, vol. 39, no.8, pp.894-902.

Freund, A., *et al*. 2010, "Inflammatory networks during cellular senescence: causes and consequences", *Trends in Molecular Medicine*, vol. 16, no. 5, pp. 238-246.

Gadbois, D.M. & Lehnert, B.E. 1997, "Cell Cycle Response to DNA Damage Differs in Bronchial Epithelial Cells and Lung Fibroblasts", *Cancer Research*, vol. 57, no. 15, pp. 3174-3179.

Gastein's Mountain, Gasteiner-Heilstollen. Available; http://www.gasteiner-heilstollen.com/home.html [2012, July 23rd]

Gerdes, J. 1990, "Ki-67 and other proliferation markers useful for immunohistological diagnostic and prognostic evaluations in human malignancies", *Seminars in Cancer Biology*, vol. 1, no. 3, pp. 199-206.

Gerdes, J., *et al*. 1983, "Production of a mouse monoclonal antibody reactive with a human nuclear antigen associated with cell proliferation", *International Journal of Cancer,* vol. 31, no. 1, pp. 13-20.

Gerdes, J., *et al*. 1984, "Cell cycle analysis of a cell proliferation-associated human nuclear antigen defined by the monoclonal antibody Ki-67", *The Journal of Immunology,* vol. 133, no. 4, pp. 1710-1715.

Gil, J. & Peters, G. 2006, "Regulation of the INK4b-ARF-INK4a tumour supressor locus: all for one and one for all", *Nature Reviews. Molecular Cell Biology,* vol. 7, no. 9, pp. 667-677.

Giovannetti, A., *et al*. 2008, "Apoptosis in the homeostasis of the immune system and in human immune mediated diseases", *Current Pharmaceutical Design,* vol. 14, no. 3, pp. 253-268.

Grudzenski, S., *et al*. 2010, "Inducible response required for repair of low-dose radiation damage in human fibroblasts", *Proceedings of the National Academy of Sciences of the United States of America,* vol. 107, no. 32, pp. 14205-14210.

Hall, E. & Brenner, D. 2008, "Cancer risks from diagnostic radiology", *British Journal of Radiology,* vol. 81, no. 965, pp. 362-378.

Hamada, N., *et al*. 2007, "Intercellular and intracellular signalling pathways mediating ionizing radiation-induced bystander effects", *Radiation Research,* vol. 48, no. 3, pp. 87-95.

Hampel, B., *et al*. 2004, "Differential regulation of apoptotic cell death in senescent human cells", *Experimental Gerontology,* vol. 39, no. 11-12, pp. 1713-1721.

Hayashi, T., *et al*. 2003, "Radiation dose-dependent increases in inflammatory response markers in A-bomb survivors.", *International Journal of Radiation Biology,* vol. 79, no. 2, pp. 129-136.

Hayashi, T., *et al*. 2005, "Long-term effects of radiation dose on inflammatory markers in atomic bomb survivors", *The American Journal of Medicine,* vol. 118, no. 1, pp. 83-86.

Health Protection Agency. , *Dose Comparisons for Ionising Radiation*. Available: http://www.hpa.org.uk/Topics/Radiation/UnderstandingRadiation/UnderstandingRadiationTopics/DoseComparisonsForIonisingRadiation [2012, 23rd July].

Herbig, U., *et al*. 2004, "Telomere Shortening Triggers Senescence of Human Cells through a Pathway Involving ATM, p53, and p21CIP1, but Not p16INK4a", *Molecular Cell,* vol. 14, no. 4, pp. 501-513.

HLEG Report. 2009, *High level and expert group on european low dose risk research. High level and expert group report on european low dose risk research—Radiation protection.*, European Commission EUR 23884 edn.

Huyen, Y., *et al*. 2004, "Methylated lysine 79 of histone H3 targets 53BP1 to DNA double-strand breaks.", *Nature,* vol. 432, no. 7015, pp. 406-411.

Ichijima, Y., *et al*. 2005, "Phosphorylation of histone H2AX at M phase in human cells without DNA damage response.", *Biochemical and Biophysical Research Communications,* vol. 336, no. 3, pp. 807-812.

ICRP. 2007, *The 2007 Recommendations of the International Commission on Radiological Protection. ICRP Publication 103.*, Annals of the ICRP 37 (2-4) edn, Elsevier Science Ltd, Oxford, UK.

Ilnytskyy, Y., Koturbash, I. & Kovalchuk, O. 2009, "Radiation-induced bystander effects in vivo are epigenetically regulated in a tissue-specific manner", *Environmental and Molecular Mutagenesis,* vol. 50, no. 2, pp. 105-113.

Iwabuchi, K., *et al*. 1998, "Stimulation of p53-mediated Transcriptional Activation by the p53-binding Proteins, 53BP1 and 53BP2", *Journal of Biological Chemistry,* vol. 273, no. 40, pp. 26061-26068.

Janzen, V., *et al*. 2006, "Stem-cell ageing modified by the cyclin-dependent kinase inhibitor p16INK4a", *Nature,* vol. 443, no. 7110, pp. 421-426.

Jeyapalan, J.C., *et al*. 2007, "Accumulation of senescent cells in mitotic tissue of aging primates", *Mechanisms of Ageing and Development,* vol. 128, no. 1, pp. 36-44.

Jun, J. & Lau, L. 2010, "The matricellular protein CCN1 induces fibroblast senescence and restricts fibrosis in cutaneous wound healing", *Nature Cell Biology,* vol. 12, no. 7, pp. 676-685.

Kastan, M.B., *et al*. 1992, "A mammalian cell cycle checkpoint pathway utilizing p53 and GADD45 is defective in ataxia-telangiectasia", *Cell,* vol. 71, no. 4, pp. 587-597.

Kaufman, J., *et al*. 2001, "Fibroblasts as sentinel cells: role of the CDcd40-CDcd40 ligand system in fibroblast activation and lung inflammation and fibrosis", *Chest,* vol. 120, no. 1, pp. 53S-55S.

Kaul, S.C., *et al*. 2003, "Overexpressed mortalin (mot-2)/mthsp70/GRP75 and hTERT cooperate to extend the in vitro lifespan of human fibroblasts", *Experimental Cell Research,* vol. 286, no. 1, pp. 96-101.

Kill, I. 1996, "Localisation of the Ki-67 antigen within the nucleolus. Evidence for a fibrillarin-deficient region of the dense fibrillar component", *Journal of Cell Science,* vol. 109, no. 6, pp. 1253-1263.

Knight, D.A., Holgate, S.T. 2003, " The airway epithelium: structural and functional properties in health and disease", *Respirology*, vol 8, no. 4, pp. 432-46.

Kortlever, R., Higgins, P. & Bernards, R. 2006, "Plasminogen activator inhibitor-1 is a critical downstream target of p53 in the induction of replicative senescence", *Nature Cell Biology*, vol. 8, no. 8, pp. 877-884.

Kosar, M., *et al*. 2011, "Senescence-associated heterochromatin foci are dispensable for cellular senescence, occur in a cell type- and insult-dependent manner and follow expression of p16^{ink4a}", *Cell Cycle*, vol. 10, no. 3, pp. 457-468.

Krewski, D., *et al*. 2006, "A Combined Analysis of North American Case-Control Studies of Residential Radon and Lung Cancer", *Journal of Toxicology and Environmental Health, Part A*, vol. 69, no. 7-8, pp. 533-597.

Krishna, D.R., *et al*. 1999, "Does pH 6 β-galactosidase activity indicate cell senescence?", *Mechanisms of Ageing and Development*, vol. 109, no. 2, pp. 113-123.

Kristnamurthy, J. 2006, "p16INK4a induces an age-dependent decline in islet regenerative potential", *Nature*, vol. 443, pp. 443-457.

Krizhanovsky, V., *et al*. 2008, "Senescence of Activated Stellate Cells Limits Liver Fibrosis", *Cell*, vol. 134, no. 4, pp. 657-667.

Krtolica, A. & Campisi, J. 2002, "Cancer and aging: a model for the cancer promoting effects of the aging stroma", *The International Journal of Biochemistry & Cell Biology*, vol. 34, no. 11, pp. 1401-1414.

Krtolica, A., *et al*. 2001, "Senescent fibroblasts promote epithelial cell growth and tumorigenesis: A link between cancer and aging", *Proceedings of the National Academy of Sciences of the United States of America*, vol. 98, no. 21, pp. 12072-12077.

Kuilman, T. & Peeper, T. 2009, "Senescence-messaging secretome: SMS-ing cellular stress", *Nature Reviews Cancer*, vol. 9, no. 2, pp. 81-34.

Kuilman, T., *et al*. 2010, "The essence of senescence", *Genes & Development*, vol. 24, no. 22, pp. 2463-2479.

Kuilman, T., *et al*. 2008, "Oncogene-Induced Senescence Relayed by an Interleukin-Dependent Inflammatory Network", *Cell*, vol. 133, no. 6, pp. 1019-1031.

Kulju, K.S. & Lehman, J.M. 1995, "Increased p53 Protein Associated with Aging in Human Diploid Fibroblasts", *Experimental Cell Research*, vol. 217, no. 2, pp. 336-345.

Kusunoki, Y., *et al*. 1998, "Flow cytometry measurements of subsets of T, B and NK cells in peripheral blood lymphocytes of atomic bomb survivors", *Radiation Research,* vol. 150, no. 2, pp. 227-236.

Kusunoki, Y., *et al*. 2003, "Long-last changes in the T-cell receptor V beta repertoires of CD4 memory T-cell populations in the peripheral blood of radiation-exposed people", *British Journal of Haematology,* vol. 122, no. 6, pp. 975-984.

Kusunoki, Y., *et al*. 2010, "T-cell immunosenescence and inflammatory response in atomic bomb survivors", *Radiation Research,* vol. 174, no. 6, pp. 870-876.

Labinskyy, N., *et al*. 2006, "Comparison of endothelial function, O2–· and H2O2 production, and vascular oxidative stress resistance between the longest-living rodent, the naked mole rat, and mice", *American Journal of Physiology - Heart and Circulatory Physiology,* vol. 291, no. 6, pp. H2698-H2704.

Law, Y.L., Wong, T.P.W. & Yu, K.N. 2010, "Influence of catechins on bystander responses in CHO cells induced by alpha-particle irradiation", *Applied Radiation and Isotopes,* vol. 68, no. 4-5, pp. 726-729.

Leatherbarrow, E.L., *et al*. 2006, "Induction and quantification of γ-H2AX foci following low and high LET-irradiation", *International Journal of Radiation Biology,* vol. 82, no. 2, pp. 111-118.

Lee, J. & Paull, T. 2005, "ATM activation by DNA double-strand breask through the Mre11-Rad50-Nbs1 complex", *Science,* vol. 308, pp. 551-554.

Lee, J., *et al*. 2010, "PTEN status switches cell fate between premature senescence and apoptosis in glioma exposed to ionising radiation", *Cell Death and Differentiation,* .

Lehnert, B.E. & Goodwin, E.H. 1997, "Extracellular Factor(s) following Exposure to α Particles Can Cause Sister Chromatid Exchanges in Normal Human Cells", *Cancer Research,* vol. 57, no. 11, pp. 2164-2171.

Little J, B., *et al*. 2003, "Involvement of the nonhomologous end joining DNA repair pathway in the bystander effect for chromosomal aberrations", *Radiation Research,* vol. 159, no. 2, pp. 262-267.

Little, J.B., *et al*. 1997, "Radiation-induced genomic instability: delayed mutagenic and cytogenetic effects of X rays and alpha particles", *Radiation Research,* vol. 148, no. 4, pp. 299-307.

Liu, D. & Hornsby, P.J. 2007, "Senescent Human Fibroblasts Increase the Early Growth of Xenograft Tumors via Matrix Metalloproteinase Secretion", *Cancer Research,* vol. 67, no. 7, pp. 3117-3126.

Lorimore, S., *et al*. 1998, "Chromosomal instability in the descendants of unirradiated surviving cells after alpha-particle irradiation", *Proceedings of*

the National Academy of Sciences of the United States of America, vol. 95, no. 10, pp. 5730-5733.

Lyng F, M., Seymour C, B. & Mothersill C. 2002, "Initiation of apoptosis in cells exposed to medium from the progeny of irradiated cells: a possible mechanism for bystander-induced genomic instability?", *Radiation Research*, vol. 157, no. 4, pp. 365-370.

Mailand, N., *et al*. 2007, "RNF8 ubiquitylates histones at DNA double-strand breaks and promotes assembly of repair proteins.", *Cell*, vol. 131, no. 5, pp. 887-900.

Martin, L., *et al*. 1997, "Airway epithelium as an effector of inflammation: molecular regulation of secondary mediators", *European Respiratory Journal*, vol. 10, no. 9, pp. 2139-2146.

Maser, R.S., *et al*. 1997, "hMre11 and hRad50 nuclear foci are induced during the normal cellular response to DNA double-strand breaks.", *Molecular and Cellular Biology*, vol. 17, no. 10, pp. 6087-6096.

McVean, A., *et al*. 2012, "Development and validation of 'AutoRIF': software for the automated analysis of radiation-induced foci", *Genome Integrity*, vol. 3, no. 1, pp. 1.

Meaburn, K.J., *et al*. 2007, "Primary laminopathy fibroblasts display altered genome organization and apoptosis", *Aging Cell*, vol. 6, no. 2, pp. 139-153.

Mehta, I.S., *et al*. 2007, "Alterations to Nuclear Architecture and Genome Behavior in Senescent Cells", *Annuals of the New York Academy of Sciences*, vol. 1100, no. 1, pp. 250-263.

Mochan, T.A., *et al*. 2003, "53BP1 and NFBD1/MDC1-Nbs1 Function in Parallel Interacting Pathways Activating Ataxia-Telangiectasia Mutated (ATM) in Response to DNA Damage", *Cancer Research*, vol. 63, no. 24, pp. 8586-8591.

Mothersill, C. & Seymour, C. 1997, "Medium from irradiated human epithelial cells but not human fibroblasts reduces the clonogenic survival of unirradiated cells", *International Journal of Radiation Biology*, vol. 71, no. 4, pp. 421-427.

Mothersill, C. & Seymour, C.B. 1998, "Cell-cell contact during gamma irradiation is not required to induce a bystander effect in normal human keratinocytes: evidence for release during irradiation of a signal controlling survival into the medium", *Radiation Research*, vol. 149, no. 3, pp. 256-262.

Muthna, D., *et al*. 2010, "Irradiation of adult human dental pulp stem cells provokes activation of p53, cell cycle arrest, and senescence but not apoptosis", *Stem Cells and Development*, vol. 19, no. 12, pp. 1855-1862.

Nagasawa, H. 1992, "Effect of dose rate on the survival of irradiated human skin fibroblasts", *Radiation Research*, vol. 132, no. 3, pp. 375-379.

Nagasawa, H. & Little, J.B. 1992, "Induction of Sister Chromatid Exchanges by Extremely Low Doses of α-Particles", *Cancer Research*, vol. 52, no. 22, pp. 6394-6396.

Nakachi, K., *et al*. 2004, "Perspectives on cancer immuno-epidemiology", *Cancer Science*, vol. 95, no. 12, pp. 921-929.

Nakamura, A., *et al*. 2008, "Both telomeric and non-telomeric DNA damage are determinants of mammalian cellular senescence", *Epigenetics and Chromatin*, vol. 1, no. 1, pp. 6.

Nakamura, H., *et al*. 1991, "Interleukin-8 gene expression in human bronchial epithelial cells", *Journal of Biological Chemistry*, vol. 266, no. 29, pp. 19611-19617.

Narita, M., *et al*. 2003, "Rb-Mediated Heterochromatin Formation and Silencing of E2F Target Genes during Cellular Senescence", *Cell*, vol. 113, no. 6, pp. 703-716.

Neriishi, E.N. 2001, "Persistent subclinical inflammation among A-bomb survivors", *International Journal of Radiation Biology*, vol. 77, no. 4, pp. 475-482.

Nijnik, A., *et al*. 2007, "DNA repair is limiting for haematopoietic stem cells during ageing", *Nature*, vol. 447, no. 7145, pp. 686-690.

Nikjoo, H., *et al*. 1997, "Computational modelling of low-energy electron-induced DNA damage by early physical and chemical events", *International Journal of Radiation Biology*, vol. 71, no. 5, pp. 467-83.

Nikjoo, H., *et al*. 1998, "Track structure in radiation biology: theory and applications", *International Journal of Radiation Biology*, vol. 73, no. 4, pp. 355-364.

NRC (National Research Council). 2006, *Health risks from exposure to low levels of ionizing radiation. BEIR VII Report, Phase II.*, National Academy Press, Washington DC.

Ohtani, N., *et al*. 2004, "The p16INK4a-RB pathway: molecular link between cellular senescence and tumour supression", *The Journal of Medical Investigation*, vol. 51, no. 3-4, pp. 146-153.

Olivieri, G., Bodycote, J. & Wolff, S. 1984, "Adaptive response of human lymphocytes to low concentrations of radioactive thymidine.", *Science*, vol. 223, no. 4636, pp. 594-597.

Park, H. & Jo, S. 2011, "Lasting effects of an impairment of Th1-like immune response in γ-irradiated mice: A resemblance between irradiated mice and aged mice", *Cellular Immunology*, vol. 267, no. 1, pp. 1-8.

Parrinello, S., *et al*. 2005, "Stromal-epithelial interactions in aging and cancer: senescent fibroblasts alter epithelial cell differentiation", *Journal of Cell Science*, vol. 118, no. 3, pp. 485-496.

Paull, T.T., *et al*. 2000, "A critical role for histone H2AX in recruitment of repair factors to nuclear foci after DNA damage", *Current Biology*, vol. 10, no. 15, pp. 886-895.

Pazolli, E. & Stewart, S.A. 2008, "Senescence: the good the bad and the dysfunctional", *Current Opinion in Genetics & Development*, vol. 18, no. 1, pp. 42-47.

Pearce, M.S., *et al*. 2012, "Radiation exposure from CT scans in childhood and subsequent risk of leukaemia and brain tumours: a retrospective cohort study", *The Lancet*, vol. 380, no. 9840, pp. 499-505.

Price, J.S., *et al*. 2002, "The role of chondrocyte senescence in osteoarthritis", *Aging Cell*, vol. 1, no. 1, pp. 57-65.

Ramirez, R.D., *et al*. 2001, "Putative telomere-independent mechanisms of replicative aging reflect inadequate growth conditions", *Genes & Development*, vol. 15, no. 4, pp. 398-403.

Rappold, I., *et al*. 2001, "Tumor suppressor p53 binding protein 1 (53BP1) is involved in DNA damage-signaling pathways", *The Journal of Cell Biology*, vol. 153, no. 3, pp. 613-620.

Rave-Fränk, M., *et al*. 2001, "In vitro response of human dermal fibroblasts to X-irradiation: relationship between radiation-induced clonogenic cell death, chromosome aberrations and markers of proliferative senescence or differentiation", *International Journal of Radiation Biology*, vol. 77, no. 12, pp. 1163-1174.

Reddel, R.R. 2000, "The role of senescence and immortalization in carcinogenesis", *Carcinogenesis*, vol. 21, no. 3, pp. 477-484.

Robles, S. & Adami, G. 1998, "Agents that cause DNA double strand breaks lead to P16INK4a enrichment and the premature senescence of normal fibroblasts", *Oncogene*, vol. 16, no. 9, pp. 1113-1125.

Rochette, P.J. & Brash, D.E. 2008, "Progressive apoptosis resistance prior to senescence and control by the anti-apoptotic protein BCL-xL", *Mechanisms of Ageing and Development*, vol. 129, no. 4, pp. 207-214.

Rodier, F., *et al*. 2005, "Cancer and aging: the importance of telomeres in genome maintenance", *The International Journal of Biochemistry & Cell Biology,* vol. 37, no. 5, pp. 977-990.

Rogakou, E.P., *et al*. 1999, "Megabase Chromatin Domains Involved in DNA Double-Strand Breaks in Vivo", *The Journal of Cell biology,* vol. 146, no. 5, pp. 905-916.

Rogakou, E.P., *et al*. 1998, "DNA Double-stranded Breaks Induce Histone H2AX Phosphorylation on Serine 139", *Journal of Biological Chemistry,* vol. 273, no. 10, pp. 5858-5868.

Rossi, D., *et al*. 2007, "Deficiencies in DNA damage repair limit the function of haematopoietic stem cells with age", *Nature,* vol. 449, no. 7160, pp. 288-291.

Rothkamm, K. & Löbrich, M. 2003, "Evidence for a lack of DNA double-strand break repair in human cells exposed to very low x-ray doses", *Proceedings of the National Academy of Sciences of the United States of America,* vol. 100, no. 9, pp. 5057-5062.

Rubin, P., *et al*. 1995, "A perpetual cascade of cytokines postirradiation leads to pulmonary fibrosis", *International Journal of Radiation Oncology, Biology, Physics,* vol. 33, no. 1, pp. 99-109.

Ryu, S., Oh, Y. & Park, S. 2007, "Failure of stress-induced down regulation of Bcl-2 contributes to apoptosis resistance in senescent human diploid fibroblasts", *Cell Death and Differentiation,* vol. 14, no. 5, pp. 1020-1028.

Sabin, R. & Anderson, R. 2011, "Cellular Senescence - its role in cancer and the response to ionizing radiation.", *Genome Integrity,* vol. 2, no. 1, pp. 7.

Sawant, S., *et al*. 2001, "Adaptive response and the bystander effect induced by radiation in C3H 10T(1/2) cells in culture", *Radiation Research,* vol. 156, no. 2, pp. 177-180.

Schlüter, C., *et al*. 1993, "The cell proliferation-associated antigen of antibody Ki-67: a very large, ubiquitous nuclear protein with numerous repeated elements, representing a new kind of cell cycle-maintaining proteins.", *Journal of Cell Biology,* vol. 123, no. 3, pp. 513-522.

Schultz, L., *et al*. 2000a, "The DNA damage checkpoint and human cancer.", *Cold Spring Harbour Symposia on Quantitative Biology,* vol. 65, pp. 489-498.

Schultz, L.B., *et al*. 2000b, "P53 Binding Protein 1 (53bp1) Is an Early Participant in the Cellular Response to DNA Double-Strand Breaks", *The Journal of Cell Biology,* vol. 151, no. 7, pp. 1381-1390.

Schuttman, W. 1993, "Schneeberg lung disease and uranium mining in the Saxon Ore Mountains (Erzgebirge)", *American Journal of Industrial Medicine,* vol. 23, no. 2, pp. 355-368.

Sedelnikova, O.A. 2004, "Senescing human cells and ageing mice accumulate DNA lesions with unrepairable double-strand breaks", *Nature Cell Biology*, vol. 6, no. 2, pp. 168-170.

Sedelnikova, O., *et al*. 2002, "Quantitative detection of (125)IdU-induced DNA double-strand breaks with gamma-H2AX antibody", *Radiation Research*, vol. 158, no. 4, pp. 486-492.

Sedelnikova, O.A., *et al*. 2007, "DNA Double-Strand Breaks Form in Bystander Cells after Microbeam Irradiation of Three-dimensional Human Tissue Models", *Cancer Research*, vol. 67, no. 9, pp. 4295-4302.

Serrano, M. & Collado, M. 2010, "Senescence in tumours: evidence from mice and humans", *Nature Reviews Cancer*, vol. 10, pp. 51-57.

Serrano, M. 1997, "The Tumor Suppressor Protein p16INK4a", *Experimental Cell Research*, vol. 237, no. 1, pp. 7-13.

Serrano, M. & Blasco, M.A. 2001, "Putting the stress on senescence", *Current Opinion in Cell Biology*, vol. 13, no. 6, pp. 748-753.

Severino, J., *et al*. 2000, "Is β-Galactosidase Staining a Marker of Senescence in Vitro and in Vivo?", *Experimental Cell Research*, vol. 257, no. 1, pp. 162-171.

Seymour, C.B. & Mothersill, C. 2000, "Relative contribution of bystander and targeted cell killing to the low-dose region of the radiation dose-response curve", *Radiation Research*, vol. 153, no. 5 Pt 1, pp. 508-511.

Shay, J.W., Pereira-Smith, O.M. & Wright, W.E. 1991, "A role for both RB and p53 in the regulation of human cellular senescence", *Experimental Cell Research*, vol. 196, no. 1, pp. 33-39.

Shelton, D.N., *et al*. 1999, "Microarray analysis of replicative senescence", *Current Biology*, vol. 9, no. 17, pp. 939-945.

Shimada, M. & Nakanishi, M. 2006, "DNA damage checkpoints and cancer.", *Journal of Molecular Histology*, vol. 37, no. 5-7, pp. 253-260.

Sikora, E., *et al*. 2011, "Impact of cellular senescence signature on ageing research", *Ageing Research Reviews*, vol. 10, no. 1, pp. 146-152.

Smith, J.R. & Pereira-Smith, O.M. 1996, "Replicative Senescence: Implications for in Vivo Aging and Tumor Suppression", *Science*, vol. 273, no. 5271, pp. 63-67.

Smogorzewska, A. & de Lange, T. 2002, "Different telomere damage signalling pathways in human and mouse cells", *The EMBO Journal*, vol. 21, no. 16, pp. 4338-4348.

Sokolov, M. 2005, "Ionizing radiation induces DNA double-strand breaks in bystander primary human fibroblasts", *Oncogene*, vol. 24, no. 49, pp. 4257-4265.

Soule, H., *et al*. 1973, "A human cell line from a pleural effusion derived from a breast carcinoma.", *Journal of the National Cancer Institute*, vol. 51, no. 5, pp. 1409-1416.

Spaulding, C., Guo, W. & Effros, R.B. 1999, "Resistance to apoptosis in human CD8+ T cells that reach replicative senescence after multiple rounds of antigen-specific proliferation", *Experimental Gerontology*, vol. 34, no. 5, pp. 633-644.

Staaf, E., *et al*. 2012, "Gamma-H2AX foci in cells exposed to a mixed beam of X-rays and alpha particles.", *Genome Integrity*, vol. 3, no. 1, pp. 8.

Starborg, M., *et al*. 1996, "The murine Ki-67 cell proliferation antigen accumulates in the nucleolar and heterochromatic regions of interphase cells and at the periphery of the mitotic chromosomes in a process essential for cell cycle progression", *Journal of Cell Science*, vol. 109, no. 1, pp. 143-153.

Stein, S., *et al*. 1999, *The Molecular Basis of Cell Cycle and Growth Control*. Wiley-Liss, Inc.

Suzuki, K., *et al*. 2001, "Radiation-induced senescence-like growth arrest requires TP53 function but not telomere shortening", *Radiation Research*, vol. 155, no. 1 Pt 2, pp. 248-253.

Suzuki, M. & Boothman, D. 2008, "Stress-induced premature senescence (SIPS) - influence of SIPS on radiotherapy", *Journal of Radiation Research*, vol. 48, pp. 105-112.

Suzuki, M., *et al*. 2012, "Persistent amplification of DNA damage signal involved in replicative senescence of normal human diploid fibroblasts", *Oxidative Medicine and Cellular Longevity*, vol. Article ID 310534, pp. doi: 10.1155/2012/310534.

Suzuki, M., *et al*. 2006, "Interstitial chromatin alteration causes persistent p53 activation involved in the radiation-induced senescence-like growth arrest", *Biochemical and Biophysical Research Communications*, vol. 340, no. 1, pp. 145-150.

Thomas, E., *et al*. 1997, "Different Kinetics of Senescence in Human Fibroblasts and Peritoneal Mesothelial Cells", *Experimental Cell Research*, vol. 236, no. 1, pp. 355-358.

Tirmarche, M., *et al*. 1993, "Mortality of a cohort of French uranium miners exposed to relatively low radon concentrations.", *British Journal of Cancer*, vol. 67, no. 5, pp. 1090-1097.

Tsai, K., *et al*. 2009, "Low-dose radiation-induced senescent stromal fibroblasts render nearby breast cancer cells radioresistant.", *Radiation Research,* vol. 172, no. 3, pp. 306-313.

Tsai, K.K.C., *et al*. 2005, "Cellular Mechanisms for Low-Dose Ionizing Radiation–Induced Perturbation of the Breast Tissue Microenvironment", *Cancer Research,* vol. 65, no. 15, pp. 6734-6744.

Tubiana, M. 2005, "Dose-effect relationships and estimation of the carcinohgenic effects of low doses of ionizing radiation. The Joint Report of the Academie des Sciences (Paris) and of the Academie Nationale de Me'decine.", *International Journal of Radiation Oncology Biology Physics,* vol. 63, pp. 317-319.

UNSCEAR. 2006, *United Nations Scientific Committee on the Effects of Atomic Radiation. Volume II: Non-targeted and delayed effects of exposure to ionizing radiation*, Annex C edn, UNSCEAR 2006 Report to the General Assembly with Scientific Annexes, United Nations., New York.

UNSCEAR. 2000, *United Nations Scientific Committee on the Effects of Atomic Radiation. Sources and Effects of Ionizing Radiation.*, Vol II Effects edn, 2000 Report to the General Assembly with Scientific Annexes, United Nations., New York.

Van der Meeren, A., *et al*. 2008, "Activation of alveolar macrophages after plutonium oxide inhalation in rats: involvement in the early inflammatory response", *Radiation Research,* vol. 170, no. 5, pp. 591-603.

Vaughan, M.B., *et al*. 2006, "A three-dimensional model of differentiation of immortalized human bronchial epithelial cells", *Differentiation,* vol. 74, no. 4, pp. 141-148.

Verheijen, R., *et al*. 1989, "Ki-67 detects a nuclear matrix-associated proliferation-related antigen. I. Intracellular localization during interphase", *Journal of Cell Science,* vol. 92, no. 1, pp. 123-130.

Vijg, J. & Campisi, J. 2008, "Puzzles, promises and a cure for ageing", *Nature,* vol. 454, no. 7208, pp. 1065-1071.

Wajapeyee, N., *et al*. 2008, "Oncogenic BRAF Induces Senescence and Apoptosis through Pathways Mediated by the Secreted Protein IGFBP7", *Cell,* vol. 132, no. 3, pp. 363-374.

Wang, C., *et al*. 2009, "DNA damage response and cellular senescence in tissues of aging mice", *Aging Cell,* vol. 8, no. 3, pp. 311-323.

Wang, E. 1995, "Senescent Human Fibroblasts Resist Programmed Cell Death, and Failure to Suppress bcl2 Is Involved", *Cancer Research,* vol. 55, no. 11, pp. 2284-2292.

Ward, I.M., *et al*. 2003, "Accumulation of Checkpoint Protein 53BP1 at DNA Breaks Involves Its Binding to Phosphorylated Histone H2AX", *Journal of Biological Chemistry,* vol. 278, no. 22, pp. 19579-19582.

Webley, K., *et al*. 2000, "Posttranslational Modifications of p53 in Replicative Senescence Overlapping but Distinct from Those Induced by DNA Damage", *Molecular and Cellular Biology,* vol. 20, no. 8, pp. 2803-2808.

Wei, S., Wei, W. & Sedivy, J.M. 1999, "Expression of Catalytically Active Telomerase Does Not Prevent Premature Senescence Caused by Overexpression of Oncogenic Ha-Ras in Normal Human Fibroblasts", *Cancer Research,* vol. 59, no. 7, pp. 1539-1543.

Wright, W.E. & Shay, J.W. 2001, "Cellular senescence as a tumor-protection mechanism: the essential role of counting", *Current Opinion in Genetics & Development,* vol. 11, no. 1, pp. 98-103.

Wu, L.J., *et al*. 1999, "Targeted cytoplasmic irradiation with alpha particles induces mutations in mammalian cells", *Proceedings of the National Academy of Sciences of the United States of America,* vol. 96, no. 9, pp. 4959-5964.

Wu, X. & Pandolfi, P. 2001, "Mouse models for multistep tumorigenesis", *Trends in Cell Biology,* vol. 11, no. 11, pp. 2-9.

Xie, A., *et al*. 2007, "Distinct Roles of Chromatin-Associated Proteins MDC1 and 53BP1 in Mammalian Double-Strand Break Repair", *Molecular Cell,* vol. 28, no. 6, pp. 1045-1057.

Xue, W., *et al*. 2007, "Senescence and tumour clearance is triggered by p53 restoration in murine liver carcinomas", *Nature,* vol. 445, no. 7128, pp. 656-660.

Yamada, M., *et al*. 2004a, "Noncancer disease incidence in atomic bomb survivors, 1958-1998", *Radiation Research,* vol. 161, no. 6, pp. 622-632.

Yamada, M., *et al*. 2004b, "Noncancer disease incidence in atomic bomb survivors, 1958-1998.", *Radiation Research,* vol. 161, no. 6, pp. 622-632.

Yanishevsky, R. & Stein, G. 1980, "Ongoing DNA synthesis continues in young human diploid cells (HDC) fused to senescent HDC, but entry into S phase is inhibited", *Experimental Cell Research,* vol. 126, no. 2, pp. 469-472.

Yap, D., *et al*. 1999, "mdm2: a bridge over the two tumour suppressors, p53 and Rb", *Oncogene,* vol. 18, no. 53, pp. 7681-7689.

Yeager, T.R., *et al*. 1998, "Overcoming cellular senescence in human cancer pathogenesis", *Genes & Development,* vol. 12, no. 2, pp. 163-174.

Yegorov, Y.E., *et al*. 1998, "Endogenous β-Galactosidase Activity in Continuously Nonproliferating Cells", *Experimental Cell Research*, vol. 243, no. 1, pp. 207-211.

Yentrapalli, R., *et al*. 2013, "Quantitative proteomic analysis reveals induction of premature senescence in human umbilical vein endothelial cells exposed to chronic low-dose rate gamma radiation", *Proteomics*, vol. 13, no. 7, pp. 1096-1107.

Zglinicki, T.V., *et al*. 2005, "Human cell senescence as a DNA damage response", *Mechanisms of Ageing and Development*, vol. 126, no. 1, pp. 111-117.

Zhang, H. 2006, "p53 plays a central role in UVA and UVB induced cell damage and apoptosis in melanoma cells", *Cancer Letters*, vol. 244, no. 2, pp. 229-238.